Design and synthesis of non uniform high impedance surface based wearable antennas

Design and Synthesis of Non Uniform High Impedance Surface based Wearable Antennas

by

Shahid Bashir

A Doctoral Thesis Submitted in Partial Fulfilment of the Requirements for the Award of Doctor of Philosophy of Loughborough University

October 2009

Abstract

This thesis is concerned with the design and fabrication of flexible textile wearable antennas integrated with the newly introduced artificial materials known as high impedance surfaces (HIS). With the rapid growth and use of wireless communication systems more and more people are taking advantage of portable computing systems on daily basis. Also with the advancement in electronic industry new and sophisticated wireless devices have been introduced which are being used closed to human body. For user convenience there is an increasing need for integrating antennas on or in the clothing. The conventional antennas being rigid and obtrusive to user movements have limitations. There is a need of antennas made of flexible textile materials that can be part of user clothing defined as wearable antennas. Also with the miniaturisation trend in electronic industry, antenna designers are facing a challenge to come up with a compact, low profile, multi function efficient antenna designs occupying a small physical space. By integrating antennas in user clothing this limited space problem can also be resolved.

With the easy availability of electro textile materials it is now possible to manufacture complete fabric antennas. The entire design cycle of wearable fabric antennas starting from material selection to prototype fabrication and antenna testing was carried out in this thesis. A novel technique for antenna fabrication using electro textile material is proposed that will have major implications on wearable computing industry.

The use of HIS for antenna performance enhancement is growing at a rapid pace. In this thesis a modified wearable form of HIS defined as non uniform HIS is presented and successfully integrated with antenna for improved performance under low profile limitation. The HIS was also integrated with normal patch antenna to reduce its size and improve its gain and impedance bandwidth.

These wearable antennas were then tested under real operating conditions. The measured results validated the design idea and showed that there are many possibilities for these unique artificial materials to be exploited for future wearable on body communication antennas.

Acknowledgements

First of all, I would like to express my sincere and foremost gratitude to my supervisor, Dr. Rob Edwards for his continuous support, guidance and valuable discussions thought out the course of my PhD studies.

His outstanding supervision and precious advice were essential to the achievements of this project. This work would not have come through without his valuable information and suggestions.

I would also like to thank my colleagues at CMCR and WiCR labs for their advice, encouragement and friendship. The time spent with them is the most memorable experience of my life. I would specially like to thank Dr. Chauraya, Dr. Panagamuwa and Dr. Whittow for their knowledgeable discussions and encouragement throughout my studies.

I am also very grateful to Mr. Brister from Antennas and Microwave Measurement Lab for his prompt support and help in fabricating antennas and invaluable advice on many occasions.

Last but not least, I would like to express my appreciation and gratitude to my parents and all my family members for their encouragement, understanding, and patience during the course of my PhD.

Publications

1. S. Bashir, M. Hosseini, R. M. Edwards, M. I. Khattak and L. Ma, "Bicep mounted low profile wearable antenna based on a non-uniform EBG ground plane - flexible EBG inverted-l (FEBGIL) antenna," *Antennas and Propagation Conference, 2008. LAPC 2008. Loughborough,* pp. 333-336, 2008.

2. M. Hosseini and S. Bashir, "Circularly polarized radiation by a dipole antenna over an innovative artificial ground plane," *Antennas and Propagation Conference, 2008. LAPC 2008. Loughborough,* pp. 453-456, 2008.

3. L. Ma, R. M. Edwards, S. Bashir and M. I. Khattak, "A wearable flexible multi-band antenna based on a square slotted printed monopole," *Antennas and Propagation Conference, 2008. LAPC 2008. Loughborough,* pp. 345-348, 2008.

4. W. Whittow, C. Panagamuwa, R. Edwards, S. Bashir and J. Vardaxoglou, "Changes in specific absorption rate in the head due to metallic gap loops and a simulated mobile phone source in a study of the effects of jewellery," *Antennas and Propagation Conference, 2008. LAPC 2008. Loughborough* , pp.197-200, 2008.

5. L. Ma, R. Edwards and S. Bashir, "A wearable monopole antenna for ultra wideband with notching function," *Wideband and Ultrawideband Systems and Technologies: Evaluating Current Research and Development, 2008 IET Seminar on,* 2008, pp. 1-5.

6. S. Bashir, A. Chauraya, R. M. Edwards and J. Vardaxoglou, "A flexible fabric metasurface for on body communication applications," *Antennas and Propagation Conference, 2009. LAPC 2009. Loughborough,* 2009, pp. 725-728.

Table of contents

List of Abbreviations

AMC	Artificial Magnetic Conductor
AUT	Antenna Under Test
BW	Bandwidth
EBG	Electromagnetic Bandgap
F/B	Front-to-Back Ratio
FFT	Fast Fourier Transform
FIT	Finite Integration Technique
HPBW	Half Power Beam Width
HIS	High Impedance Surface
MoM	Method of moment
PBA	Perfect Boundary Approximation
PBC	Periodic Boundary Condition
PEC	Perfect Electric Conductor
PMC	Perfect Magnetic Conductor
PML	Perfectly Matched Layer
TST	Thin Sheet Technique
WLAN	Wireless Local Area Network

List of Figures

1 INTRODUCTION

1.1 Background

The ever growing miniaturization of electronic devices, combined with recent developments in wearable computer technology, are leading to a creation of a wide range of devices that can be carried by users in their pockets or in some cases attached to their bodies [1, 2]. These trends in computing tools are consistent with society's historical need to evolve its tools and products into more portable, mobile and even wearable form factors. Watches, radios and telephones are important examples of this trend. Communications technologies are heading towards a future in which user specified information is no longer limited to the static environment of the office or home. Well designed mobile and wearable products can offer more portable and effective ways for people to access this information on demand. In recent years the development of wearable computer systems has been rapid. They are becoming more and more light weight and quite soon there will be a wide range of unobtrusive wearable and ubiquitous computing devices integrated into daily clothing to create a so called Body Area Network (BAN) [3]. To reach this featherweight level requires optimization of every single part and subpart of the wearable system. The main parts of a typical body worn wearable system is shown in Figure 1-1. As can be seen a body worn wearable system consists of electronic devices normally situated on or in close proximity to the human body. The wired connection between devices in a BAN may be inconvenient for a user. This may be due partly to weight and partly to restriction in movement and prescriptions placed on clothing design and manufacture. Therefore the need for comfortability is pushing the trend of wireless communication in place of wired one.
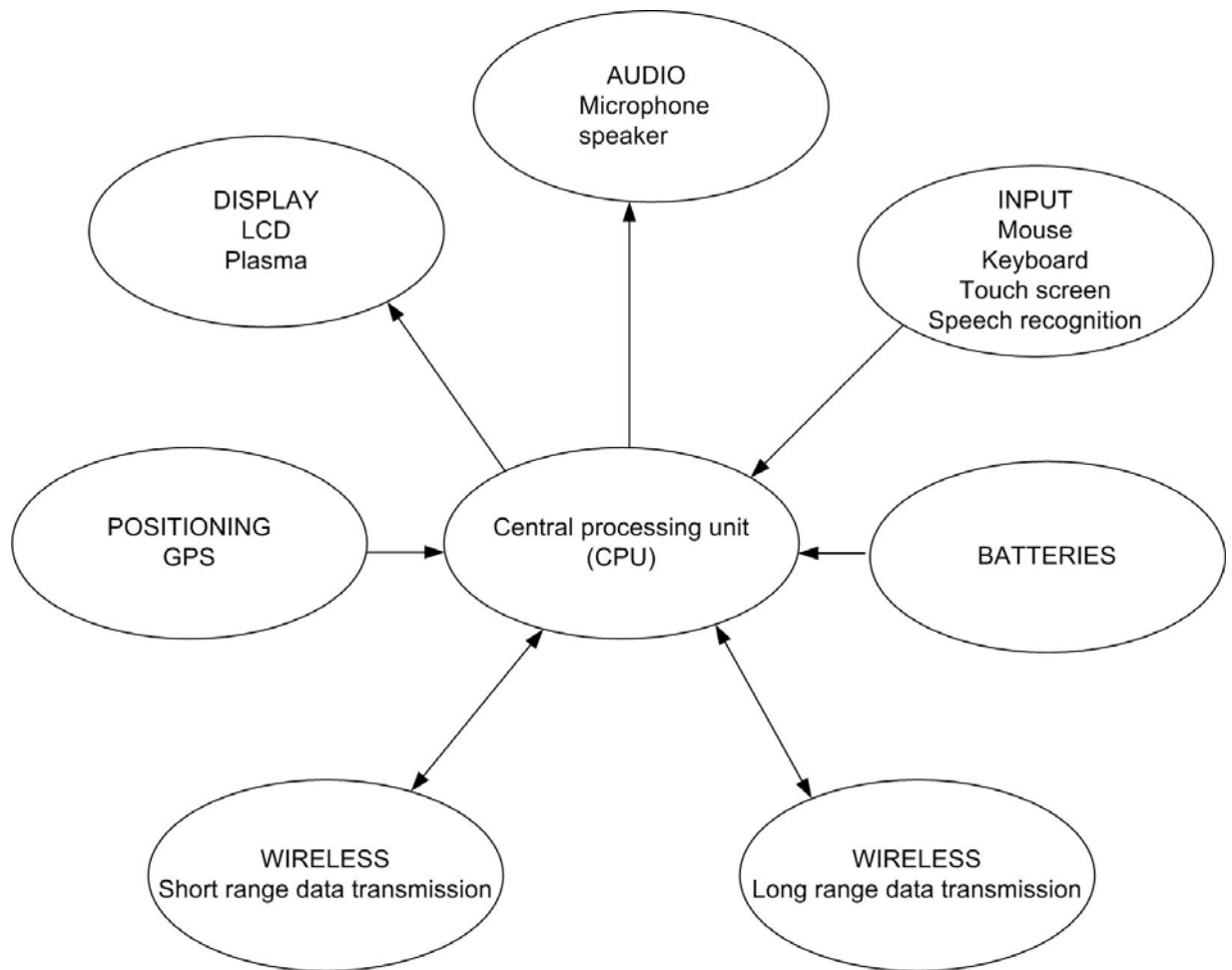
Figure 1-1 Block diagram of a typical body worn wearable system

As shown in Figure 1-1 both short range and long range wireless communication plays an important role in mobile wearable systems. However these communication systems consist of several subparts of which antenna is the most essential one. As radio wave transmitting and receiving devices, they establish a connection between devices which are part of a BAN. And the quality and reliability of a connection will depend a great deal on optimal design of antennas. Compared with conventional antennas which are designed inside electronic gadgets like mobile phones, laptops, Personal Digital Assistant (PDA) and pagers, antennas for wearable systems operate in a near human body environment. The lossy human body reduces the radiation efficiency by absorbing radiating energy and also changes the radiation characteristics like operating frequency and input match bandwidth of wearable antenna [4].

Also conventional antennas are typically fabricated using metals and insulators which are rigid and thus not comfortable and flexible to be worn. Also to increase portability antennas need to be low profile, light weight and tolerant to bending. It can therefore be concluded that conventional antennas are not suitable for wearable applications. And there is need for antennas which make use of flexible materials to design so called wearable antennas. The wearable antenna can be defined as an antenna that is designed and meant to be a part of clothing [5].

Having identified wearable antennas as the main focus of this project the wearable textile system will be discussed in the next section. The salient features of wearable textile system and its applications will be explored.

1.2 Wearable Textile System

The so called "wearable textile systems" aim is to improve quality of life by enhancing the functionalities of clothing through a combination of textiles and electronics. The vision is a future electronic system as an integral part of everyday clothing and serving as an intelligent personal assistant. The new generation of garments known as "smart clothes" have the ability to monitor user's bio signal and communicate this information to the health control centre to provide real time information about person's health. However optimum integration of an antenna into a garment can be achieved by making an antenna out of textile material. The implementation of an antenna in textiles is the straightforward way following the philosophy of wearable computing. However making an antenna truly wearable introduces additional constraints [6]. Compared with conventional antennas, textile antennas must be drapable. Drapability means that something can be bent in all directions at the same time. A textile satisfies this property in contrast to standard flexible substrates with their preferred bending direction. Additionally, a textile antenna must have a flat and planar structure such that it does not affect wearing comfort [7]. The availability of conducting textile materials, known as electro textiles has enabled the manufacturing of truly textile antennas and makes them an unobtrusive part of the wearable textile system [8, 9].

The earliest demand for wearable antennas was set by military for concealing the identity of soldiers carrying radio in the battlefield. The conventional monopole antenna was clearly visible from the distance so it was proposed to incorporate the antenna into the soldier's uniform which has added advantage of eliminating devices that can tangle in trees, foliage and low height obstructions. This idea let to development of RF helmet antenna [10, 11] and RF vest antenna [12-14]. These antennas were constructed using conductive cloth and have advantages of being light weight, inexpensive and low maintenance cost. There was no visual signature provided and they permitted all weather operation.

Another potentially demanding area of wearable antennas is in the health sector for detection of early cancer using imaging methods. One of the new imaging methods "microwave imaging", involves using non-ionising radiation to image the human body. The reflected waves are processed and used to make a comparison between healthy tissues and abnormal tissues [15]. A monopole antenna has been used for this work. However, research is also going on to develop better antennas for microwave imaging and textile antennas which are comfortable against skin and would seem to be a natural choice in this area. Some other interesting applications of wearable textile systems are:

- Assistance to emergency services such as police, paramedics and fire fighters
- Navigation support in the car or while walking
- Pulse rate monitoring in sports
- Space applications

Having defined wearable textile system and its application, desirable features and critical design issues of wearable antennas will be put forward in the next section.

1.2.1 Wearable Antennas: Desirable Features and Critical Design Issues

Wearable antennas have drawn more and more attention in recent years due to the fact that they can be seamlessly integrated into clothing [9, 16-19] which is a desired feature for

hands free applications and military applications requiring low visibility. More importantly wearable antennas can use all the space on clothing that can be utilized to improve quality of signal in wireless communications. Secondly multi path fading is one of the most severe problems in wireless communication since the signal strength drops as the mobile terminal moves over a distance comparable to wavelength. Antenna diversity is a very effective way to combat multipath fading. However antenna diversity requires at least half a wavelength separation between each antenna in the diversity system. This is not possible on small form factor hand held units which limits the use of antenna diversity. On the other hand antenna diversity can be utilized on a large scale of a body worn wireless system [20] . Wearable textile antennas has also attracted consumer electronics industry because it fulfils the increasing demands from the rapidly evolving wireless world. Wearable antenna desirable features common to all applications require light weight, functional, robust, unobtrusive, inexpensive, zero maintenance and no setup requirements.

The important factors that can influence the wearable antenna performance are:

- *Human body interaction with the antenna.* The human body is an irregularly shaped medium with frequency dependent permittivity and conductivity. The distribution of the electromagnetic field inside the body and the scattered field depends largely on the body physiological parameters, geometry, frequency and polarisation of the incident field. Due to high permittivity of body tissues [21] the antenna resonant frequency will change and detune to a lower one. Another important parameter is the antenna Gain that directly affects the power transmitted in a maximum radiation direction. Due to lossy human body some part of radiating power of an antenna will be absorbed by it and it will result in lower Gain.

- *Variations in dimensions.* Due to stretching and compression which are typical for fabric, the antenna structure can easily deform and affect its performance characteristics. As a result it will be difficult to mass produce an antenna with the same radiation characteristics even using same materials.

- *Water absorption*. Fabric antennas made of textile material contain voids that can easily absorb water and moisture and can consequently change the resonant frequency and impedance bandwidth of an antenna.

Most often the wearable antenna requirements are application specific. However common requirements for many applications are:

  (1) Light weight

  (2) Low fabrication cost

  (3) Low maintenance cost

  (4) No setup requirement

  (5) Flexible and stable to withstand bending and stretching

  (6) Robust to withstand damage from obstacles

  (7) Hidden and water proof to avoid wet weather conditions

  (8) Capable of providing shielding from the adverse affects of human body

In the next section the literature review that has contributed to the evolution of wearable antennas will be briefly summarised. This extensive review will help to point out the area of wearable antennas that needs further research study.

1.3 Literature Review of Wearable Antennas

The research work done on wearable antennas can be categorised not only on the basis of type of antennas used like microstrip patch antenna, PIFA antenna, E-shaped and U-slot patch antenna but also on their intended applications like FM radio and TV, cellular mobile communications, WLAN, GPS and UWB applications. The up to date research that has been done so far on wearable antennas and their applications is summarised below:

The first published research work on wearable antennas dates back to 1999 when a dual band planar antenna was designed for wearable and ubiquitous equipment [5]. In this work the conventional Planar inverted F antenna (PIFA) was modified by inserting a U shaped slot to make a dual band antenna that works at mobile cellular band GSM 900 and Bluetooth 2.4GHz band. Although the materials used in this design were conventional rigid type but the proposed idea was to put this antenna on the sleeve to make it a wearable antenna design. The effect of the human body on the radiation characteristics of this antenna was minimized due to the presence of the ground plane.

After this idea of antennas for wearable communication systems the research on wearable antennas generated significant interest among different university and industry researchers. To make wearable antennas comfortable to be worn a fabric based mobile phone antenna for GSM 900 was designed [22]. The conducting parts were constructed with copper plated rip-stop nylon and a foam spacer was used as the dielectric. The antenna was placed on the outside of the upper arm in order not to be affected by human and on body efficiency was reported to be 50%. A flexible substrate based printed IFA wearable antenna for 2.4GHz WLAN and UMTS 2100MHz was proposed for smart clothing in [23]. A microstrip based fleece fabric antenna for an emergency workers outfit was designed working in the 2.4GHz WLAN band [16]. The effect of bending on wearable Microstrip patch antenna designed for 2.5GHz was studied in [24]. It was observed that the resonant frequency changed when antenna was bent in the E-plane while H-plane bending has minimal effect on the resonant frequency.

Wearable antennas are finding increasing use in military uniforms [25] as radio operators are easily identified by their protruding antennas and can be targeted by the enemy. In addition, the antennas can be easily broken by trees and bushes which prohibit their mobility. To overcome this problem different wearable antenna designs seamlessly integrated into soldier uniform have been proposed [10, 14, 26-28]. As any conducting structure can radiate if designed properly some researchers proposed to use the metal button of jackets and belts as antennas [29-31]. The first U shaped patch antenna design was successfully implemented for wearable applications using copper tape and fleece fabric [18].

With the increasing success of wearable antenna designs some researchers started exploring new applications. One wearable antenna design for FM reception was proposed [32]. Different antenna types including half wave thin and wide dipole, Meandered dipole and helical antenna were fabricated using copper tape on fleece fabric. As textile conducting materials continue to find use in wearable antenna design it was deemed necessary to characterise their electrical properties. The measurement techniques of surface resistivity and conductivity of electro textiles was carried out in [33, 34]. The use of electro textiles in wearable antennas applications was explored in [35]. For this purpose a fabric antenna was designed and its efficiency was reported to be 80%. This research supported

the idea of using textile conducting materials in place of traditional copper for light weight wearable antennas.

The effect of conductivity of electro textiles on wearable antennas performance was explored in [36, 37]. Six WLAN fabric antennas were fabricated with different conducting materials and it was concluded that for optimal performance of the antenna i.e. the same as a conventional copper made antenna, the conducting fabric should not be discontinuous in the direction of current flow. Also it must have good conductivity and must be densely knitted. In order to enhance the accuracy of modelling conducting textile based wearable antennas, one experimental method to retrieve the radio frequency material parameters of electro textiles has also been proposed [38]. Similarly the effect of low conductivity of conducting textiles on the input matching, resonant frequency and gain has been explored in [39].

As different textile materials start appearing in wearable antenna design it was deemed necessary to characterise the performance of wearable antenna with different textiles. In [40] six different fabrics were tested as wearable antenna substrates. It was concluded that the textile material should be inelastic and it should have a smooth surface so that there is uniform separation distance between antenna and textile substrate.

As wearable antennas are meant to work in close proximity to human body it is very important to characterise the effect of human body on its performance. The first in depth results showing textile antenna performance in the vicinity of human body was given in [4]. The results showed that wearable antennas performed well near human body and performance was only marginally affected by human body interaction.

Most of wearable antenna designs reviewed so far are linearly polarized. The first circular polarized wearable antenna was presented in [7]. The conventional corner truncated patch was employed for this purpose. Another conventional technique of feeding along the diagonal of square patch was employed in [41] to design WLAN wearable antenna with circular polarization. The promising results showed that standard antenna design techniques works equally well for textile based antennas. Applying conventional designs for wideband and dual band antennas an E-shaped wearable antennas was also proposed

for dual band operation [42] and results were quite similar to conventional E-shaped patch design.

In order to make wearable antenna for people working in tough and harsh environments like fire-fighters Microstrip patch antenna working in 2.4GHz WLAN band was designed using flame resistant Aramid fabric [17, 43]. As this fabric is thin so multilayer structure was used to enhance the impedance bandwidth. The circular polarization was achieved by exciting two orthogonal modes by probe feeding along the diagonal. Similarly a GPS wearable antenna was proposed using fire resistant and water resistant foam substrate [44]. This antenna was particularly suitable for integration into rescue worker's garments. This antenna was shown to work well even when covered with textiles and when integrated into a jacket or worn on the human body. In order to improve the bond between the conducting layer and textile fabric a new assembly technique based on adhesive sheet and ironing was proposed [45] by designing a rectangular ring antenna using fleece fabric and electro textile. Wearable antennas based on modified dipole and folded dipole array design were presented in [46, 47].The use of wearable antennas was also explored for Radio frequency identification (RFID) applications [48, 49]. To make wearable antenna feather light for athletes as they use very light clothes a flexible and light weight antenna at 2.4GHz for athletes was proposed in [50]. To improve the wireless communication link reliability diversity antenna configuration of body worn textile antenna system at 2.4GHz was proposed in [51]. An extensive treatment of design and characterization of purely textile patch antennas was carried out in [9]. In this research work Microstrip line feed patch antennas were fabricated for Bluetooth applications. Both linear as well circular polarised designs were investigated. To simulate the bending behaviour antennas were put on a cylinder of 37mm and 100mm which are typical dimensions of human arm and leg. It was observed that circular polarisation can deteriorate if bending radius is too small.

As the number of wireless communication systems is increasing there is a need for multiple antenna systems. Distributed body worn transceiver system using an electro textile antennas was investigated in [20]. As there is a large space available on human body or clothing so multi textile antennas are proposed to combat multipath fading in wireless channels. In [52] different fabrication techniques of textile antennas were discussed. For conducting part of the antenna copper tape, copper thread and conductive spray was used to see their affect on wearable antenna performance. The affect of human body presence on

the antenna reflection coefficient and radiation pattern was also discussed. It was concluded that for wearable antenna to be accepted by general public they should be hidden, small in size and weight. The first dual polarized textile patch antenna for integration into protective garments and working in the 2.4GHz band was proposed in [53]. The first multiband wearable antenna that works in GSM 900, DCS 1800, PCS 1900, UMTS 2100 and 2.4GHz WLAN was designed [54] using neoprene substrate which is normally used by scuba divers.

The feeding method has an important role in the overall characteristics of the devices specially the impedance bandwidth of antenna [55]. The first aperture coupled patch antenna for integration into wearable textile systems was explored in [8]. In this feeding method the feeding transmission line is totally isolated from the antenna this allowed optimal selection of antenna substrate and feed substrate material. Also this feeding method is more convenient and comfortable for the user and thus results into highly efficient and fully flexible wearable antenna.

The large space available on the human body or clothing can be utilized for designing a high gain antenna array. This concept was explored in [56] for a body worn electro textile antenna array. An eight element patch antenna array was constructed in the 2.45GHz industrial, scientific and medical (ISM) band. They were shown to have comparable performance to their conventional antenna counterparts.

Ultra wide band (UWB) is an emerging wireless technology recently approved by Federal Communications Commission (FCC). It allowed high data rate over short distances with low power consumption [57]. The first UWB textile antenna was proposed in [58]. Two design topologies were investigated. The first was a coplanar waveguide (CPW) fed disc monopole antenna and other a microstrip fed annular slot antenna. All designs had small thickness of 0.5mm and were flexible enough to be easily integrated into clothing. An UWB antenna based on a button structure was proposed in [59, 60].

Electromagnetic bandgap (EBG) structures also known also known as High Impedance surface (HIS) or Artificial Magnetic Conductor (AMC) [61] surfaces are finding increasing use in conventional antenna designs [62-66]. The reason for this being their unique electromagnetic properties of in-phase reflection of plane waves and stop band for

propagation of surfaces waves. These properties have been exploited in designing low profile antennas [66] and improving the bandwidth, gain and backward radiation in patch antenna designs [67].

The use of EBG structures in wearable antennas designs has not been explored to a great extent. However some designs have been proposed which have incorporated them. The first EBG based antenna design for wearable application was proposed in [68]. Although it was not a truly wearable antenna as it was constructed of traditional rigid FR4 substrate however the idea was to use this for wearable applications. A 2.45GHz patch antenna was fabricated on a thin FR4 substrate and EBG pattern was etched on the ground plane of the antenna. It was observed that the effect of EBG was to increase the impedance bandwidth, gain and reduce the backward radiation as well as reduce the size of the antenna.

The first truly wearable EBG antenna was put forward in [69]. In this design a patch antenna was fabricated on top of periodic square patch array working as EBG. Copper tape was used to make conducting parts of an antenna while fleece fabric was used as an antenna substrate. The affect of the EBG structure was two fold. Firstly to increase the input match bandwidth by 50% and secondly to reduce the antenna size for a fixed frequency by 30%. The effect of wearable EBG antenna bending on input match and impedance bandwidth was examined in [70]. It was shown that when antenna is bent along the direction which determines its resonant length affects it has the greatest effect on the input matching and impedance bandwidth.

A dual band triangular patch antenna integrated with dual band EBG was proposed in [71]. The dual band was achieved by a parasitic element close to the triangular patch. The dual band EBG was realised by using a combination of patches and concentric rings. It was shown that EBG structure helped in reducing the back radiation by up to 15dB. In [72] a CPW fed dual band wearable antenna was integrated with a dual band EBG structure. The antenna operated in the 2.45GHz and 5GHz WLAN bands. The EBG structure consisted of only 3 x 3 EBG elements but helped in reducing the backward radiation towards the body by over 10dB and also improved the antenna gain by 3dB.

After this extensive review of research work done in the wearable antenna design field the aims and objectives of this thesis will be highlighted in the next section.

1.4 Research Aims and Objectives

The aims and objectives of this research study stems from the literature review summarised above. It is clear that wearable antennas for wireless body centric communications to be accepted by the general public they need to be low profile, light weight, comfortable against skin and unobtrusive to be worn. Although most of the new wearable antenna designs reported in literature are planar and thus given that they can be made flexible, they may be embedded into clothing. However associated with these types of antennas are some inherent drawbacks and they therefore do not properly fulfil the requirements set for wearable antennas in Section 1.2. For example microstrip antennas when made small tend to low efficiency, narrow bandwidth and poor front-to-back (F/B) ratio. Similarly printed monopole antenna is very sensitive to human body detuning effects as they do not have ground plane under the antenna. Their resonant frequency, impedance bandwidth, radiation pattern and gain are all affected by lossy human body.

It is the hypothesis of this thesis that there is a need to select suitable flexible conducting and non conducting materials for fabricating fully textile wearable antennas. For this purpose there should be a reliable and non destructive method to measure the antenna relevant electromagnetic properties of these materials. Also for mass production and rapid prototyping of wearable antennas there is a need for industry standard fabrication technique. With the growing use of HIS structures into conventional antenna design and their benefits there is a need for incorporating them into wearable antenna field. It can be said that by integrating periodic structures known as High Impedance Surface (HIS) with wearable antennas not only the physical characteristics of antenna can be improved like making them low profile and compact in size but the radiation characteristics of antennas can be greatly enhanced in terms of input match bandwidth, radiation pattern, gain and F/B ratio. Also due to surface wave suppression property (which will be explained in chapter 2) of HIS structures the backward radiation towards human body will be reduced and hence the degradation effect of a lossy human body on antenna performance can be minimized. Thus the antenna can work equally well whether it is away from the body or on the body.

Although as mentioned in Section 1.3 some wearable antenna designs incorporating HIS structures have been proposed with significant improvements in wearable antenna

performance. But there is still some research work need to be done to design novel HIS and their integration into wearable antennas.

In short the following are the main objectives for this research work:

- Selection of suitable non conducting material as antenna substrate for flexible wearable antennas.
- Selection of suitable conducting textile material (electro textile) as antenna radiating element and ground plane to design fully textile wearable antennas.
- Proposing a suitable technique to measure the electromagnetic properties of wearable materials.
- Finding the PCB industry standard fabrication technique for wearable antennas.
- Design of novel High Impedance Surfaces (HIS).
- Integration of HIS with wearable antenna design.
- Performance study of wearable antennas integrated with novel HIS.

1.5 Research Contributions

The research in this thesis concerns designing and fabricating fully textile wearable antennas integrated with a novel HIS. The selection of materials and their characterisation for wearable antenna design has received limited attention in scientific journals. In this research full classification of different techniques available for characterising electromagnetic properties of materials is given. The advantages and disadvantages of different methods clearly mentioned. The cavity method was best due to its accuracy and non destructive nature. The split post dielectric resonator (SPDR) working on the principle of cavity method and used in this research was discussed in detail. Different fabric samples as potential wearable antenna substrates were then measured for the first time using SPDR. The accuracy of this device was verified with the values of the published results.

To date wearable antennas were fabricated using copper tape or electro textiles using conventional knife cutting or laser ablation [73]. In this research a novel technique to fabricate wearable antennas using electro textile was employed. The traditional printed

circuit board (PCB) etching method was modified for the thin electro textiles. This is the first time such a technique has been implemented in wearable antenna design. This method allows rapid prototyping with industry standard accuracy. Also this opens a new possibility of complex wearable antenna design shapes that were never reported before in open literature. This has major implications for wearable computing industry as well.

The use of HIS with antenna has been studied in detail in past. However the majority of HIS structures reviewed are uniform with unit cell repeating itself uniformly over the whole periodic structure. There is a variation of uniform HIS known as non uniform HIS [74, 75] in which the parameters of unit cell varies from one cell to other cell. By introducing non uniformity the performance of some types of antenna had been shown enhanced in relation to input match bandwidth and F/B ratio [74, 76]. This design concept was modified to wearable form factor and successfully design low profile and compact non uniform HIS based wearable antennas [77] in this research.

1.6 Thesis Outline

This chapter has provided an introduction to the motivation and the need behind the research study in this thesis. The design of fully textile wearable antennas integrated with novel HIS has been identified as the key part of this thesis.

Chapter 2 will discuss the important steps relevant to wearable antenna design. It will also provide the relevant theory of high impedance surfaces (HIS). Their unique electromagnetic properties of in phase reflection and surface wave suppression will be discussed. The simulation models that have been used to design HIS will be presented. The effect of introducing non uniformity to the uniform HIS will also be discussed.

Chapter 3 will present the important electromagnetic properties of conducting textiles and non conducting textile substrates used in this project. The experimental setup that has been used to characterize the permittivity and loss tangent of textile fabrics will be explained. Prototype textile patch antennas will be fabricated using novel PCB etching technique. The measured reflection coefficient results will be used to select suitable electro textile for this research.

In chapter 4 a novel inverted L 2.4GHz WLAN wearable antenna will be introduced. This antenna will be integrated with uniform HIS as well as non uniform HIS for performance enhancement. The two layer design will be modified to single layer for further reduction in profile. The simulated as well as measured results will be presented for reflection coefficient and radiation patterns.

In Chapter 5 the thesis introduces a novel non uniform HIS based patch antenna. The miniaturisation and improvement in input match bandwidth will be highlighted. The simulated and measured results will be presented for reflection coefficient and radiation patterns.

In chapter 6 the performance characteristics of prototype wearable antennas in real life like situations like bending condition and on human body will be discussed. The input match performance and radiation patterns will be given for these operating environments.

Finally chapter 7 highlights the main conclusions of this research and key findings and gives suggestions for further work in this area.

2 DESIGN AND SYNTHESIS OF HIGH IMPEDANCE SURFACES FOR LOW PROFILE ANTENNAS

2.1 Introduction

As discussed in Chapter 1, planar antennas with low profiles are natural choices of antennas for wearables. The microstrip antenna [78] is a good example of a planar antenna that has many desirable properties. Typically, they consist of one or more radiating elements and a dielectric substrate which is supported by a sheet of conducting material known as a ground plane which, like the radiating elements, is often assumed to be a perfect electric conductor (PEC). Any energy radiated by an antenna into body tissue will be readily absorbed and is therefore wasted since it does not radiate. The boundary condition on the surface of a PEC requires total reflection of a normally incident wave [79] and therefore, theoretically at least, one could use a ground plane both to isolate an antenna from the body (no field can exist within the ground plane) and also use the reflected energy to constructively reinforce waves away from the body. However, there are several properties of microstrip antennas that need special attention. Firstly the ground plane in use is not infinite. This means that the image of the conducting elements seen upon it causes currents that creep beyond the edge of the ground plane and around the back of it will form a back lobe that radiates into the skin. It would be useful if this effect could somehow be limited.

Secondly, to achieve constructive interference the separation between the ground plane and radiator will need to be λ/4. For example for a substrate having a relative permittivity of 1 (air), would need to have a separation of 32mm at 2.4GHz operating frequency to optimally reinforce the wave propagating out from the body. It would be helpful if somehow thickness could be reduced.

Thirdly, there is a component of the energy produced by microstrip antennas known as a surface wave [65] . These types of evanescent waves travel along the interface between the air and the dielectric and do not radiate and are therefore a loss. It would be helpful if this type of wave could somehow be suppressed.

In recent years, periodic structures known as High Impedance Surfaces (HIS) have attracted significant attention due to their unique electromagnetic properties of in phase reflection and surface wave suppression [61]. These types of surfaces have a boundary condition that is satisfied by zero tangential magnetic fields, a normal incident wave is therefore reflected with no phase change (Note that PEC surfaces invert the reflected wave). Theoretically HIS behave like Perfect Magnetic Conductors (PMC) which doesn't exist in nature. Hence HIS is also called Artificial Magnetic Conductor (AMC). If an AMC surface could be realised that was infinitely thin then the reflected wave normal to the surface would be constructive with the incoming wave which would allow to place the radiating element/s of microstrip antenna also in the interface with no need for a λ/4 thick dielectric substrate. However, it turns out that practical HIS are not infinitesimally thin and that in any case since a substrate is required to support the wave in a microstrip antenna some thickness is needed. Nevertheless as will be seen later in this chapter the AMC can substantially reduce the thickness of an antenna.

HIS also exhibits frequency bands (band gaps) inside which no surface waves can propagate along the surface [65]. HIS structures exhibiting a surface wave band gap are called Electromagnetic Bandgap (EBG) structures. EBG structures have been successfully utilised to improve the radiation pattern in the forward direction, reduce backward radiation and hence increase in the gain and improve Front to Back (F/B) ratio of low profile printed antennas [80].

As the aim of this research is the design of wearable antennas with low profiles, compact sizes, reduced backward radiation and improved input match bandwidths, the integration of HIS into wearable devices has been of benefit.

In this chapter HIS and their unique properties will be formally defined. The two main characteristics of in phase reflection and surface wave suppression will be presented with

examples for this purpose. The variation in resonant frequency and bandwidth of conventional HIS due to change in incident angle is explained with computed results. Subsequently angularly stable non uniform HIS are proposed using an equivalent circuit model of parallel conducting strips.

2.2 Perfect Electric Conductor as Ground Plane

The perfect electric conductor (PEC) is a theoretical material having infinite conductivity σ (S/m). It turns out that conducting material such as copper (typically 6×10^7 S/m) although having finite conductivity can be approximated as a PEC. A flat copper sheet has been used in numerous antenna designs as a reflector or a ground plane [81]. The conducting ground plane reflects an incident electromagnetic wave. Given the correct position of the antennas radiating element/s the use of a ground plane has two advantages. One it may improve the antenna gain by up to 3dB and two, it shields a body underneath the ground plane. The amount of gain increase and shielding depends on the ground plane size [55] .

While a simple conducting surface has these desirable properties, it also exhibits one undesirable property of inverting the phase of the reflected wave for antenna applications. As the electric field inside a perfect conductor is zero the boundary condition at the metal/air interface forces the tangential electric field at the surface to be zero. When an electromagnetic wave is incident on a conductor, the reflected wave undergoes a phase reversal to satisfy boundary conditions of electric field node and magnetic field antinode [82].

Unfortunately, antennas do not operate efficiently if positioned very close and parallel above a PEC ground plane. By image theory [83] the parallel electric source placed very close above the PEC surface will generate negative image currents on the PEC surface. The image currents in the conductive sheet cancel the currents in the antenna resulting in reduced radiation efficiency.

This phenomenon can also be explained by considering the phase shift that occurs as incident wave propagates and than reflects back from the PEC and finally adding with the

incident wave to form an interference pattern on the front side of the radiator. This sequence of operation is shown in Figure 2-1 for a $\lambda/4$ distance between the radiator and PEC ground plane. When an electromagnetic wave travels a distance of $\lambda/4$ it undergoes a phase change of 90 degrees.
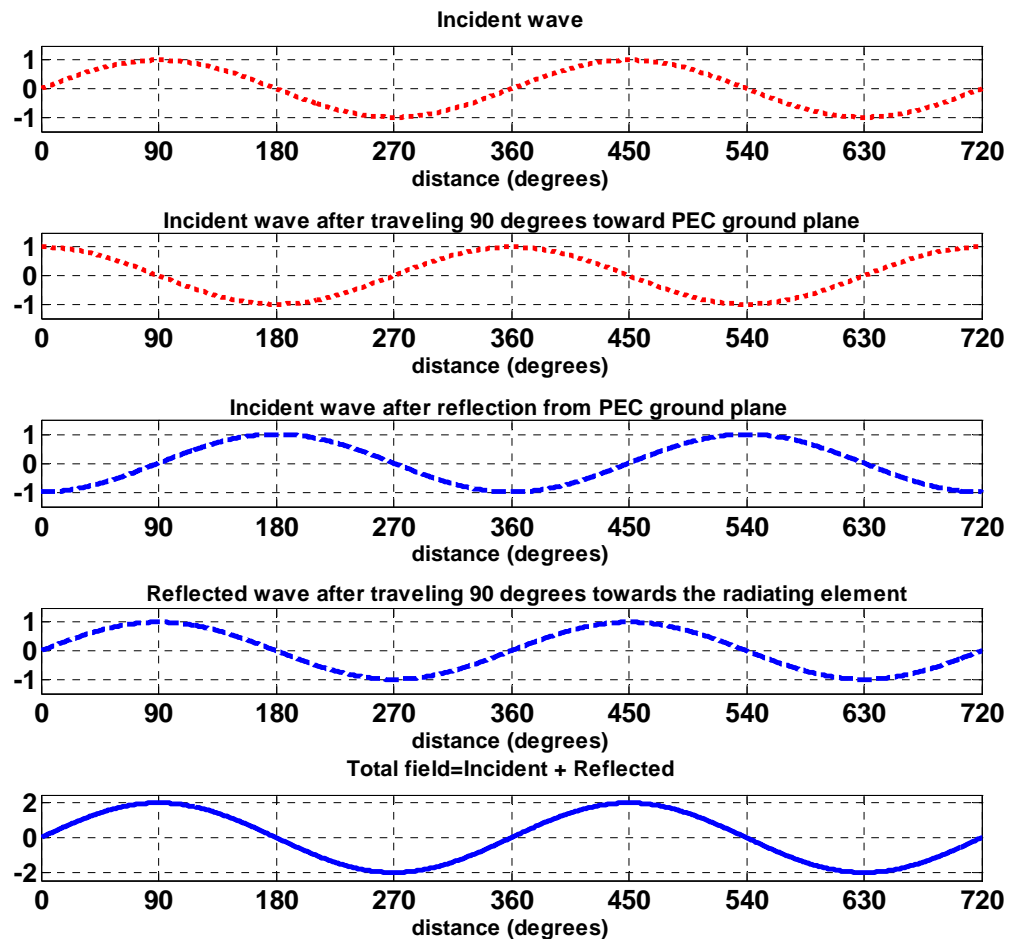
Figure 2-1 Phase changes of incident wave for a λ/4 spacing between the radiator and PEC ground plane

When it impinges the PEC ground plane, it is reflected back and undergoes further 180 degrees phase change. It than travels towards the radiator by travelling $\lambda/4$ distance again and in the process its phase changes by further 90 degrees. Now as shown in Figure 2-1 this wave and the incident wave are in phase. They add up constructively in the forward direction. However if this spacing of $\lambda/4$ is not there, the reflected will be 180 degrees out of phase with the incident wave and destructive interference will take place accordingly.

This destructive interference phenomenon is shown in Figure 2-2 for a dipole antenna placed horizontally and very close to a PEC ground plane. Due to destructive interference between reflected waves and original waves emitted directly by the radiating element, the antenna is effectively shorted out by the metal surface and radiation efficiency is reduced significantly.
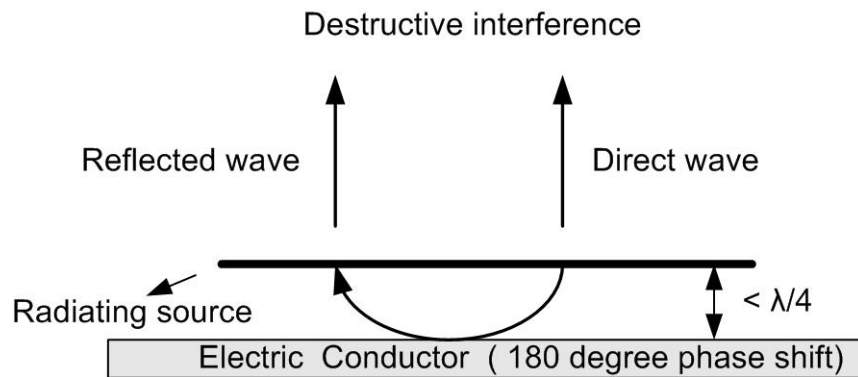
Figure 2-2 A Radiating element lying parallel and close to electric conductor

This problem can be solved by separating the radiating element from the ground plane by at least one quarter of operating wavelength as explained in Figure 2-1. This situation is depicted in Figure 2-3, the total round trip phase shift from the radiating element, to the conductor surface and back to the element equals one complete cycle. Therefore, the two waves will be in phase and will interfere constructively. In this way the antenna will radiate efficiently even when placed close to the electric conductor. However the entire structure requires a minimum thickness of $\lambda/4$ which limits its applications in low profile antenna designs. The low profile design usually refers to the antenna structure whose overall height is less than one tenth of a wavelength at the operating frequency. Therefore this minimum thickness requirement is the limitation in reducing the antenna profile and also in achieving broadband design as quarter wavelength separation only exists at a certain frequency range.

Constructive interference
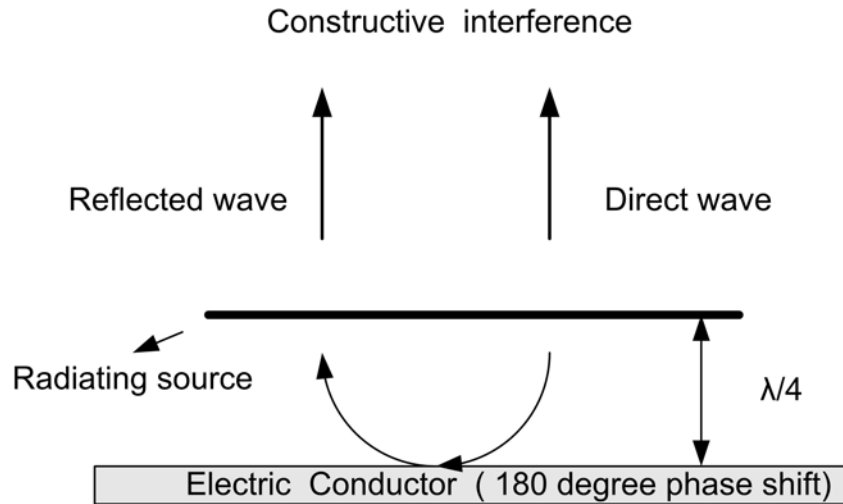
Figure 2-3 Radiating element separated by ¼ wavelength from the electric conductor

Another property of conductor surfaces is that they support surface waves [84]. These are propagating electromagnetic waves that are bound to the interface between conductor and free space. When an antenna operates close to a metal sheet, it will radiate plane waves into free space; however it will also induce surface currents that will propagate along the conducting sheet. If the conductor is smooth and infinite in extent, the surface currents will not radiate into free space and would result only as slight reduction in radiation efficiency. In a real situation, the conducting ground plane is always finite in size and not perfectly smooth. So these surface currents will propagate until they reach a discontinuity like an edge or corner. They will radiate and interfere with the antenna radiation. The combined radiation from the antenna and different parts of the conducting ground plane will form series of lobes and nulls at various angles which will be seen as ripples in the far field radiation pattern [85]. In addition part of the surface currents will also radiate on the back side of the ground plane, decreasing Front-to-back ratio. Moreover when multiple antennas share the same ground plane to form an array, surface currents in addition to free space coupling also cause unwanted mutual coupling among them [65]. This may cause scan blindness in phased arrays [86].

In the next section the antenna performance behaviour in the presence of Perfect Magnetic Conductor (PMC) will be discussed.

2.3 Perfect Magnetic Conductor as Ground Plane

In contrast to a PEC, the Perfect Magnetic Conductor (PMC) will generate in phase image currents when a horizontal electric source is placed above it. This image current will reinforce the antenna current and increase the radiation efficiency of antenna. Because the reflected wave has no phase shift on reflection from PMC surface, the λ/4 minimum distance is no longer needed. The in phase reflected waves and the waves radiating directly from the source will combine constructively as shown in Figure 2-4. This helps to significantly reduce the antenna profile. However, unfortunately no natural material has been found to realise such a magnetic conductive surface.
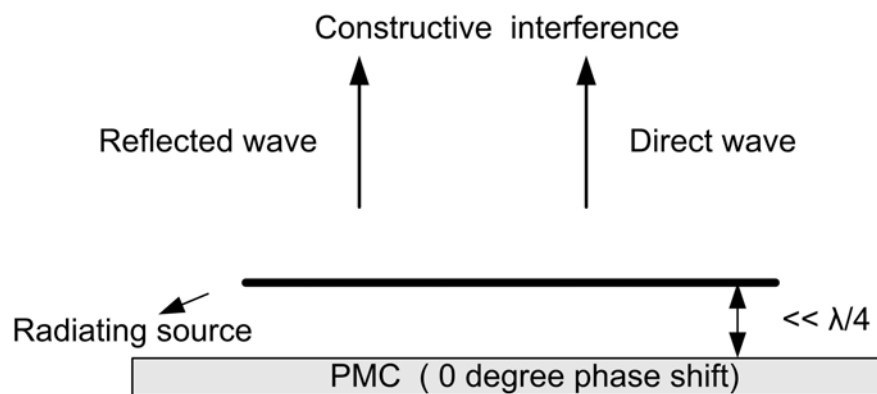
Figure 2-4 A radiating source lying parallel above PMC ground plane

Much effort was therefore devoted to realise a PMC like surface artificially. In the next section the artificially engineered High Impedance Surfaces (HIS) will be discussed that can mimic PMC behaviour and has many interesting applications in antenna and microwave field.

2.4 High Impedance Surfaces (HIS)

In 1999 [61] it was shown that by incorporating a periodic pattern on a conducting surface it is possible to alter its radio frequency surface properties. A smooth conducing surface has low surface impedance while with a specially designed geometry; the periodic structure can have high surface impedance. Such structures have therefore been named high impedance surfaces (HIS).

The two main electromagnetic properties of HIS are:

- *In phase reflection or Artificial Magnetic conductor (AMC) behaviour*. As discussed previously that PEC exhibits 180º phase shift while PMC, which doesn't exist in nature, has a reflection phase of 0º. The reflection phase of HIS varies from -180º to +180º with frequency. When it is between -90 to +90 the image currents are more in phase than out of phase. It means that in a certain frequency band, HIS behave as PMC. And therefore HIS showing such characteristics have been called Artificial Magnetic Conductor (AMC). This in phase reflection behaviour enables low profile antenna design using AMC as ground plane [66].

- *Surface wave suppression or Electromagnetic Band gap (EBG) behaviour*. The frequency band within HIS shows high surface impedance it doesn't allow free propagation of surface waves [87]. In other words there is a band gap for surface wave, hence the name Electromagnetic band gap (EBG). EBG structures have been integrated with antennas to improve the antenna Gain and reduce backward radiation [88, 89].

These periodic structures after their introduction have attracted a lot of attention because of these unique electromagnetic properties. One particular application exploiting the in-phase reflection property is using them as ground plane for low profile antenna.
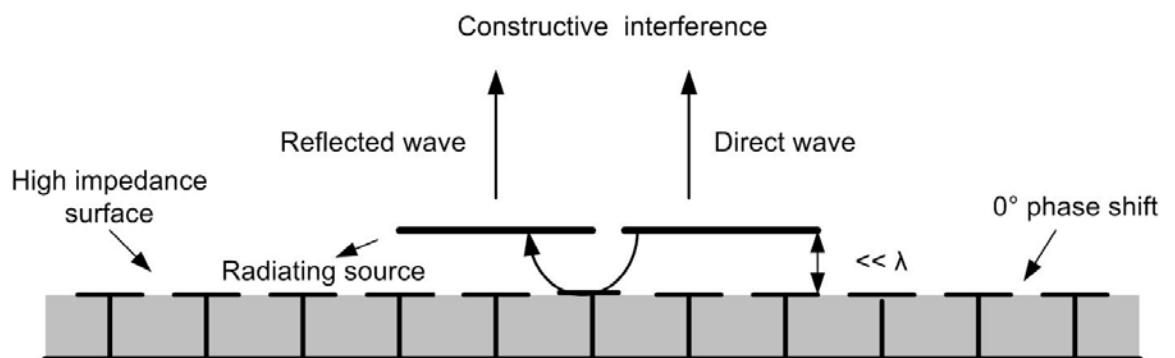
Figure 2-5 A radiating dipole lying above a high impedance surface (HIS) ground plane

In Figure 2-5 a radiating element lying horizontally above a HIS ground plane is not shorted out as it would on a normal metal ground plane. The HIS ground plane reflects

most of the power just like a metal ground plane however its reflection phase is 0º unlike 180º of metal sheet, thus allowing the radiating element to be placed directly above the surface. In other words, the image current aid rather than oppose antenna current. In other applications the surface wave suppression property is exploited to enhance printed antenna performance. Surface waves usually occur on the interface between two different materials, such as air and metal. They are bound to the interface and attenuate exponentially in the direction normal to the interface. The fields associated with surface waves usually extend thousand of wavelengths into the surrounding space at radio frequency and are frequently depicted as surface currents [90]. Surface wave exists mostly because of finite size of the antenna ground plane. They reduce antenna gain, efficiency and bandwidth. By integrating HIS structure as ground plane with printed antennas surface waves cannot propagate due to band gap behaviour and increased amount of power couples to the space waves. Thus antenna embedded with HIS ground plane show much improved radiation pattern performance as compared to normal PEC ground plane.

These desirable electromagnetic properties of HIS structures have been exploited in wearable antenna designs as well. They can help to reduce backward radiation towards human body and enhance the radiation towards the desired direction and result in improvement in antenna performance in terms of radiation efficiency and gain [69, 70, 73, 77].

In the next section the theoretical background is provided on the working of typical HIS structure. This will help to design HIS for wearable antenna applications pertinent to this research.

2.4.1 Operation Mechanism of High Impedance Surfaces (HIS)

High impedance surface normally consists of periodic arrangement of dielectric and/or metallic elements. To better understand the operation mechanism of HIS structure some circuit models have been proposed [90-93]. The working principle of a simple two dimensional planar periodic structure shown in Figure 2-6 will be now explained. This structure was first proposed in [61]. It consists of four main parts: a metal ground plane, a dielectric substrate, periodic metal patches on top of the substrate and vertical metallic vias connecting the patches to the ground plane. It is also called mushroom EBG structure as its

shape is similar to a mushroom. The parameters of HIS structure are labelled in Figure 2-7 as patch width *W*, gap width *g*, substrate thickness *h*, dielectric constant ε_r, vias radius *r*. When the periodicity (*W*+*g*) is small compared to the operating wavelength, the operation mechanism of this HIS structure can be explained by using an effective medium model in which the electromagnetic properties of the surface are reduced to an equivalent lumped LC circuit as shown in Figure 2-7 (b).
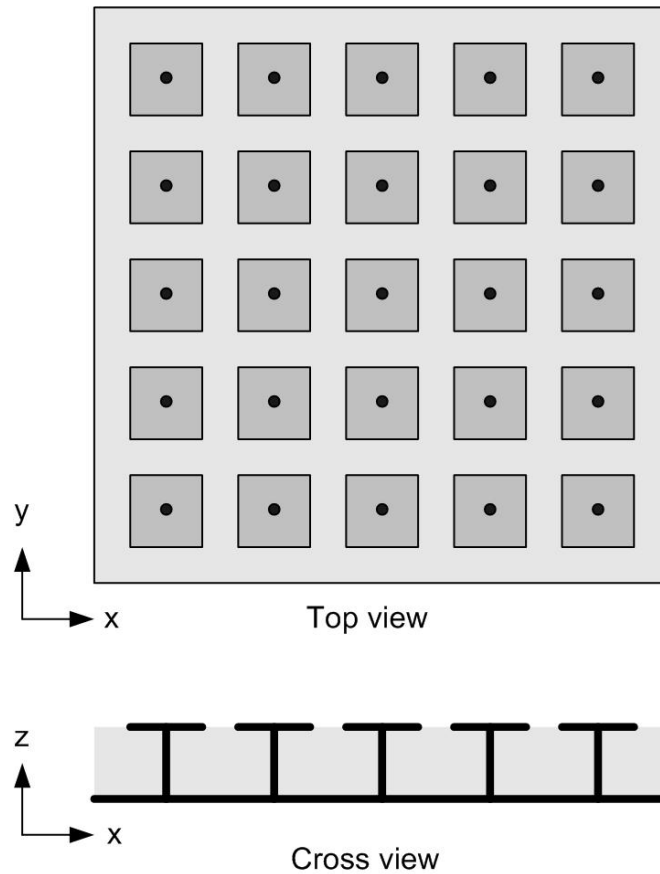
Figure 2-6 A mushroom like HIS structure top and cross view

(a)   (b)
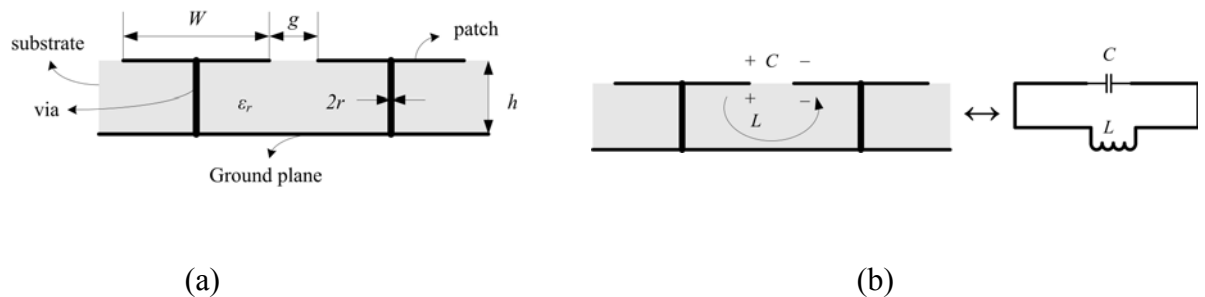
Figure 2-7 LC model for the mushroom like HIS structure (a) HIS parameters (b) equivalent LC model

In this equivalent model the capacitance C is due to the gap between the patches and the inductance L results from the current path between the patches through vias. The impedance of a parallel resonant LC circuit is given by:

$$Z = \frac{j\omega L}{1 - \omega^2 LC} \tag{2.1}$$

The resonant frequency of the equivalent circuit is computed as follows:

$$\omega_o = \frac{1}{\sqrt{LC}} \tag{2.2}$$

Examining Equation (2.1) it can be seen that at low frequencies, the unit cell is generally inductive and Transverse Magnetic (TM) surface waves are supported by this surface. As the frequency of excitation increases the unit cells first become resonant and then capacitive with Transverse Electric (TE) waves becoming the dominant mode. In a narrow band around resonant frequency ω_o, the surface exhibits high impedance. At resonance the structure suppresses the propagation of both TE and TM surface waves and results in a band gap of frequency (EBG behaviour). Surface waves are therefore suppressed (choked off) and a greater proportion of the energy into the system is reflected back due to the high level of mismatch. Note that in this case the surface is excited by microstrip line.

According to [61] the values of the reactive values of the unit cells are dependent on the fringing effects between neighbouring co-planar metal patches. For edge reactance for structures in which the gap g (Figure 2-6) is narrow the following equation is true[90]:

$$C = \frac{W\varepsilon_o(1 + \varepsilon_r)}{\pi} \cosh^{-1}\left(\frac{W + g}{g}\right) \tag{2.3}$$

The value of the inductance can be derived from the current loop in Figure 2-7(b), consisting of the vias and metal patch. For a solenoid current (current where the magnetic flux is parallel to the direction of the axis of the lumped inductance) the magnetic field can be computed using Ampere's Law. The equivalent inductance is then calculated from the stored magnetic field energy and excitation. The inductance therefore depends only on the

thickness of the structure and the permeability of the media and according to [90] is given by the following equation:

$$L = \mu h \tag{2.4}$$

By substituting (2.3) and (2.4) into (2.1) and (2.2), the surface impedance Z and resonant frequency ω_o for a given structure can be computed.

2.5 Classification and Characterisation of High Impedance Surfaces (HIS)

After their introduction a wide variety of HIS structures have been proposed and studied in the microwave and antenna community [85, 87, 94-98]. Because of their diverse shapes and EM properties it's important to classify them. One simple way to classify them is based on their geometry. They have been classified into three groups:

1. Three dimensional volumetric surface
2. Two dimensional planar surfaces
3. One dimensional transmission lines

Another way to classify them is based on the exhibited EM properties. There are two main structures under this classification:

1. Electromagnetic bandgap (EBG) structures
2. Artificial Magnetic Conductor (AMC) structure

The structures which inhibit the propagation of electromagnetic waves are called EBG structures. The electromagnetic wave can be either plane wave with a specific incident angle and polarization state or it can be a surface wave bounded to a ground plane. Most of the three dimensional HIS structures, such as the periodic array of dielectric rods [99] comes under this category. Some two dimensional surfaces [100, 101] can also be put into this category when the surface waves are inhibited.

The structure which shows in phase reflection phase behaviour is called AMC structures. Usually two dimensional surfaces with a very thin profile come under this category. It usually consists of Frequency Selective Surfaces (FSS) [102] backed by a thin grounded slab [103, 104].

It is important to point out that there are some structures which show both EBG and AMC characteristics. For example, the mushroom like EBG [61] and the uni-planar EBG [88] belong to both groups. Initially it was proposed that if there are no vias in the mushroom like HIS it does not show EBG behaviour [105]. However in [106] it was experimentally proved that when via is removed form the mushroom like HIS the EBG phenomenon still exists but the spectral position moves to the higher frequency band while AMC band remains at the same position as in mushroom like HIS. This is due to different phenomenon responsible for AMC and EBG resonance. The EBG behaviour occurs due to array resonance while Fabry-Perot resonance is responsible for AMC characteristics. It was then proposed that by varying the periodicity of the HIS structure but keeping the patch size fixed the AMC and EBG bands can be tailored independently and designed to overlap for simultaneous EBG and AMC operation.

In the next section the models used for reflection phase and surface wave band gap characterisation of HIS structure will be discussed.

2.5.1 Reflection Phase Characterisation of HIS Structures

Reflection coefficient is an important parameter to describe the reflection property of an object. It is defined as the ratio of the reflected field over the incident field at the reflecting surface. It is a complex number with both magnitude and phase. HIS structures of the type considered here always have an integrated ground plane which is generally assumed to be both PEC and infinite. Thus in analysis the reflection coefficient magnitude is always unity (all energy reflected). However the reflection coefficient phase does vary and of special interest to HIS operating as AMC.

The reflection coefficient phase of HIS structure can be computed by illuminating the surface with a plane wave and evaluating/measuring the phase difference between the reflected wave and the incident wave at the reflecting surface. The authors of [107]

considered a single unit cell of the HIS structure with Periodic Boundary Conditions (PBC) on four sides to model an infinite structure. The model setup is shown in Figure 2-8. Other then PBCs it can be seen that the perfectly matched layers (PML) are positioned above the HIS to absorb the reflected energy. The total field/scattered field formulation was used to incorporate the plane wave excitation into the computational domain. An observation plane was located on the scattered field region to record the reflected field from the HIS surface.
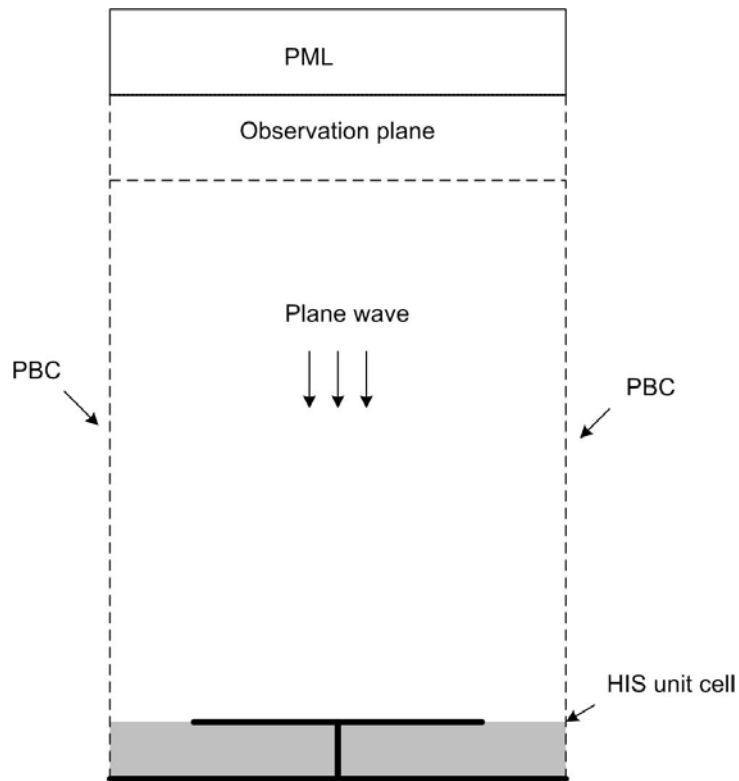
Figure 2-8 A unit cell setup for reflection phase characterisation

Because of the different locations of the observation plane and reflecting HIS surface an ideal PEC surface located at the same height as the HIS top surface was used as a reference. The scattered field from a PEC surface were also calculated. Then the reflection phase from the HIS structure is normalised to the reflected phase from the PEC surface using:

$$\phi = \phi_{HIS} - \phi_{PEC} + \pi \qquad (2.5)$$

Where,

ϕ : Reflection coefficient phase at the surface of HIS

ϕ_{HIS} : Reflection coefficient phase of HIS at the observation plane

ϕ_{PEC} : Reflection coefficient phase of PEC at the observation plane

The propagation phase added due to the distance between the reflecting surface and observation plane is thus cancelled out. A factor of π is added to the phase result to account for the surface reflection phase of PEC surface which is known to have a reflection coefficient phase of π radians.

The simulation software CST MWS (discussed in Section 2.8) can be used to model this setup for reflection phase characterisation. However the waveguide port with Perfect Electric and Perfect Magnetic boundary conditions on the opposite side walls of unit cell can also be used to simulate plane wave incidence. This model setup is shown in Figure 2-9.
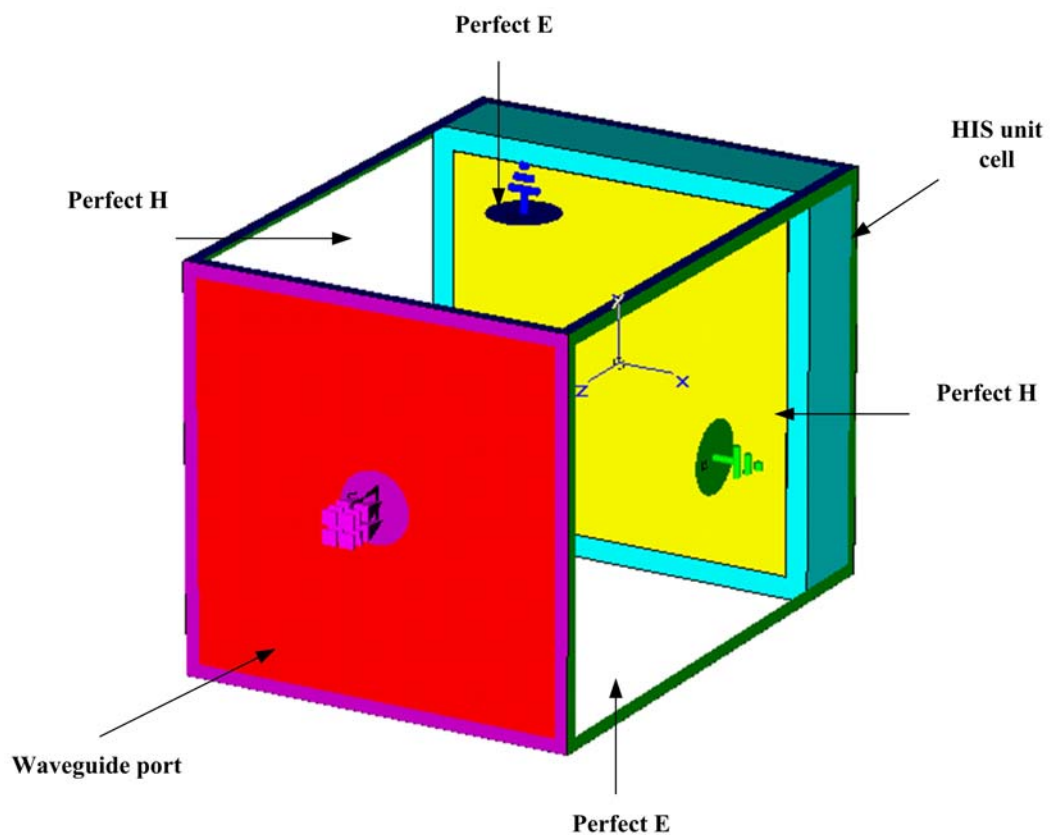
Figure 2-9 A unit cell model setup in CST MWS for reflection phase characterisation

The waveguide port and Perfect **E** and Perfect **H** boundary conditions are used to simulate normal incident plane wave. To find the reflection coefficient phase at the HIS surface the waveguide port must be de-embedded up to the reflecting surface. The evaluated reflection coefficient phase of a typical HIS operating as AMC structure is shown in Figure 2-10.
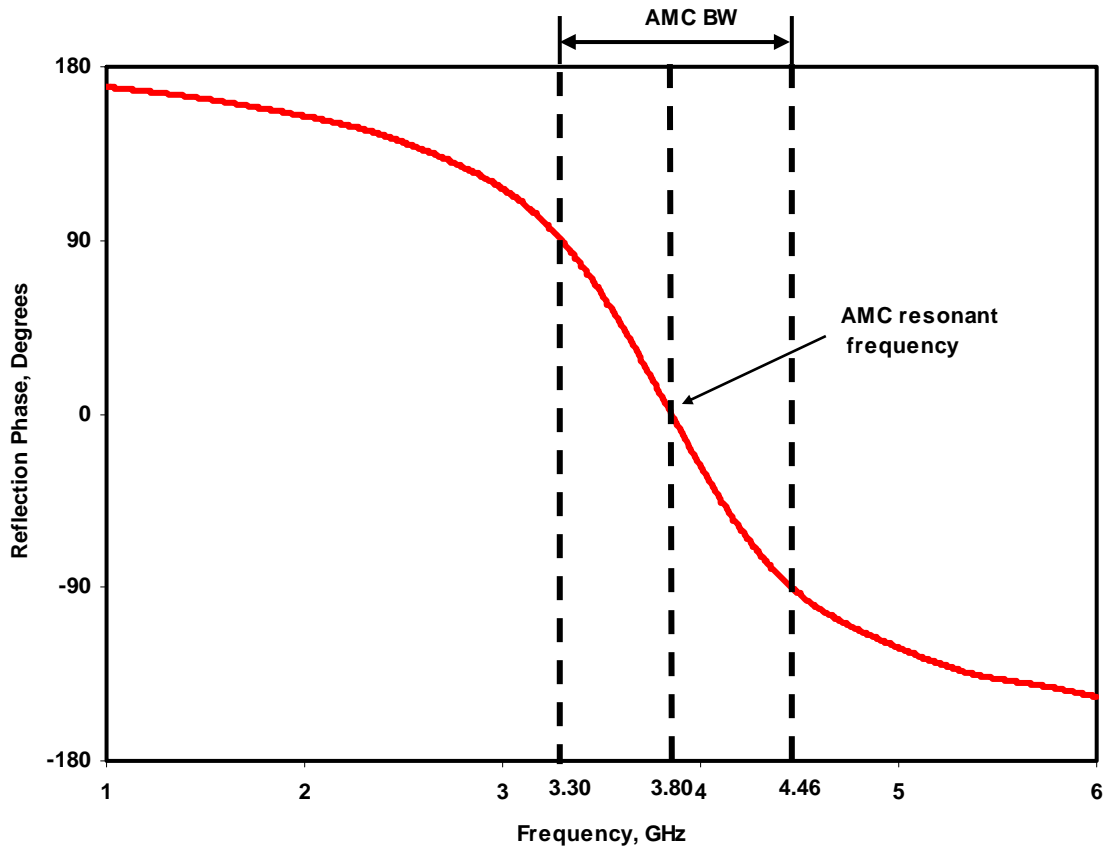
Figure 2-10 Reflection phase of a typical HIS for normal plane wave incidence

As can be seen from Figure 2-10 the reflection coefficient phase of AMC surface varies with frequency from +180° to -180°. At low and high frequencies the HIS surface exhibits a phase similar to a PEC, that is 180º. For this design the reflection coefficient phase crosses zero degrees at 3.8GHz which is the AMC resonant frequency. Previously the useful bandwidth of an AMC surface has been defined as the range ±90°. The usefulness criteria is that within this bandwidth the reflected wave is more in phase than out of phase with the incident wave (constructive for radiating elements in the interface). Outside this frequency range the reflected waves are mostly out of phase with the incident waves and from the known literature survey it has no useful applications for antenna and microwave devices.

2.5.2 Surface Wave Suppression Characterisation using a Suspended Transmission Line Method

The degree to which an HIS structure suppresses the propagation of surface waves can be measured by several techniques. For the types of finite size HIS structures which are discussed in this thesis a useful method is that proposed in [108] which is known as the suspended transmission line method. In this method an insulated microstrip transmission line is placed over the HIS structure to be characterised. Model geometry is shown in Figure 2-11. In this technique the microstrip is used to excite the travelling wave in the HIS and by its attenuation across a bandwidth, infer by S_{21} the ability of the structure to suppress surface waves. Typically the two ports of the microstrip line would be connected to a Vector Network Analyser. Note that when in use as an antenna ground plane the microstrip would be absent and a radiating element would be added.
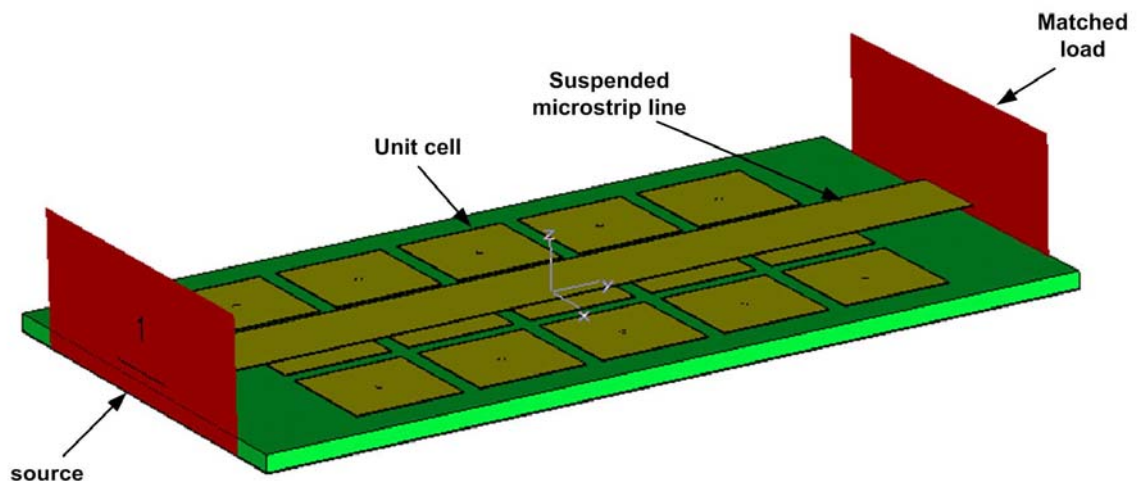
Figure 2-11 Suspended Microstrip line model setup for surface wave suppression characterisation

The simulated scattering parameters for a typical HIS operating as EBG are shown in Figure 2-12. If $S_{12} < $ -20dB is set as surface wave suppression criteria it can be seen that this HIS is able to effectively suppress surface waves in the 2.4GHz-2.8GHz frequency band (EBG band). Outside this operating band it work as a normal PEC allowing surface waves to pass through it normally. Therefore if an antenna is designed which operates in this EBG band, surface waves are suppressed resulting in improvement of radiation pattern

shape and radiation efficiency. The authors of [107] equate illumination by a TM polarised incident plane wave to excitation by the insulated microstrip. This technique therefore allows for the measurement of surface wave bandgap without the use of plane wave chamber setup.
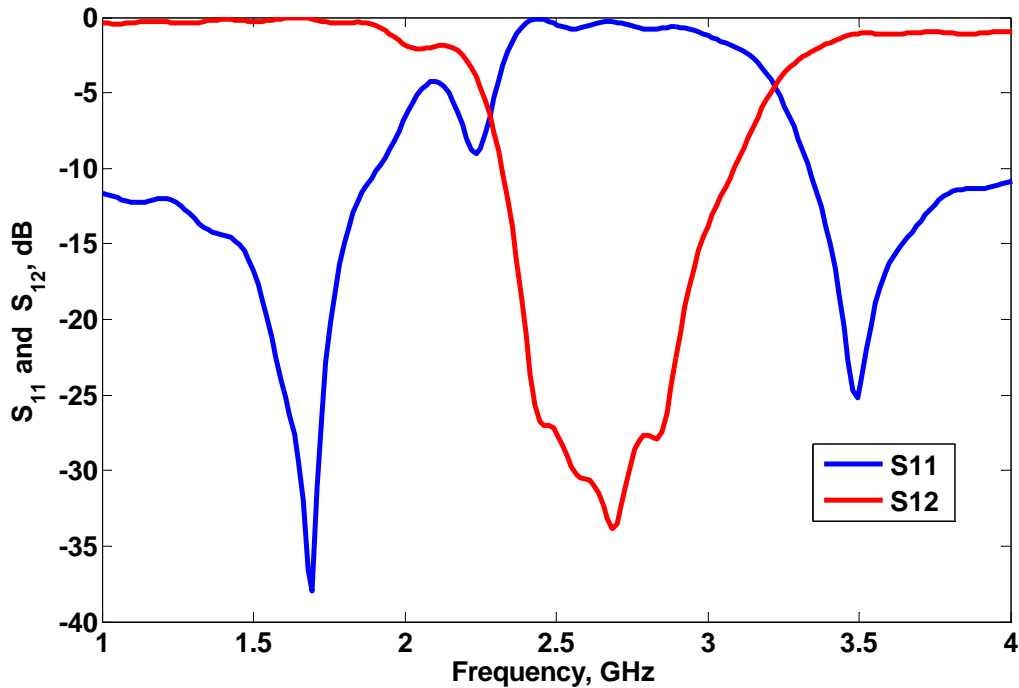
Figure 2-12 Simulated Scattering parameters for a typical HIS showing bandgap behaviour

2.6 Effects of Obliquely Incident Plane Waves on the Reflection Coefficient Phase of HIS Structures

The measurement technique described in section 2.5 proposes illumination by a normally incident wave for AMC characterization. Typical HIS structure use equi-spaced square conducting elements as part of their unit cells. This HIS is therefore symmetric in the plane of incidence as shown in Figure 2-6. Thus the reflection coefficient phase is independent of the polarisation direction for the normally incident plane wave and remain stable for both TE and TM polarisations. However, it is observed that when a plane waves obliquely illuminates the HIS surface, the phase of the reflected wave depends on the incidence angle and polarisation [109]. To verify this the reflection phase of a typical mushroom type HIS shown in Figure 2-6 was computed for oblique incidence considering both TE and TM polarisation cases.

The dimensions of the analysed HIS structure were:

$$W = 0.10\lambda, \quad g = 0.02\lambda, \quad h = 0.04\lambda, \quad \varepsilon_r = 2.94, \quad r = 0.005\lambda \qquad (2.6)$$

To model the oblique incidence in CST MWS a unit cell template in Frequency domain solver was used. Cell boundaries along *x* and *y* directions model an infinite periodic structure. For TE plane wave illumination, the electric field was set along the *y* axis and the plane wave was incident on the *xz* plane. The incident angle is defined as the angle between the propagation vector and the *z*-axis and would vary from 0º to 90º. Figure 2-13 shows the reflection coefficient phase results for 0º, 20º and 40º angle of incidence. As the angle increased, the resonant frequency (0 degree reflection coefficient phase), also increased from 6.44GHz for normal incidence to 6.57GHz at 20º and 6.88GHz at 40º incidence. It is important to observe that the slope near the resonant frequency also became steeper when the incidence angle increased. This resulted in decreased AMC bandwidth.
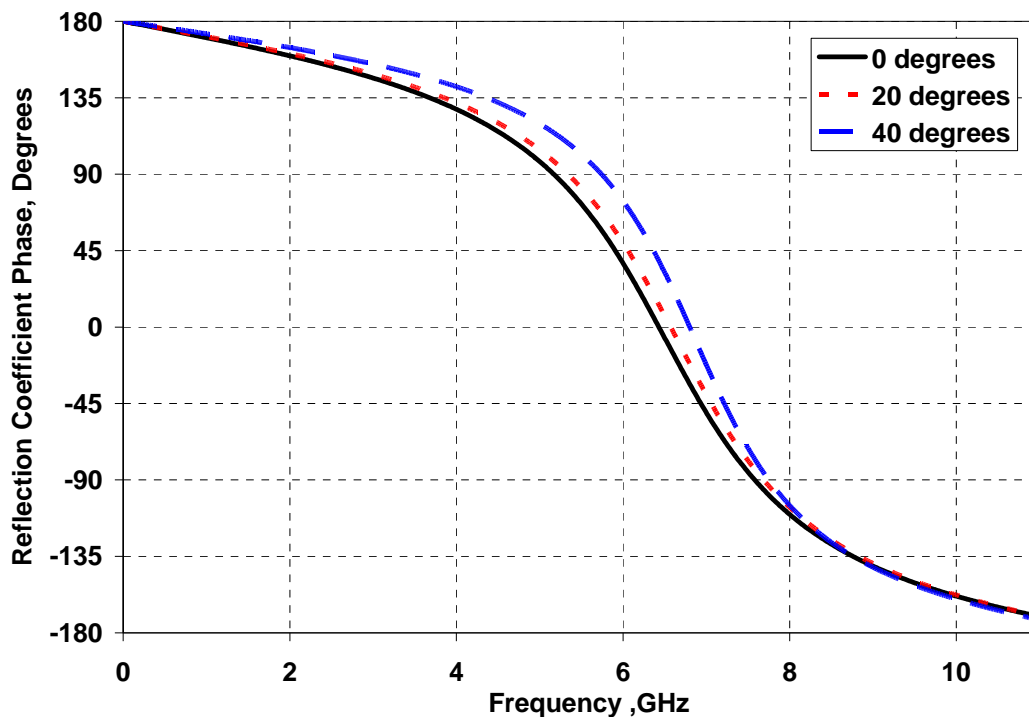
Figure 2-13 Simulated Reflection Coefficient phase of a mushroom HIS structure for the TE incidence at different incident angles of plane wave illumination.

For the TM incident case, the electric field was again set along the *y* direction however the plane wave was incident on the *yz* plane. Figure 2-14 shows the simulated results for 0, 20 and 40 degrees of incidence. The reflection phase response was significantly different for oblique incidence due to dual band reflection phase behaviour. As the incident angle of the

TM wave changed from normal, one resonance appeared at a frequency lower than the original frequency and other at the higher. With the increase in the incident angle, the lower resonant frequency decreased from 5.54GHz at 20º to 5.5GHz at 40º whereas the upper resonant frequency increased from 6.77GHz at 20º to 7.38GHz at 40º. It was observed that the separation between the two resonant frequencies increased as the incident angle increased.
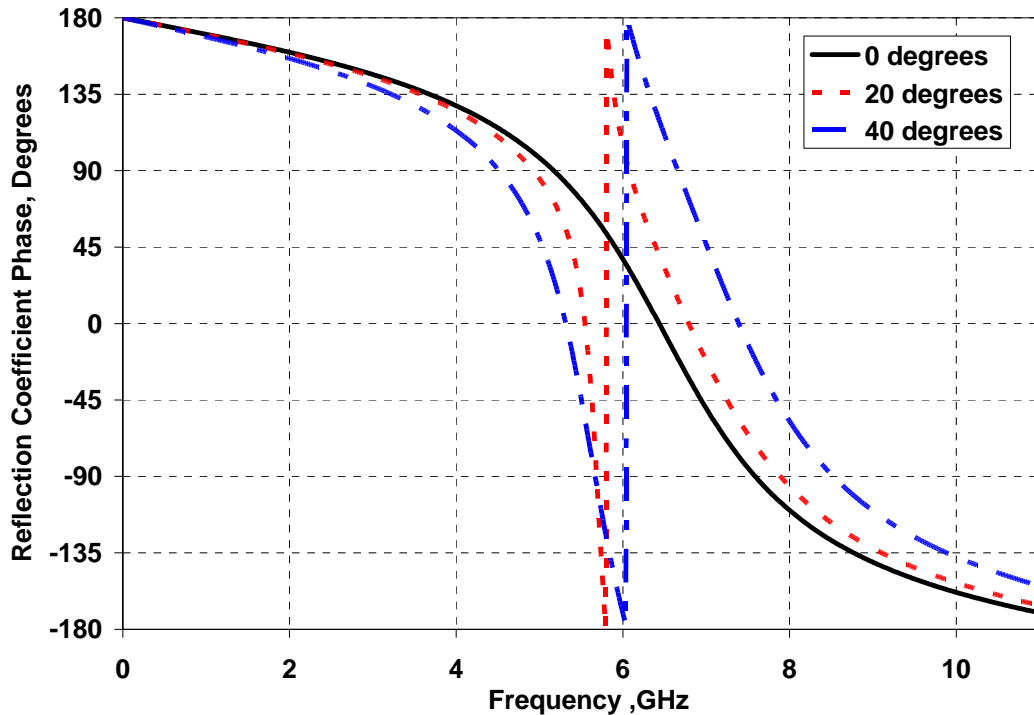
Figure 2-14 Simulated reflection coefficient phase of a mushroom HIS structure for the TM incidence at different incident angles of plane wave illumination.

One possible explanation for different TE and TM oblique incidence results is the existence of vertical vias connecting the HIS patches to the ground plane. For the TE incidence case, the electric field is oriented perpendicular to the vias. Thus centre via has no effect on the TE incidence fields and the reflection phase is determined only by the induced current on the HIS patch.

For the obliquely incident TM waves, the electric field has a component parallel to the vias. Thus the boundary condition is enforced on the vias, and an electric current is induced on the vertical vias as well. The magnitude of current changes with incidence angle. Therefore in this case reflection phase is determined both by the induced current on

the patch and induced current on the vias. As a result there are two AMC resonances in the reflection coefficient phase as shown in Figure 2-14.

This variation of resonant frequency with incidence angle and polarisation limits the useful operating bandwidth operation of HIS in many applications [75, 110]. Normally, if the input match bandwidth of low profile antenna placed near a typical HIS is within the resonance bandwidth of HIS, a significant improvement in the radiation performance is observed as compared to the conventional design using PEC ground plane [111, 112]. However this improvement is within a limited operating bandwidth. One explanation for this behaviour is that the HIS does not exhibit uniform surface impedance with respect to the different spatial harmonics radiated by an antenna. For instance, it is known that a small horizontal antenna radiates a large angular spectrum of TE and TM polarized plane waves [93]. And due to change in the resonant behaviour of HIS for different spatial harmonics, the total interaction between antenna and HIS is a combination of constructive and destructive interference.

In order to reduce this effect angularly stable HIS structures have been proposed. These will be briefly discussed in the next section along with novel non uniform HIS proposed in this research.

2.7 Angularly Stable HIS for Enhanced Performance

As discussed in the previous section there is a need for developing HIS structures which exhibit stable resonant behaviour with the change in incidence angle. Some work has been done in designing angularly stable HIS [93, 104, 110, 113]. In these designs the unit cell element shape is optimised for angular stability. Subsequently the optimised unit cell is then repeated periodically to create a uniform periodic HIS.

It is proposed that by varying the uniformity of periodic structures, angular stability can be achieved. These new structures have been termed as non uniform or tapered HIS structures. They can be employed in wearable antennas to design low profile antennas and to improve the input match bandwidth, radiation efficiency and gain.

2.7.1 Non Uniform HIS Structure Concept

The starting point of developing non uniform HIS for wearable antenna design is the one dimensional planar conductive strips array. One of the aims in this research study is to design wearable antennas which will occupy a small space on the human body. By using HIS designs based on one dimensional periodic structure the space occupied by the whole structure can be reduced. This design criteria reduces the bending affect on the antenna performance [70]. The circuit representation of an infinite parallel conducting strip was developed in [114]. The development of the strip array formulation for TE incidence is shown in Figure 2-15. The metal strips are infinitely thin with width '*w*' and period '*p*'. The plane wave is incident onto the strips at an angle '*θ*'. The equivalent circuit representation for this HIS is given in Figure 2-16.
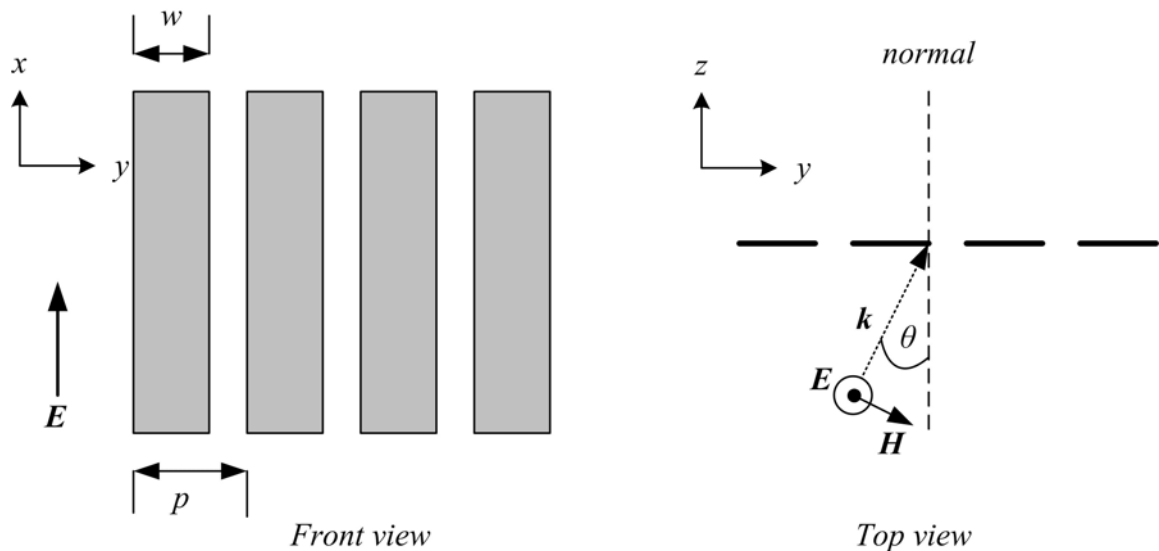
Figure 2-15 A 1-D array of HIS unit cells with parameters for TE incidence
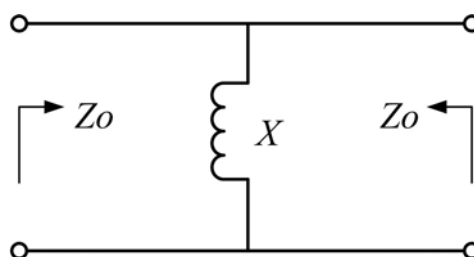
Figure 2-16 Equivalent circuit model for TE incidence

The equivalent circuit inductive reactance [114] normalised to free space characteristic impedance Z_o is given by :

$$\frac{X(w)}{Z_o} = F(p,w,\lambda) = \frac{p\cos\theta}{\lambda}\left\{\ln\left[\frac{1}{\sin\left(\frac{\pi w}{2p}\right)}\right] + G(p,w,\lambda,\theta)\right\} \tag{2.7}$$

Where λ the free space wavelength and G is a correction term for large angles of excitation of wave incidence and is given by:

$$G(p,w,\lambda,\theta) = \tfrac{1}{2}\frac{(1-\beta^2)^2\left\{\left(1-\frac{\beta^2}{4}\right)(A_+ + A_-) + 4\beta^2 A_+ A_-\right\}}{\left(1-\frac{\beta^2}{4}\right) + \beta^2\left(1+\frac{\beta^2}{2}-\frac{\beta^2}{8}\right)(A_+ + A_-) + 2\beta^6 A_+ A_-} \tag{2.8}$$

Where

$$A_\pm = \frac{1}{\sqrt{\left(\frac{p\sin\theta}{\lambda}\right)^2 - \left(\frac{p}{\lambda}\right)^2}} - 1 \tag{2.9}$$

$$\beta = \sin\frac{\pi w}{2p} \tag{2.10}$$

Similarly, the TM incidence case and corresponding equivalent circuit representation are shown in Figure 2-17 and Figure 2-18. In this case the magnetic field vector *H* is parallel to the strips and wave is incident at an angle θ. The strips have a period '*p*' and a gap spacing '*g*'.

The capacitive susceptance is given by :

$$\frac{B(g)}{Z_o} = 4F(p,g,\lambda) \tag{2.11}$$
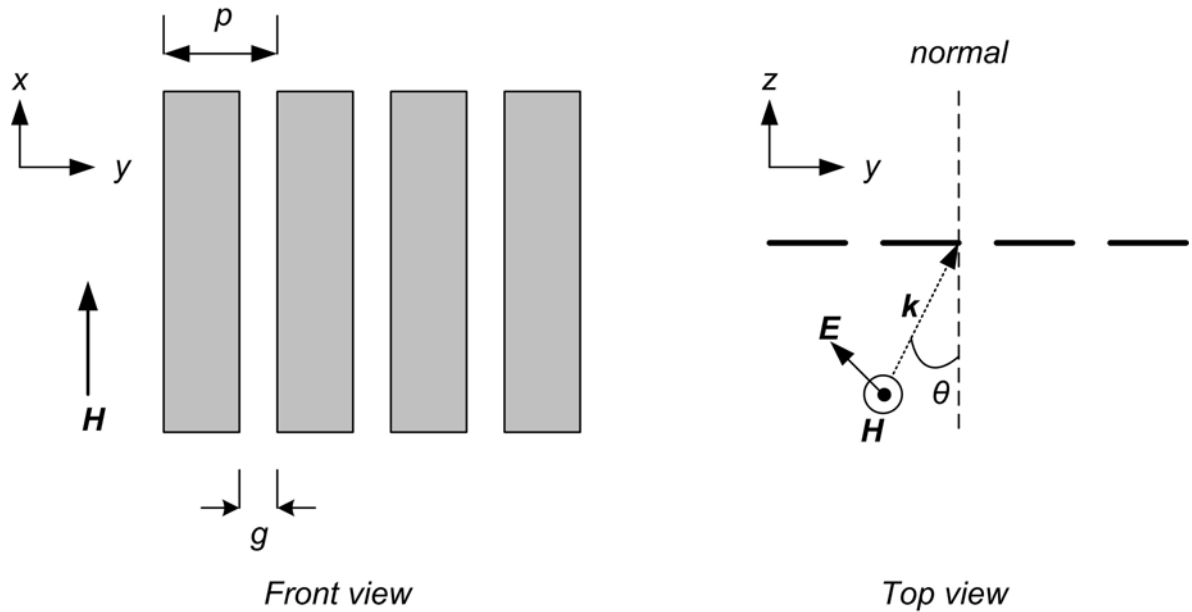
Figure 2-17 A 1-D array of HIS unit cells with parameters for TM incidence
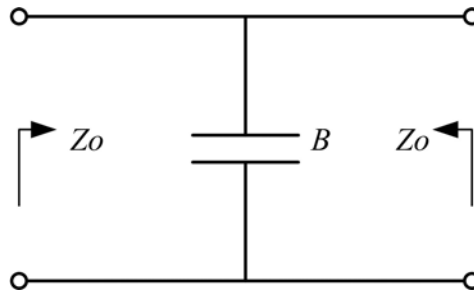
Figure 2-18 Equivalent circuit model for TM incidence

The equations presented above are valid for wavelengths and angles of incidence 'θ' in the range $p(1+\sin\theta)/\lambda < 1$. They are also only valid for plane wave incident in either **E** plane or **H** plane and hence they cannot be used to model the cross polarisation effects. This model given for infinite length strips can be adapted for the finite lengths of the strips. The equivalent reactance for the finite length strips is given by:

$$\frac{X}{Z_0} = \omega L = \frac{d}{p} F(p, w, \lambda) \tag{2.12}$$

And the susceptance is given by :

$$\frac{B}{Z_0} = \omega C = \frac{d}{p} 4F(p, g, \lambda) \tag{2.13}$$

The reactance and susceptance are each reduced by a factor d/p from the corresponding array of infinite strips to account for the finite length of the strips. From Equation (2.7) it is clear that when w and λ are fixed, X can be kept stable by appropriate increase of p against increase of θ. In other words, by gradually increasing p from centre towards outwards greater angular stability of AMC resonant frequency can be achieved.

It is important to point out that these equivalent circuits do not take into account the effect of dielectric substrates [114]. However the effects of PEC backed dielectric layers can be accounted for by considering them as short circuited transmission line connected to the equivalent circuit of the planar strip based HIS.

Another explanation for this angular stability is that as the incidence angle increases for plane wave incidence on HIS, the resonant frequency increases as shown in Figure 2-13, so in order to compensate for this increase in resonant frequency, the terminating unit cells of the HIS structure can be modified to reduce the deteriorating effect on bandwidth. For example when the terminating unit cells of a non-uniform HIS are increased in width the increase in resonant frequency can be compensated.

The comparison between the performance of uniform and non uniform HIS will be carried out in detail in Chapter 4.

2.8 Simulation Technique

In this research, simulation software played an important part in the design and evaluation of wearable antennas and HIS structures. For this purpose we used Microwave Studio® which is a product of Computer Simulation Technology (CST).

CST MICROWAVE STUDIO® is a fully featured 3D software package for electromagnetic analysis and design in the high frequency range. It simplifies the process of inputting the structure by providing a powerful solid modelling front end which is based on the ACIS modelling kernel. It is specially suited to the fast, efficient analysis and design of components like antennae (including arrays), filters, transmission lines, couplers, connectors (single and multiple pin), printed circuit boards and resonators.

The numerical method working behind this program is Finite Integration Technique (FIT). This numerical method provides a universal spatial discretisation scheme, applicable to various electromagnetic problems, ranging from static field calculations to high frequency applications in time or frequency domain. In the following section the main aspects of this procedure will be briefly explained.

2.8.1 Finite Integration Technique (FIT)

Finite Integration Technique was first proposed by Weiland in 1977 [140]. Unlike most numerical methods, FIT discretises the following integral form of Maxwell's equations, rather than the differential one :

Faraday' Law:

$$\oiint_{\partial A} \vec{E}.d\vec{S} = -\int_{\partial t} \frac{\partial \vec{B}}{\partial t}.d\vec{A}$$

Ampere's Law:

$$\oiint_{\partial A} \vec{H}.d\vec{S} = \int_A (\frac{\partial \vec{D}}{\partial t} + \vec{J}).d\vec{A}$$

Gauss's Law for electric field:

$$\oiint_{\partial V} \vec{D}.d\vec{A} = \int_V \rho.dV$$

Gauss's Law for magnetic filed:

$$\oiint_{\partial V} \vec{B}.d\vec{A} = 0$$

Where

E = electric field vector (V/m); B = magnetic flux density vector (Wb/m^2);

H = magnetic field vector (A/m); D = electric flux density vector (C/m^2);

J = displacement current density (A/m^2); ρ= volume charge density (C/m^2).

In order to solve these equations numerically a finite calculation domain is defined, enclosing the considered application problem. By creating a suitable mesh system, this domain is split up into several small cuboids, so called grid cells. There are two meshes which are orthogonal to each other. The spatial discretisation of Maxwell's equation is finally performed on this two orthogonal grid systems to obtain the complete discretised set of so called Maxwell's Grid Equations:

$$Ce = -\frac{d}{dt}b, \qquad\qquad \tilde{C}h = \frac{d}{dt}d + j$$

$$\tilde{S}d = q, \qquad\qquad Sb = 0.$$

Compared to the continuous form of Maxwell's equations, the similarity between both descriptions is obvious. Now all matrix equations are available to solve electromagnetic field problems on the discrete grid space. The process is repeated for all grid cells within the boundary until the desired accuracy is reached. The FIT formulation is a very general method and therefore can be applied to wide frequency ranges, as well as diversiform structures (from common topology to complex geometries). Compared to other numerical techniques, the major advantage of the FI-method is that the computational complexity increases linearly with problem size, while other method, like Method of Moment (MoM), forms a dense matrix increasing exponentially with problem size. Wideband results, useful for most wireless systems, can be obtained within only one simulation with FIT. Compare to the Finite Difference Time Domain (FDTD) method, which only operates time domain calculation, FIT is able to support a frequency domain solver and an Eigenmode solver which are based on Maxwell's equations in the harmonic case.

There are also a few weaknesses of the FIT method. First, the entire computational domain needs to be meshed, and the mesh grids must be small enough to assure the calculation accuracy. These will result in a large computational load for some situations. Second, it is very difficult to generate proper mesh properties for very long or very thin structures. Finally, for some curved structure or at the edge of the structure, the grid needs to be stair-cased, this will cause unstable or inaccurate results for some sensitive device.

A key feature of CST MWS is the approach of using the simulator or mesh type that is best suited to a particular problem. The software contains three different simulation techniques (transient solver, frequency domain solver, eigenmode solver) to best fit their particular applications. The most flexible tool, transient solver, which is a time domain simulator, is also the mainly used solver in this research. It can obtain the entire broadband frequency behaviour of the simulated device from only one calculation run. It is remarkably efficient for the most kinds of high frequency applications.

The transient simulator permits a broadband calculation of S-parameters from one single calculation run by applying the Finite Integration Technique (FIT) method to time signals. The calculation of the transient solver operates with time pulses, it can be easily transformed into the frequency domain by making use of a Fast Fourier Transformation (FFT). The S-parameters can then be derived from the resulting frequency domain spectra. This shows an obvious advantage of calculation in the time domain. CST Microwave Studio automatically calculates the appropriate excitation time pulse from the frequency range setting. The default Gaussian shaped pulse guarantees a smooth spectrum in the frequency domain, which allows a reliable calculation of the S-parameters.

To overcome the meshing weaknesses of the FIT, CST developed a few special meshing methods to enhance the calculating accuracy. They are the Perfect Boundary Approximation method (PBA), Thin Sheet Techniques (TST) and Multilevel Subgridding Scheme (MSS). These methods allow a better approximation of curved surfaces and finer field discretization within the mesh cells. It has been found that the computational time can be much reduced by this method without affecting the entire accuracy.

2.9 Conclusions

In this chapter the effects of several electromagnetic structures on the performance of horizontal low profile antenna have been discussed. The out of phase reflection from conventional PEC ground plane significantly degrades the performance of antenna and is therefore a limitation in the design of low profile antenna design. The newly introduced HIS structures has made it possible to circumvent this problem. The unique electromagnetic properties of in phase reflection and surface wave suppression allow antenna designer to make low profile antennas with superior performance as compared to conventional PEC ground planes. The operation mechanism of mushroom like HIS is than explained in detail. The lumped LC model has been used to derive useful parameters of HIS structure. Then the variation of resonant frequency of conventional HIS with the change in the incident angle and polarisation is discussed. Than the solution to this problem is proposed using non uniform or tapered HIS structure . The equivalent circuit model of parallel conducting strips has been used to explain the working principal of

angularly stable HIS. The simulation software used in this research is then briefly introduced. The numerical technique (FIT) working behind this program is then explained.

3 THE ELECTROMAGNETIC CHARACTERISATION OF MATERIALS SUITABLE FOR WEARABLE ANTENNAS

3.1 Introduction

In this chapter different techniques available for electromagnetically characterising materials will be discussed along with their advantages and disadvantages. The resonant method will be explained in detail which is the working principle of split post dielectric resonator (SPDR) used in this research. The experimental setup for measuring materials will then be explained along with important steps taken during measurement. The measured properties of different non conducting samples are given and discussed. The electro textiles tested in this research work are also discussed qualitatively. In the end the performance of a prototype wearable antenna using felt as a substrate and electro textile as conducting element is given. The best performance electro textile was selected using the result for antenna's input match bandwidth and resonant frequency.

A first step in the design of a textile antenna consists of choosing appropriate non conducting material for substrate and conducting material for radiating element and ground plane. As mentioned in Section 1.2.1 of Chapter 1 an ideal wearable antenna should be drapable. Therefore in this chapter the process used to design and fabricate a drapable textile antenna will be outlined. Conducting as well as non conducting textile materials are required which are comfortable enough to be worn close to the body that also have electromagnetic properties suitable for optimal antenna design. Characterising materials before using them in antenna design is the first step of this research. Some work in the past has been done to integrate electronic devices into clothing [1, 115]. The purpose of clothing in these applications was to act as a support for wires carrying information from one point to another. Its role was passive and more of mechanical type rather than electrical. Salonen [40] proposed the use of textile materials both natural and man made in

the design of a Global Positioning System (GPS) wearable antenna. This antenna operated at 1.575GHz and was circular polarized.

Although there are many factors that will influence from what materials a garment can be made, in this thesis consideration will be restricted to drapability, conductivity and electrical properties. Further, magnetic materials are difficult to obtain, they are therefore ignored and it is assumed that all of the materials considered are non-magnetic.

Classical Maxwellian theory [83] tells us that the performance of an antenna is dictated by its electrical size. This in turn is fixed by the permittivity [55] of the components of the antenna. In chapter 4 an antenna was defined as being planar with a ground plane and radiating elements, supported by a dielectric substrate. Associated with the dielectric substrate will be a permittivity and a loss [78]. Since the conducting parts used in most antenna design are metals, typically copper ($\sigma = 5.8 \times 10^7 S/m$), they are stiff and tend to be not suitable for wearable antenna application. However, recently nylon and polyester textiles coated with Copper, Nickel and Tin have been developed [34]. These conducting textiles are drapable and have low resistivity ($\leq 0.1\,\Omega$/sq) and known as "electro textiles". Previously wearable antennas have been successfully designed using electro textiles [19, 45]. This research study also employed electro textiles as conducting parts of wearable antennas.

In the next section discussion on the electromagnetic properties of the substrate materials used in wearable antenna design will be given.

3.2 The Properties of Dielectric Substrates Used in the Fabrication of Wearable Antennas

The performance of printed antennas depends a great deal on the substrate on which it is mounted [116]. The substrate not only provides mechanical support to the antenna but also affects the properties such as resonant frequency, bandwidth and most importantly radiation efficiency. In a printed antenna [117] the electromagnetic fields radiated exist within the dielectric substrate which forms a substantial proportion of the volume of the antenna. If the substrate is lossy the efficiency of antenna is decreased [118]. The thickness and permittivity of substrate has influence on the bandwidth of the antenna [119].

A suitable substrate therefore must satisfy both mechanical and electrical requirements of the design.

3.2.1 Permittivity

Permittivity is a property which is associated with how much electrical charge a material can store in a given volume. The units of permittivity are Farads/metre (F/m). The permittivity in vacuum (free space) is denoted as ε_0 its value is 8.854×10^{-12} F/m. Materials other than vacuum have permittivity higher than ε_0, often they are referred to by their relative permittivity, denoted by ε_r :

$$\varepsilon_r = \frac{\varepsilon}{\varepsilon_0} \qquad (3.1)$$

Where ε is the absolute permittivity of material. In microwaves, relative permittivity ε_r is often refer to as the "dielectric constant". Dielectric constant is a function of frequency and its important to characterise substrate material for the range of operating frequencies.

In non-TEM transmission lines such as those realised in Microstrip antennas, most of the electric fields are constrained within the substrate, but a fraction of the total field exists within the air above the substrate. The effective permittivity (effective dielectric constant) takes this into account.

Ideally dielectric materials with minimum losses are preferred to have maximum radiation efficiency of antenna. However there are always some losses associated with dielectrics. The permittivity of dielectric is in general complex and is given by :

$$\varepsilon = \varepsilon' - j\varepsilon'' \qquad (3.2)$$

Where ε' is the real part of the permittivity (dielectric constant) and ε'' is the imaginary part of the permittivity and is indicative of loss. To quantify losses of dielectric materials another term known as loss tangent is used which is explained in next section.

3.2.2 Loss Tangent

Loss tangent $\tan\delta$ (also known as dissipation factor) characterises the amount of power turned into heat in the material. It is given by the ratio of imaginary ε'' to the real part ε' of the permittivity:

$$\tan\delta = \frac{\varepsilon''}{\varepsilon'} \tag{3.3}$$

The higher the loss tangent values the more lossy the dielectric substrate. Higher losses mean reduced radiation efficiency. In this research material with low loss tangent values will be explored. For comparison Felt has a loss tangent of 0.016 whilst FR4 has a loss tangent of 0.028.

In the next section different techniques available to measure the above mentioned properties of different fabric samples will be discussed.

3.3 Dielectric Measurement Techniques

The measurement of complex dielectric properties of materials at radio frequency has gained increasing importance especially in research field, such as material science, microwave circuit design, absorber development and biological research. Dielectric measurement is important because it can provide the electrical characteristics of the materials, which proved useful in many research and development fields [120].

Several useful techniques have been developed to measure complex permittivity properties in time domain or frequency domain [121-124].

The 4 main techniques available for dielectric measurements are:

- Transmission/reflection line technique
- Open ended coaxial probe technique
- Free space technique
- Resonant technique

3.3.1 Transmission/Reflection Line Technique

This is a broadband measurement technique [125]. It involves placing a sample of the material to be measured into a length of waveguide or coaxial line. Two ports of a vector network analyser provide scattering data which can then be used to obtain the permittivity and loss tangent of the material under test.

This method requires sample preparation such as machining so that sample fit tightly into the waveguide line. As a result its accuracy is limited by air gap effects between sample and waveguide line. The techniques works well with ceramics but poorly with textiles.

3.3.2 Open Ended Coaxial Probe Technique

The open ended coaxial probe technique is a non destructive method [124] that involves a narrow ended probe being pressed against a specimen or immersed into the liquids. It uses the reflection coefficient. This technique is suitable for cases in which its not possible to obtain a separated sample of a material. With this technique the sample can be placed in close contact with the probe without causing any changes in the material characteristics.

Only reflection measurements are available and measurement accuracy is affected by air-gaps between and around the probe and the material to be measured.

3.3.3 Free Space Technique

This method utilises two antennas placed facing each other and a VNA. The sample under test is placed in between the two antennas such that the transmission path is through it. This method requires the sample to be large and flat. It is suitable for sample measurements in high temperature and hostile environments.

A limitation is the requirement of large and flat sample. Accuracy is affected by multiple reflections between antenna and surface and due to diffraction effects at sample edges.

3.3.4 Resonant Technique

The resonant technique offer the highest available accuracy for measurements of real permittivity and measurements of very low loss materials that can not be measured with other techniques. There are many types of resonant techniques available such as re-entrant cavities, Split post cylinder resonator, cavity resonators and Fabry-Perot resonators [122]. The dielectric properties can be determined by first measuring the resonant frequency and quality factor of empty cavity. A next step is to repeat the same measurement after filling the cavity with the sample under test. The permittivity and loss tangent values can than be computed using the resonant frequency, quality factor and thickness of sample.

This method requires good frequency resolution and hence a good VNA. It is limited to narrow band of frequencies. This is because the cavity sizes determined by the wavelength and the modes the cavity will support have distinct ranges of frequency.
For measurements in this research Split Post Dielectric Resonators (SPDR) was used which operates on this technique. In the next section the working principle of SPDR will be explained.

3.4 Split Post Dielectric Resonator Overview

3.4.1 Working Principle

The split post dielectric resonator (SPDR) measurement technique is one of the type of resonant method. The SPDR provides an accurate technique for measuring the complex permittivity of dielectric and ferrite substrates and thin films at a single frequency point in the frequency range of 1 to 20 GHz. A measurement at a discrete frequency point should be adequate, because lossless materials are nearly non dispersive. This means that their dielectric constant and loss tangent will stay constant over a small range of frequencies. This method is non destructive, as long as the sample can fit in the SPDR, because no special sample preparation is needed. The geometry of a typical SPDR is shown in Figure 3-1.
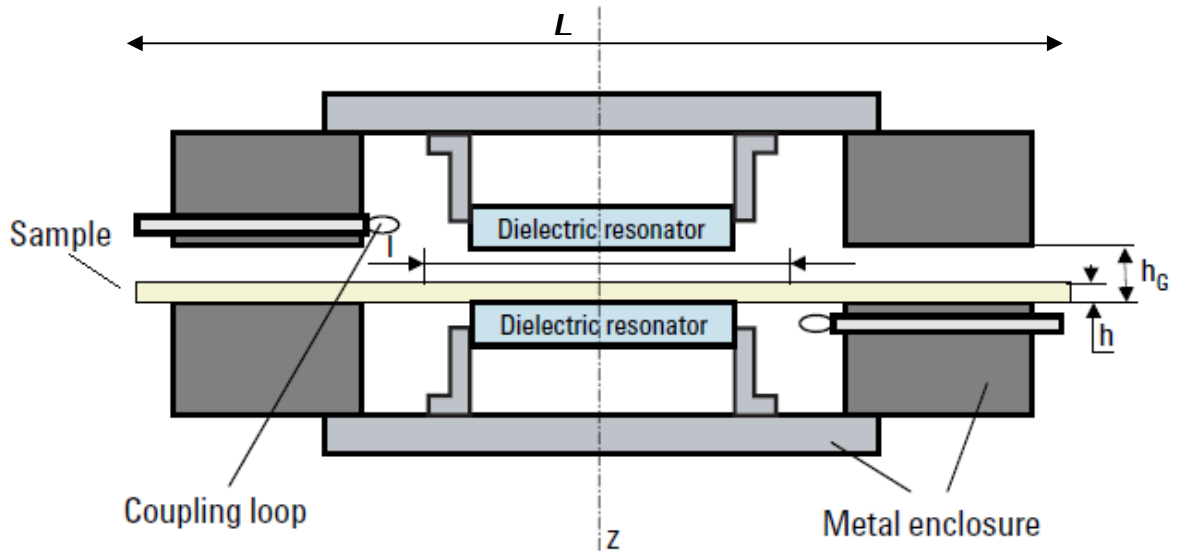
Figure 3-1 Cross sectional view of Split Post Dielectric Resonator fixture

The size of the resonator dictates that it operates in $TE_{01\delta}$ mode in which there is only an azimuthal electric field component so that the electric field is continuous on the dielectric interface. For low loss materials the influence of losses on the resonant frequencies is negligible [122]. Thus the real part of permittivity of the sample under test can be found on the basis of the resonant frequencies and physical dimensions from an iterative solution to the equation 3.4:

$$\varepsilon' = 1 + \frac{f_0 - f_s}{h f_o K_\varepsilon(\varepsilon'_r, h)} \tag{3.4}$$

Where

h - Thickness of the sample under test

f_o - the resonant frequency of the SPDR with an empty cavity

f_s – The resonant frequency of the SPDR with dielectric sample

K_ε – a coefficient function of ε'_r and h. By definition K_ε function values are found for a given SPDR and fixed ε'_r and h by:

$$K_\varepsilon(\varepsilon_r', h) = \frac{f_0 - f_s}{(\varepsilon_r' - 1)hf_0} \qquad \text{(3.5)}$$

Exact resonant frequencies and the values of K_ε are computed for a number of ε_r' and h for a given SPDR and tabulated. Interpolation is than used to compute K_ε for other values of ε_r' and h. The initial value of K_ε in permittivity evaluation (using Equation 3.4) is taken to be the same as its corresponding value for a given h and $\varepsilon_r'=1$. Subsequent values of K_ε are found for the subsequent dielectric constant values obtained in the iterative procedure. Because K_ε is a slowly varying function of ε_r' and h so the iterations using Equation 3.4 converge rapidly.

The dielectric loss tangent of the sample can be determined [121] using :

$$\tan\delta = \frac{\left(Q^{-1} - Q_{DR}^{-1} - Q_c^{-1}\right)}{P_{es}} \qquad \text{(3.6)}$$

Where:

Q - The unloaded Q-factor for the resonant SPDR containing dielectric sample

P_{es} - Electric energy filling factor of the sample defined as

$$P_{es} = h\varepsilon_r' K_1(\varepsilon_r', h) \qquad \text{(3.7)}$$

$Q_c -$ Q-factor depending on metal enclosure losses for the resonant SPDR with the sample defined as

$$Q_c = Q_{c0}K_2(\varepsilon_r', h)) \qquad \text{(3.8)}$$

$Q_{c0} -$ Q-factor depending on metal enclosures for empty SPDR

$Q_{DR} -$ Q-factor depending on dielectric losses for the resonant SPDR with the sample defined as :

$$Q_{DR} = Q_{DR0} \left(\frac{f_o}{f_s} \right) \left(\frac{P_{eDR0}}{P_{eDR}} \right) \tag{3.9}$$

P_{eDR}, P_{eDR0} - Electric energy filling factors of the SPDR with sample and without sample respectively

Q_{DR0} - Q-factor depending on dielectric losses in dielectric resonators for empty SPDR

The main sample requirements are two strictly parallel faces, the thickness of the sample h must be less than the fixture air gap h_G (see Figure 3-1), and the sample must have enough area to completely cover the gap between the resonant cavity located inside of the fixture. The air gap between the sample and the dielectric resonator (see Figure 3-1) does not affect the accuracy of the measurement. The sample may have a rectangular or round shape. For easy handling of the sample it is recommended that the sample area dimension L is bigger than the dimension of the minimum measurable area l (or active area of the fixture). The required thickness of the sample also depends on its permittivity [122]. Materials with high permittivity should have small thickness. The Figure 3-2 shows the typical resonant frequency f versus permittivity for the case of a 2.47GHz SPDR.
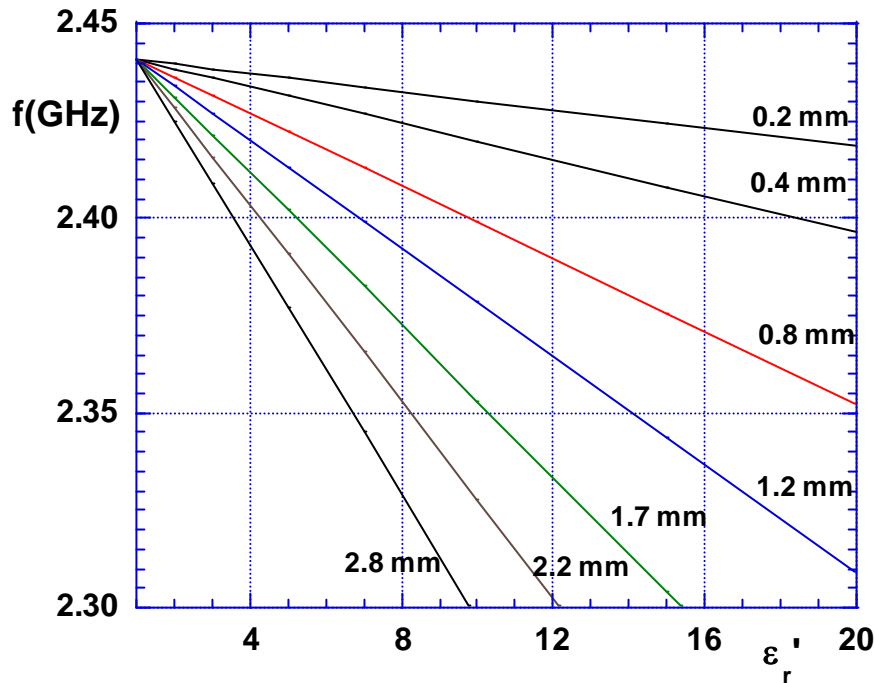
Figure 3-2 Resonant frequency f versus permittivity ε_r for 2.47GHz SPDR [126]

In the next section the experimental setup for dielectric material measurements using SPDR will be explained.

3.5 *Experimental Setup for Dielectric Measurement using SPDR*

The front and top views of 2.4GHz split post dielectric resonator (SPDR) are shown in Figure 3-3 and Figure 3-4 respectively. While Figure 3-5 shows felt sample inside the SPDR. The simplified schematic shown in Figure 3-1 illustrates the main parts of the SPDR. A pair of thin dielectric resonators and a metal enclosure of relatively small height are used in the construction of the SPDR fixture. This allows a strong evanescent electromagnetic field to occur in the air gap between the dielectric resonators and in the cavity region for radii greater than the radius of dielectric resonators. This simplifies numerical analysis.
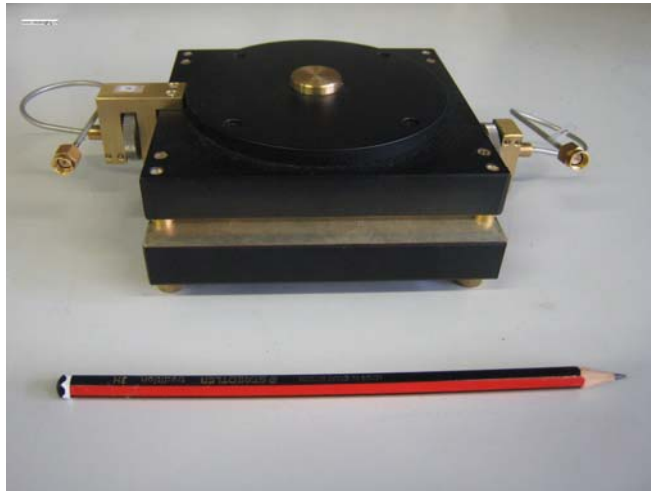
Figure 3-3 Front view of 2.4GHz Split Post Dielectric Resonator
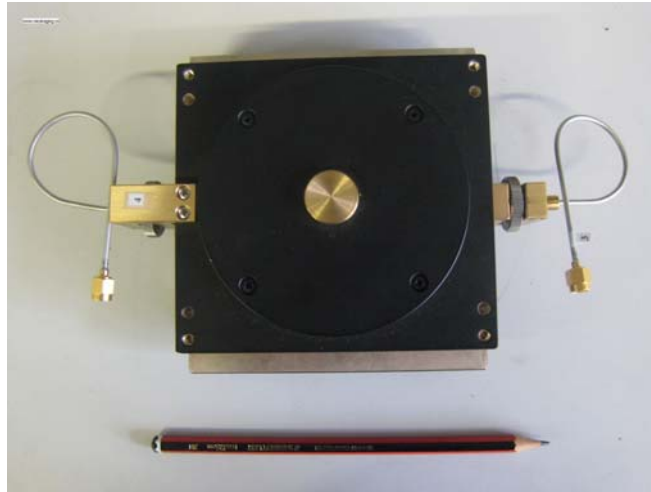
Figure 3-4 Top view of 2.4GHz Split Post Dielectric Resonator

Figure 3-5 2.4GHz Split Post Dielectric Resonator with Felt sample

The experimental setup to measure the samples is shown in Figure 3-6 and consists of the following components:

- Vector Network Analyzer
- 2.47GHz SPDR
- Software program to compute Dielectric Properties from scattering parameters
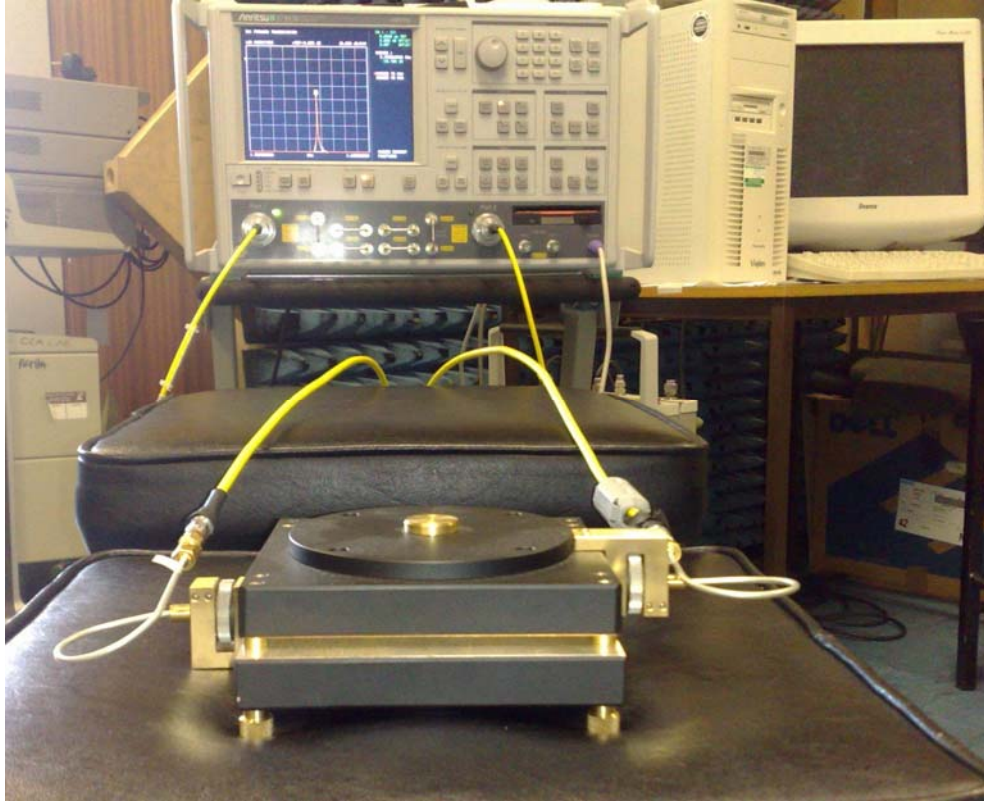
Figure 3-6 Experimental setup to measure permittivity and loss tangent values of samples

Before measuring any sample the VNA was first calibrated up to the cable connector plane using standard calibration procedure. This neutralised the affect of the connecting cables from the measured complex scattering parameters. After this the SPDR was connecting with the two ports of the VNA. After adjusting the scale on VNA the resonant frequency of the empty cavity was noted down. The 3dB bandwidth of the resonance curve was also noted down. The quality factor Q was than computed using:

$$Q = \frac{f_r}{f_{h_{3dB}} - f_{l_{3dB}}}$$

(3.10)

Where f_r is the resonant frequency and $f_{h_{3dB}}$ is the upper 3dB frequency and $f_{l_{3dB}}$ is the lower 3dB frequency. After this the sample was cut to the necessary dimensions and its thickness was also measured. The sample was then put inside the gap of the SPDR so that it completely covered the minimum coverable area as explained in the Section 3.4.1 and defined in Figure 3-1. The same steps were repeated but this time with sample. The

resonance frequency which was changed due to affect of sample and Q factors were computed from 3dB resonance curve.

The thickness of the sample and Q factor of empty cavity and filled cavity were then entered as input to the software program which than extracted the desired permittivity and loss tangent values of the tested samples.

In the next section measured values of different textile substrates will be discussed and selection of material for wearable antenna on the basis of these values will be carried out.

3.6 Measured Electromagnetic Properties of Fabrics

Five different samples for wearable antenna substrates were tested for their suitability. One reference material made of FR4 and polystyrene foam was also measured to check the accuracy of SPDR. The measured values of permittivity and loss tangent are given in Table 3-1.

As can be seen the measured values of reference samples are in good agreement with the published values. This certified the accuracy of equipment and measured electromagnetic properties. The permittivity values of most of the fabrics were less than 2 except neoprene which has a value of 5.2. The fleece fabric showed the minimum loss tangent among fabrics. This is due to the loose construction of this fabric resulting in a high concentration of air per unit volume.

Table 3-1 Measured Permittivity and loss tangent values of different samples

Material	Thickness, mm	Permittivity, ε	Loss tangent, $\tan\delta$
FR4	1.6	4.6	0.025
Polystyrene foam	2	1.02	0.00009
Felt	3	1.36	0.016
Fleece	2	1.2	0.004
Neoprene rubber	1.5	5.2	0.025
Silk	1.56	1.2	0.054
Cotton	0.44	1.54	0.058

3.7 Selection of Fabrics

After comparing the measured values of different samples it was decided to use felt as a substrate for wearable antenna design in this research. Other tested fabrics like fleece and silk showed good properties but their single layer thickness was too small to fabricate any antenna with reasonable bandwidth. The relation between thickness of the substrate and bandwidth is well known [119]: the thinner the substrate the narrower the bandwidth, the thicker the substrate the broader the bandwidth. Also some materials are too fragile for robust antenna design and sticking conducting material on them is a tedious task. The process of bonding electro textiles to the substrate is discussed in chapter 4. Neoprene was not selected because it is not too comfortable to be worn and not a common item for clothing. However, it may be useful for sports attire.

The felt material with is a soft and smooth surface is well suited for wearable application. It is a common textile used in daily clothing and is easily available from high street shops in different thicknesses ranging from 1.5mm to 12mm.

3.8 Leather as a Substrate

In order to increase selection of tested materials, leather was chosen as another drapable material to be used as potential substrate for wearable antenna design. Leather is a material with soft and smooth surface. It is available in different varieties with each type flexible to

varying degrees. It is a common material used in daily wearable items like coat, belt and hat. This mass applicability makes it a worthy idea to test its suitability for wearable antennas. In order to ensure good and reliable quality different leather samples were obtained from Andrew Muirhead & Son Ltd [127] a well known manufacturer of leather in United Kingdom. They obliged by sending 5 different types of leather samples shown in Figure 3-7.

Figure 3-7 Different samples of leather characterised by SPDR

The measured values of permittivity and loss tangent are given in Table 3-2.

Table 3-2 Measured values of Permittivity and loss tangent for leather samples

Leather Type	Thickness, mm	Permittivity, ε_r	Loss tangent, $\tan\delta$
Sateen Rockall	1.3	2.39	0.069
Red	1.4	2.25	0.058
Oxford Blue	1.5	2.32	0.071
Sateen Sunflower	1.5	2.21	0.054
Purple Polka	1.3	1.83	0.049

From measured values its clear that all leather samples have permittivity values in the range of 1.8 - 2.4 and their loss tangent values in the range of 0.049 – 0.071.

The permittivity values and loss tangent values are a bit higher as compared to Felt. The higher loss tangent values have a significant detrimental affect on radiation efficiency of antenna. Leather is also a non homogenous material, its properties vary across its surface. This will make it difficult to construct a consistent property antenna on leather of same type. Also leather naturally absorbs water. So if wearable antenna is radiating in open wet environment, the characteristics of leather antenna will change significantly. Due to these reasons leather was not preferred for wearable antenna design in this research.

3.9 Conducting Materials

All antennas need a conducting material either as a ground plane or as a radiating element. The current flowing on the conductor which is responsible for radiation depends on the electrical conductivity of the material. The electrical conductivity is the ability of material to allow unhindered flow of charges through it and is measured in Siemens per metre (S/m). Ideally perfect electric conductor (PEC) is preferred which has infinite conductivity. However in reality all materials have limited conductivity. For example commonly used copper has a conductivity of 5.8×10^7 S/m. In the next section characterization of conducting textile materials will be discussed.

3.9.1 Measurement of Electro textiles for High Frequency Applications

Conducting textile materials have been used in past in place of ordinary metals in many applications [34, 128]. Its potential use in wearable antenna design has been realised after number of researchers proposed antenna design using them [9, 36, 37, 58, 70].

The following are essential requirements for conducting fabrics in wearable antenna design:

- *High conductivity* -A low (less than 1 Ω/sq) and stable resistance to minimize losses
- *Homogeneity*- it should be homogenous with minimum variation of resistance
- *Drapability*- it should be flexible enough to be worn comfortably

- *Elasticity*- it should be elastic so that its properties doesn't change too much when it is bent or stretched

After doing research on conducting textiles it was decided to procure electro textile samples from Less EMF Inc [129]. Four different conducting textiles namely Flectron, Shieldit, Zelt and Pure Copper Polyester Taffeta shown in Figure 3-8 were obtained. All of them can be cut and sewn like ordinary fabric.
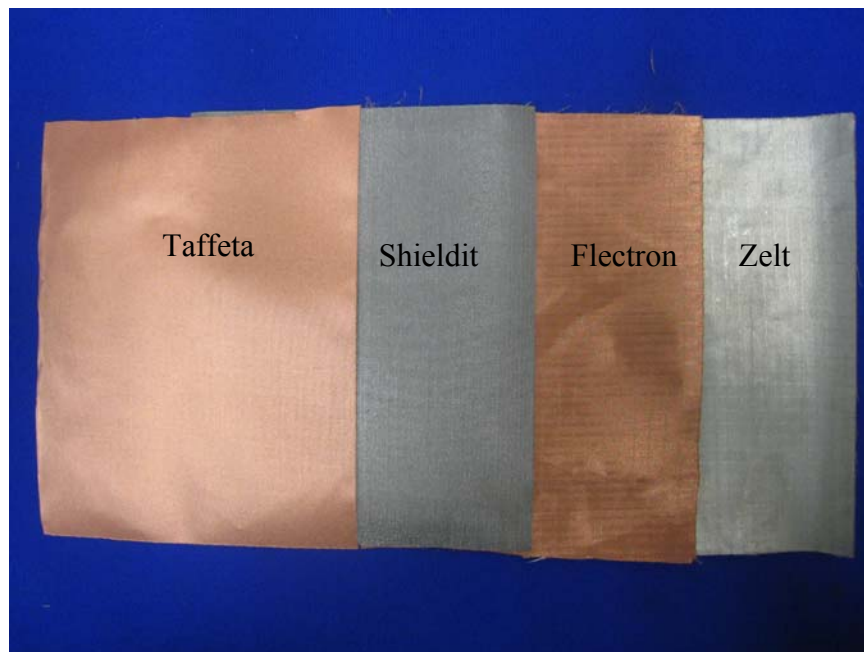
Figure 3-8 Samples of Taffeta, Shieldit, Flectron and Zelt electro textiles

Both Zelt and Flectron are nylon based fabrics with the former coated with Tin/Copper while the latter coated with copper only. Shieldit and Taffeta are polyester based fabrics with the former plated with Nickel and copper plus a hot melt adhesive on one side while the latter is coated with pure copper only.

These conducting textiles with different conducting properties need to be tested for their suitability to optimal antenna design. For this purpose a simple patch antenna resonating at 2.45GHz was designed and fabricated using these conducting fabrics. The patch was etched on electro textiles using a novel technique by modifying the traditional printed circuit board (PCB) etching method (Appendix A). An adhesive spray (commonly used for photo mount) was used to attach conductive fabric to the Felt substrate. The fabricated prototype antennas are shown in Figure 3-9 .To better understand affect of conductive

fabrics of different composition and electrical properties on antenna performance a reference antenna was also fabricated using ordinary copper metal. A measured and simulated reflection coefficient (S_{11}) comparison of different fabric antennas is shown in Figure 3-10.
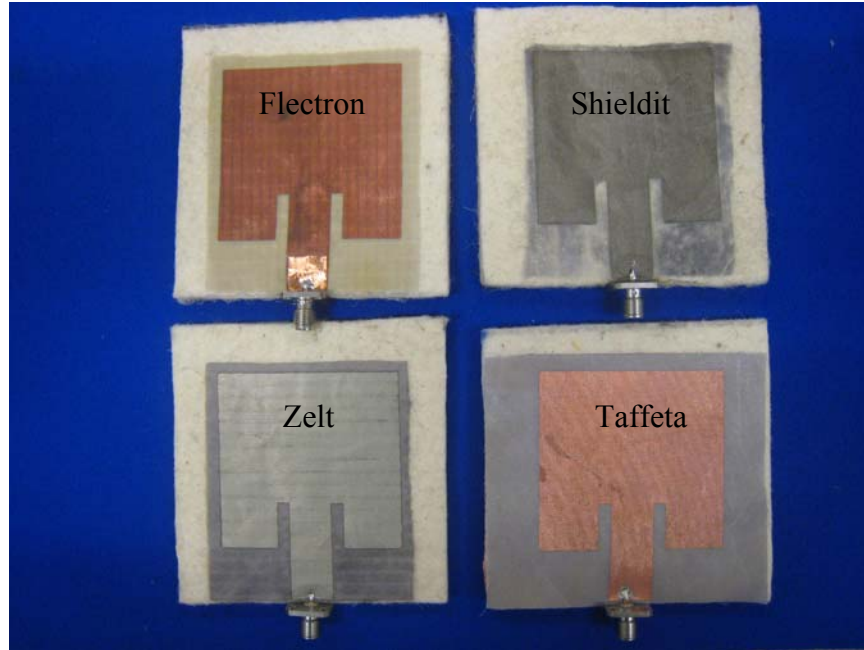
Figure 3-9 Fabricated prototype wearable patch antennas using different electro textiles
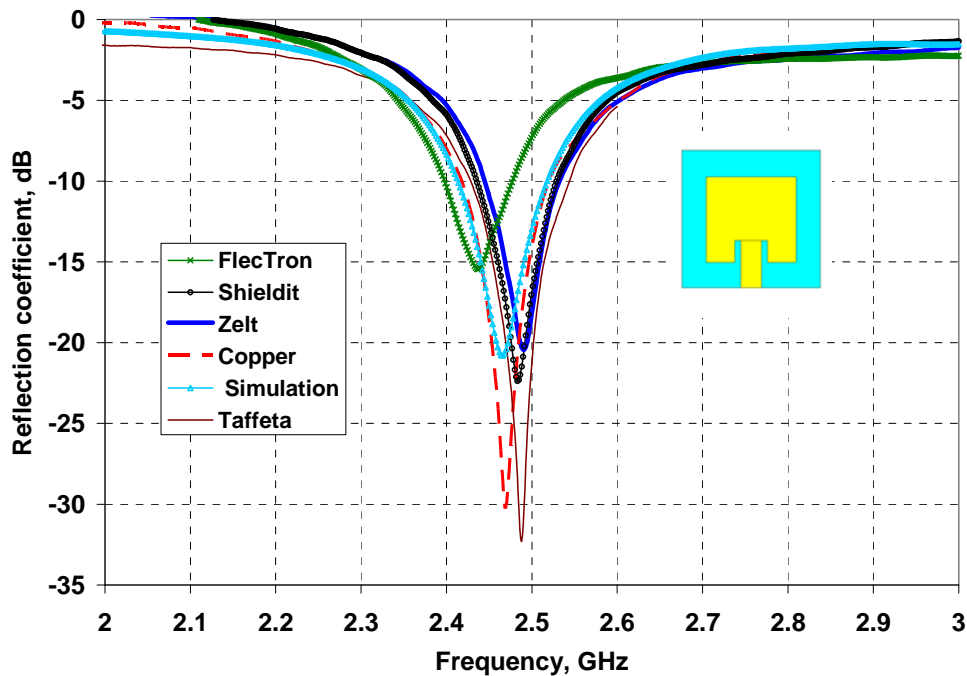
Figure 3-10 Measured Reflection coefficient (S_{11}) of 2.45GHz prototype patch antennas with different electro textiles

As can be seen all fabric antennas showed acceptable performance in relation to copper based antenna. Other than the Flectron based patch there was close agreement of resonant frequency for all the electro textiles patches with the simulation and conventional copper patch. The antenna fabricated with Flectron showed reasonable bandwidth for $S_{11} < -10dB$ however the resonant frequency was shifted downward to 2.43GHz from the desired frequency of 2.48GHz. The reflection coefficient of copper based Taffeta fabric showed the best agreement with the reference copper patch and the level of matching at the resonant frequency was also quite good ($S_{11} < -32dB$).

The reason for better performance with Taffeta is due to it is highest conductivity among the tested fabrics. It has quite low surface resistivity of less than 0.05 Ohms/sq which makes it well suited for highly efficient RF devices. It is also Light weight with a weight of $72g/m^2$ and thickness 0.08mm. It is also flexible in 3 dimensions and can be conformed to any shape with ease. It is also highly tear resistant. Its large temperature range makes possible soldering a connector to it without burning holes in the fabric.

Also during etching process satisfactory results were achieved with Taffeta in terms of etching accuracy as well as processing time. While with other electro textiles results were not consistently accurate. The processing time was also almost double as compared to Taffeta.

In summary the measured results of electro textile based antennas have shown that they can be used in wearable antenna design just like normal Copper and the superior performance of Taffeta fabric as mentioned before make it an easy decision to use it as a conducting element in wearable antenna designs of this research.

3.10 Conclusions

In this chapter the importance of characterising materials used in wearable antenna designs was discussed. Some basic properties of conducting and non conducting materials which are important from antenna's design point of view were defined.

Different methods for characterizing dielectric materials were discussed. It was concluded that resonant method of characterizing dielectric materials was the best because of its non destructive nature and accuracy. The split post dielectric resonator (SPDR) operating on resonant method was then used to find the properties of materials. The accuracy of measured values was validated by measuring the properties of well known material and it showed good agreement with the actual values. Some minor errors were due to uncertainty in the height of samples being measured.

After measuring different samples it was decided to use Felt in this research as its permittivity and loss tangent values were within this research requirements. Other materials were rejected, some due to very low single layer thickness and other due to drapability issues.

The study on conducting materials defined as electro textiles was also discussed . The prototype patch antennas were fabricated and copper based Taffeta fabric was selected for this thesis because of its easy etching and good agreement of its input match performance with reference to Copper patch antenna.

In summary, the study on both flexible conducting and non conducting materials has shown a possibility to design an optimal textile antenna. In next chapter the design and fabrication of novel wearable antennas using these materials will be discussed.

4 LOW PROFILE WEARABLE ANTENNAS USING HIGH IMPEDANCE SURFACES

4.1 Introduction

In this chapter a novel wearable antenna is introduced which was designed using the theory written out in Chapter 2. For antennas to be integrated into everyday clothing it is desirable that they are compact in size (to lessen severe bending with movement of the body), and have low profile (to help wearability if they are conformal to the skin). Microstrip patch antennas belong to a well known class of low profile antennas that have gained popularity in research and commercial use in the last few decades [78, 116, 130]. They have the desired properties of being low profile and if made of a flexible material can be highly conformal. However they are inherently narrow bandwidth and for many applications a half wave microstrip antenna is still too large to be accommodated in an available space [131]. Nevertheless, extensive research has been done on patch antennas to reduce their size (miniaturisation) [132]. Work has also been done to increase their inherent bandwidth [133] Currently as of 2009 microstrip antennas should be considered as a first choice for wearable antennas for body worn communication systems. Many wearable antennas based on microstrip patch design have already been proposed [8, 9, 18, 24, 40, 42, 134] which shows the growing popularity of this type of antenna among wearable antenna design engineers. Further to the discussion on HIS provided in Chapter 2, this chapter illustrates the benefits of using an HIS in antenna designs via simulation and measurement.

The radiation mechanism of microstrip patch antenna can be represented using a magnetic current above a PEC ground plane [78]. With the recent advancement in HIS structures an equivalent has emerged which is basically an electric current above a HIS ground plane [135].

As discussed in Chapter 2 electric current on a wire cannot radiate efficiently near a traditional PEC ground plane because of the reverse image current. The creation of in phase reflection from HIS ground plane partially overcomes this difficulty. As a result, the design of low profile electric current type of antenna becomes possible. Since the electric current flows along a metal wire, this new type of low profile antenna may be referred to as a wire-HIS antenna [135].

In line with the theme of this research an aim here is to design a novel low profile high bandwidth wearable antenna. Firstly, the radiation performance of a wire dipole over PEC, PMC and HIS ground planes will be shown. The enhanced performance of a dipole over a HIS ground plane will be seen to confirm the validity of the design idea. Secondly, in this chapter a wire antenna will be modified to a planar strip antenna which is more suitable for wearable design applications.

The WLAN (2.40- 2.48GHz) band is chosen as the operating frequency band of wearable antenna. Based upon encouraging results a further modification of design from two layers to single layer is performed. This will further reduce the profile of wearable antenna with out deteriorating the input match performance.

4.2 Simulated Results for the Characteristics of a Half Wave Dipole over a PEC, a PMC and a HIS Ground Plane

4.2.1 A Half-Wave Dipole in Free Space

 In order to show the performance enhancement introduced by HIS based ground plane a reference is established by considering a dipole antenna in free space. Figure 4-1(a) depicts the geometry of thin dipole antenna with length L$\cong\lambda/2$ = 52mm and radius r=0.2mm (r$<<\lambda$). The simulated dipole is centre fed with 50Ω discrete port. The input resistance and reactance of dipole is computed and plotted in Figure 4-2(b) . The resonant frequency in this case is defined as the frequency at which S$_{11}$ is minimum. The Figure 4-2(a) shows that the dipole is resonant at frequency f_0 =2.52GHz and its length in terms of free space wavelength λ_0 is 0.44 λ_0 . The S$_{11}$ < -10dB bandwidth is $\cong$ 10.6%.
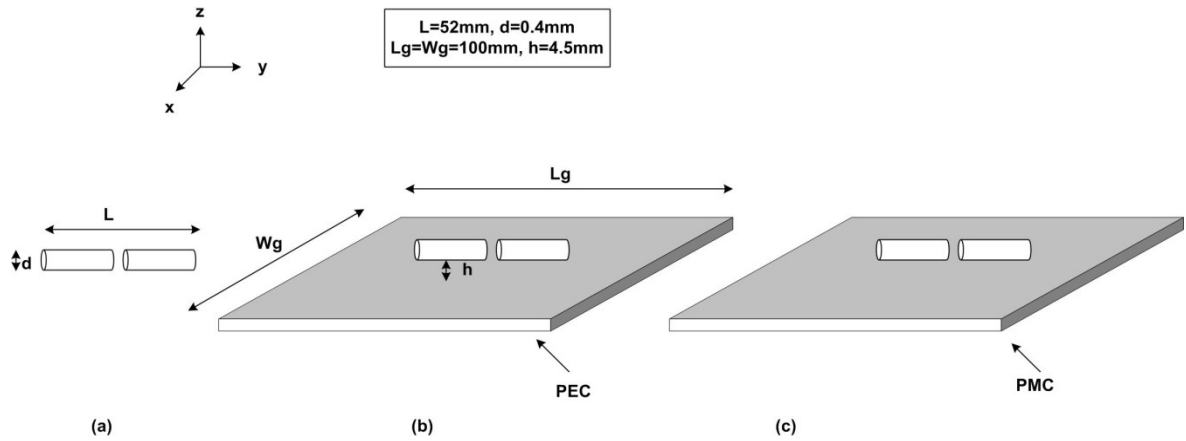
Figure 4-1 A λ/2 horizontal dipole antenna. (a) Free space, (b) over a PEC, (c) over a PMC.

(a)   (b)
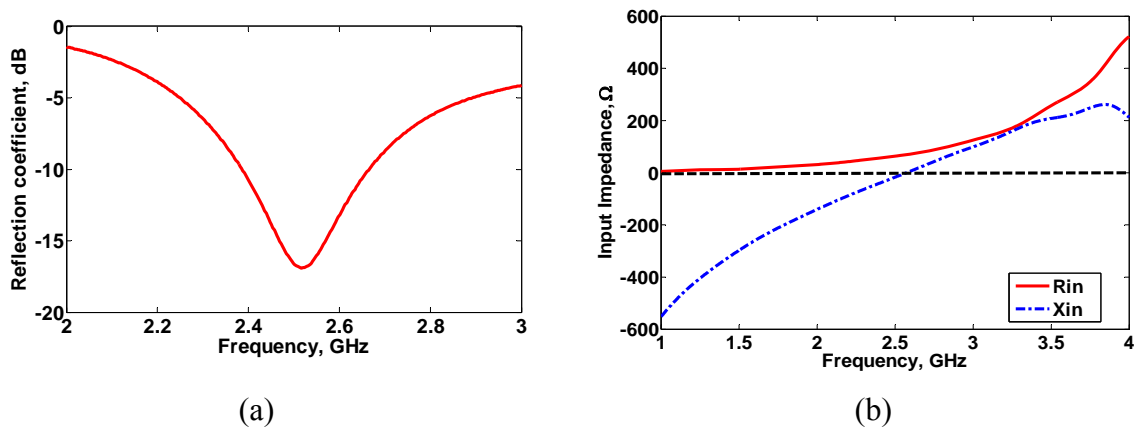
Figure 4-2 A λ/2 dipole antenna in free space. (a) Reflection coefficient (S$_{11}$), (b) Input Impedance.

4.2.2 A Horizontal Dipole Over a Finite Size PEC Ground Plane

In this second experiment a half-wave horizontal dipole parallel and close to a PEC was modelled. The air space between the dipole and the PEC was 4.5mm. The PEC size was 100mm×100mm as shown in Figure 4-1(b). This experiment is analogous to reducing the profile of a dipole above a ground plane to make the antenna more suitable for wearable applications.

The input impedance results are shown in Figure 4-3(b). The presence of the PEC changed the impedance behaviour of the dipole antenna significantly. The antenna resonated at $f_0 =$

2.61GHz where minimum S_{11} occurs as shown in Figure 4-3(a). At resonance the match was severely degraded from -17dB for the free space case to only -2dB for a low profile dipole antenna over a PEC. The value of input resistance at the resonant frequency was so small (close to zero) that the efficiency of the antenna was reduced significantly. Also impedance matching with the external matching network would be difficult to achieve. This simulation model thus showed that the dipole antenna cannot operate efficiently if placed horizontally very close the PEC ground plane.

(a)   (b)
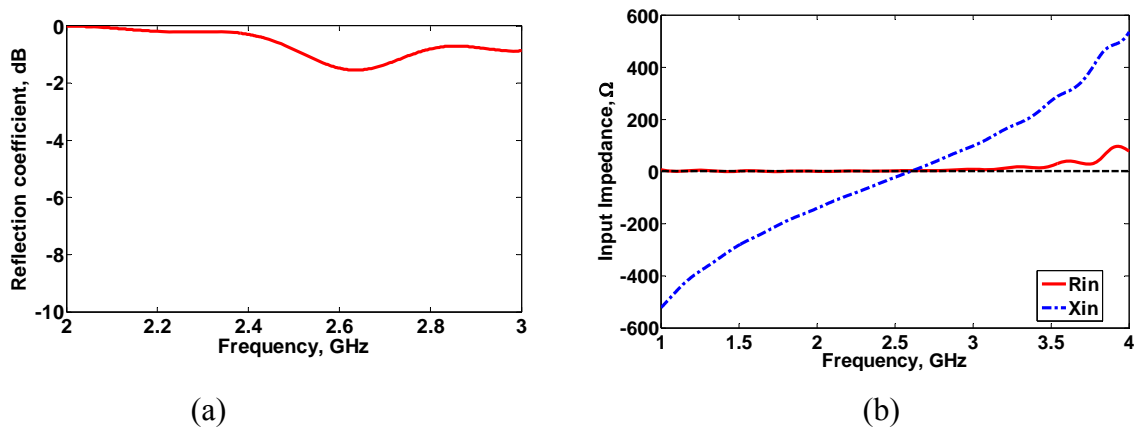
Figure 4-3 A λ/2 dipole antenna over PEC. (a) Reflection coefficient (S_{11}), (b) Input impedance

4.2.3 A Horizontal Dipole Over Finite Size PMC Ground Plane

Now the performance of dipole above an ideal PMC ground plane would be analysed. The dipole was placed at the same height from PMC as in the previous case of PEC shown in Figure 4-1(c). The results for the input impedance of a dipole over a finite size PMC ground plane are shown in Figure 4-4(b). The resonant frequency corresponding to minimum S_{11} is $f_0 = 2.5$GHz as shown in Figure 4-4(a). These simulated results suggest that although not as good as the free space case the match of the antenna was improved by the use of a PMC. It is important to mention that compared to dipole in free space, the input resistance was almost doubled and the slope of the input reactance versus frequency was increased. It is clear from S_{11} comparison that performance of dipole over PMC was much better than the dipole over the PEC surface. However the minimum value of S_{11} was only -6dB and thus could not satisfy the $S_{11} < $ -10dB BW criteria. Even if antenna was matched to 50Ω system impedance using external matching network, the increase reactance slope would limit the bandwidth lower as compared to free space case. One

reason for this behaviour is the strong coupling between the PMC surface and the antenna above it due to in phase image currents. This observation clearly demonstrates that the ideal PMC surface does not improve the antenna performance as desired.

It turns out that currently whilst ideal PEC surfaces can be closely approximated using conductive surfaces (copper is commonly used as a substitute PEC), PMC surfaces are more complex in design and do not exist in nature.

In the next section the artificially created PMC surface would be introduced that exhibit high surface impedance to the closely placed horizontal radiator and improves its performance significantly.

(a)   (b)
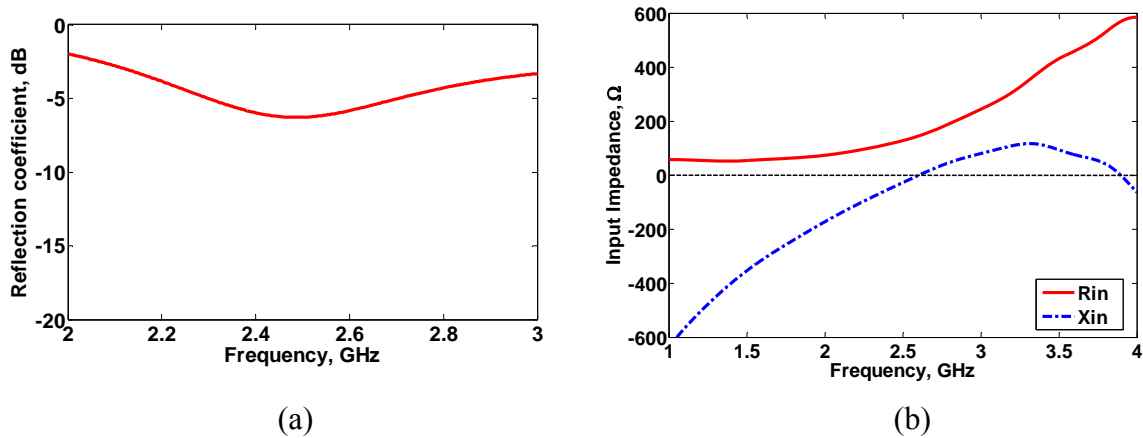
Figure 4-4 A horizontal λ/2 dipole over a PMC. (a) Reflection coefficient (S$_{11}$), (b) Input impedance

4.2.4 A Horizontal Dipole Over a High Impedance Surface

In line with theory and results presented thus far in this thesis an artificial PMC or high impedance surface was synthesized. This practical structure was then used in place of the theoretical PMC discussed in previous section. Note that as discussed in Chapter 2 Section 2.3 the artificial PMC is also known as a High Impedance Surface (HIS).

The HIS was based on the work of [75]. According to the results given in previous section and based upon the theory presented in Chapter 2 Section 2.7 a unit cell of the HIS was first synthesised and in the model the cell was illuminated by a plane wave normal to the x-

y plane. The cell consisted of a straight wire above a PEC. The length of each straight wire was set to 46mm with a radius r=0.2mm. The height of each dipole from the ground plane was h=3mm. The unit cell was thus 10mm wide with 0.2mm radius dipole in the centre and height of 3mm.

A single unit cell is shown in Figure 4-5 Also shown in Figure 4-5 (c) is the reflection coefficient phase plotted against frequency for the cell. The reflection coefficient phase is zero at 2.95GHz which was to be the HIS resonant frequency. The authors of [66] suggest that the frequency range where the HIS surface has a reflection phase in the range 90°±45° can improve the input match of the antenna. This corresponds to frequency range 2.7 – 3.0GHz for dipole HIS reflection phase shown in Figure 4-5(c).

This unit cell was repeated uniformly to create the so called uniform HIS structure. The reflection phase behaviour of infinite structure made of this unit cell would show the same reflection phase response as the single unit cell. However in practice an infinite structure does not exist so 7 unit cells were employed to make a finite dimension uniform HIS structure. The 7-cell HIS is shown in Figure 4-6 and below in Figure 4-7 is shown the reflection coefficient phase plotted versus frequency.
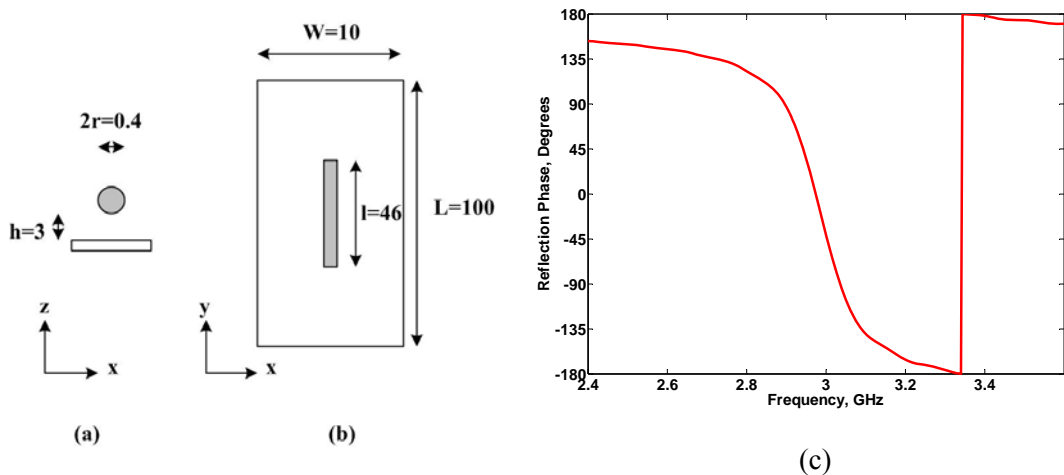
Figure 4-5 Geometry of Unit cell. (a) Side view, (b) Top view, all dimensions in mm (c) Reflection coefficient phase of unit cell.
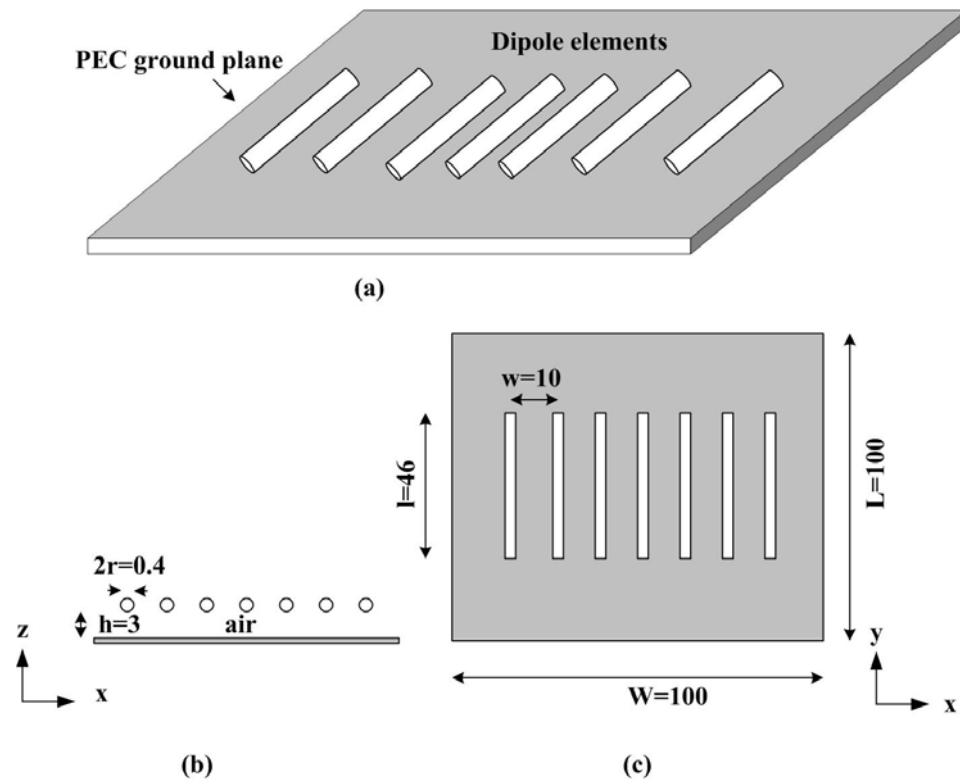
Figure 4-6 High Impedance Surface implemented using λ/2 parallel strips over a PEC. (a) 3D view, (b) side view, (c) top view. Note all dimensions are in mm (not to scale).
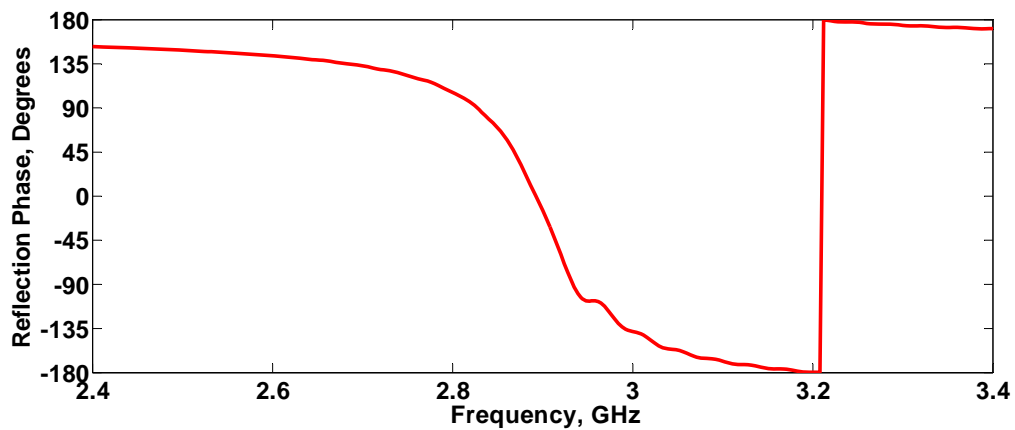
Figure 4-7 Reflection Phase of 7 cell finite size HIS.

It can be seen that total size of 7 cell HIS is $L \times W = 100\text{mm} \times 100\text{mm}$. The resonant frequency corresponding to zero degree reflection phase is 2.9GHz which is not much different from infinite size HIS.
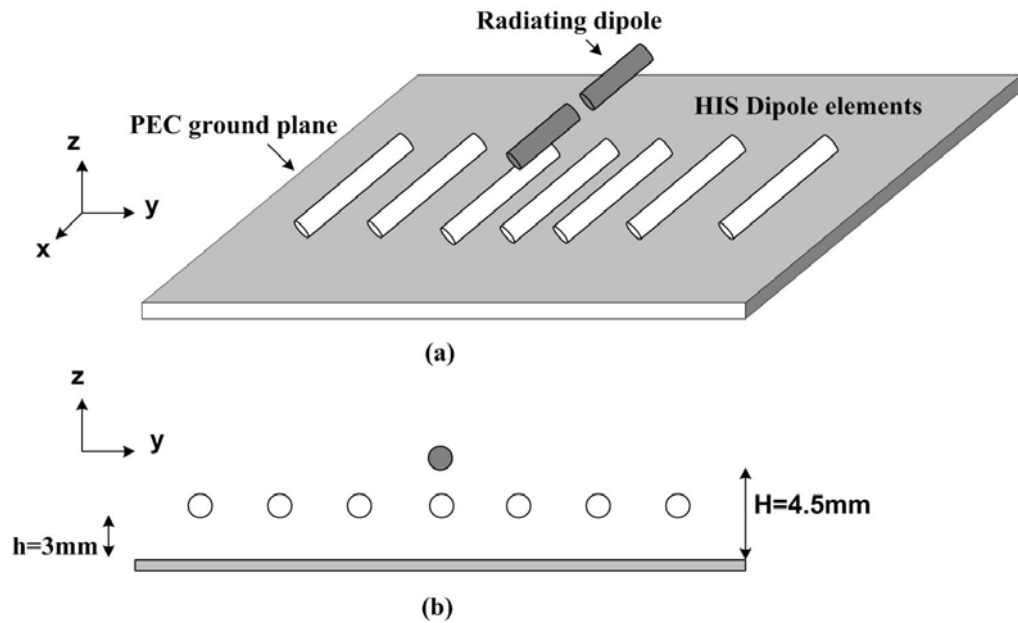
Figure 4-8 λ/2 dipole over HIS structure. (a) Perspective view, (b) Cross view.

The next stage was the synthesis of a dipole above a 7-cell HIS. This new iteration is shown in Figure 4-8. The simulated reflection coefficient (S_{11}) and input impedance results are shown in Figure 4-9.
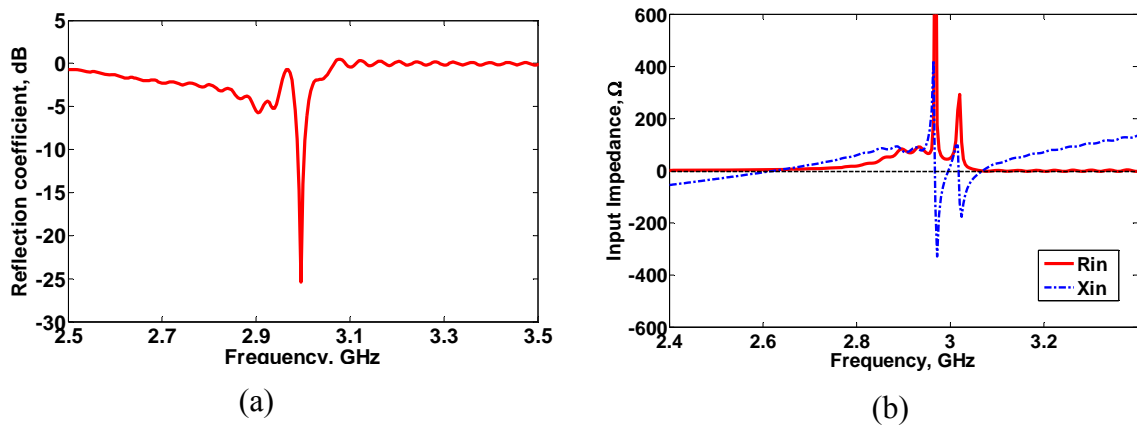
Figure 4-9 λ/2 Dipole over uniform HIS. (a) Reflection coefficient (S_{11}), (b) Input impedance.

Examining first the S_{11} for the new structure it can be seen that the Q of the antenna was improved by the 7-cell HIS with a deep resonance <-25dB at $\cong$ 3GHz. This compares well with the -17dB for the free space λ/2 dipole. However, it can also be seen from this result that the -10dB bandwidth has been much reduced from $\cong$ 10.6% down to $\cong$ 1%. In addition

there is a ripple on the S11 plot that was associated with the new structure. As the structure was both finite so this ripple could be a function of this and the periodicity of the cell elements of the HIS. It can also be seen from the simulated results that this structure had a second resonance and that the null in S_{11} was due to a superposition of two resonance at slightly above and slightly below 3GHz. It can be rationalized that one resonance was due to the dipole and a second resonance due to the HIS structure. The input impedance result in Figure 4-9 (b) also shows the decrease in real part of input impedance at the resonant frequency which helped in matching

The bandwidth of the new system is a function of the bandwidth of the HIS. This in turn is a function of the range of frequencies that HIS of the type used here will perform well as a PMC. Detailed discussion on these properties can be found in Chapter 2.

Thus, in order to improve the input match bandwidth of this design a non-uniform high impedance surface was synthesised.

4.2.5 Dipole Over Non Uniform High Impedance Surface

In the transformation to non uniform HIS design from the uniform HIS described in previous section only the distance between the dipoles needed to be altered. With the central cell straight wire as the origin the gaps were altered symmetrically with increasingly larger gaps between the straight wires toward the extent of the HIS structure. A diagram of the new system is shown in Figure 4-10.
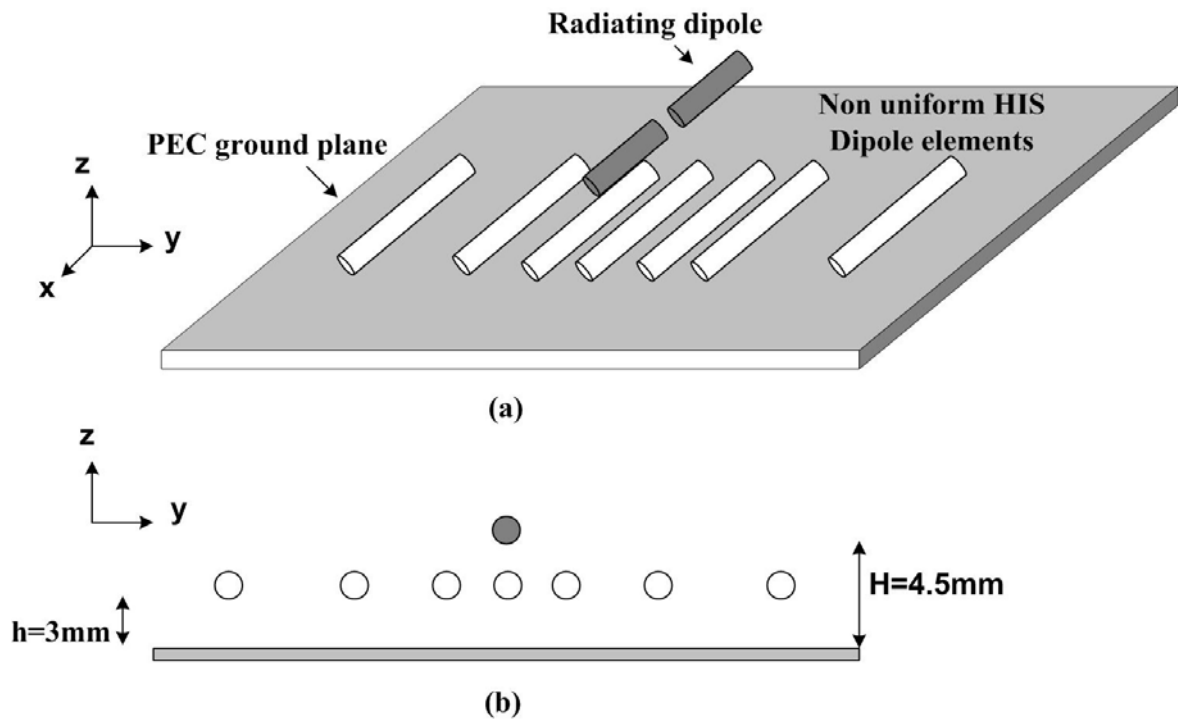
Figure 4-10 λ/2 dipole over Non Uniform High Impedance Surface. (a) Perspective view, (b) cross view.

Many simulations were carried out to find the optimal tapered distance between the unit cell dipoles. When the distances between the dipoles on both sides of the centre dipole were set to 7mm, 10mm and 13mm the optimal input match bandwidth was obtained. The results for S_{11} and input impedance of the dipole simulated over the non-uniform version of the dipole based HIS structure are shown in Figure 4-11.
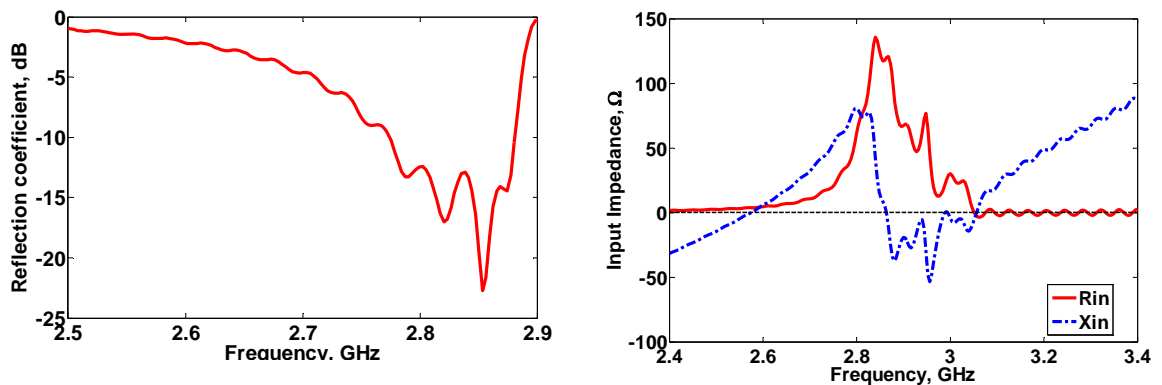
Figure 4-11 λ/2 dipole over Non Uniform straight wire HIS. (a) Reflection coefficient (S_{11}), (b) Input Impedance.

The resonant frequency corresponding to minimum S_{11} criteria was 2.85GHz. The input match bandwidth for $S_{11} < $ -10dB was 3.5% which is more than the uniform HIS structure.

The scale of input impedance shown in Figure 4-11 (b) clearly showed that input resistance is reduced significantly as compared to uniform HIS structure.

It is pertinent to mention that height of the dipole from PEC ground plane is only $0.04\lambda_0$ where λ_0 is the operating wavelength. While the height required for dipole over PEC ground plane is $0.25\lambda_0$. Thus dipole based HIS ground plane has reduced the profile of the antenna system by a factor of approximately 6.5. A non uniform HIS ground plane also improves the -10dB impedance bandwidth when compared with a uniform HIS ground plane.

4.3 A Three Layer Wearable Antenna for 2.4GHz WLAN Applications

A wearable antenna for WLAN (2.4-2.484GHz) was chosen as a useful and novel first application for the HIS researched thus far. In order to make use of the advantageous techniques discussed in previous sections there was a need to further modify the half wave dipole above a PEC. Firstly the final structure needed to be flexible and secondly it needed to be planar. Therefore all current supporting elements of both the HIS as well as the driven antenna would need to be flexible. In addition fabrication of the antenna would require spacing between the straight wires and the PEC for the HIS and isolation between the driven element on the HIS. A flexible dielectric substrate and conducting elements were therefore needed. Also to make a planar antenna all of the straight wires in the design were now replaced with strips

Based upon a brief survey of suppliers for the dielectric substrate it was decided to use commonly used Felt [136]. The felt was available in different thicknesses ranging from 1.5mm to 12mm. The electromagnetic properties of Felt were determined using the cavity resonator technique discussed in detail in Chapter 3. The measured permittivity of Felt is ε_r =1.36 and dielectric loss tangent is $\tan\delta$ =0.023.

Conducting surfaces were made using copper Polyester Taffeta Fabric [129]. This is a shiny, smooth polyester fabric with copper integrated into it. It is light weight and flexible

and can be cut and sewn like ordinary fabric. The material used had an approximate thickness of 0.08mm and surface resistivity of 0.05 Ωm^{-2}.

4.3.1 Design Detail and Simulated Results

For integration into wearable clothing and to make feeding more practical the centre fed dipole driven element of Figure 4-10 was modified to an end fed planar inverted L antenna [119]. Also to appreciate the performance enhancement introduced by non uniform HIS the design stages are shown starting from the inverted L antenna without HIS to the inverted L antenna with uniform HIS and finally the optimal wearable design of inverted L antenna with non uniform HIS structure.

The design stages of wearable inverted L antenna are shown in Figure 4-12. Using the analysis written up in Chapter 2 but combined now with the optimised results for the HIS iterations in Section 4.2.5 as a first design stage a textile 5×16 ($\cong \lambda_{eff}/4$) conductive strip was chosen on top of 4.5mm thick Felt over a flexible PEC. This replaces the dipole antenna with an inverted planar L antenna.
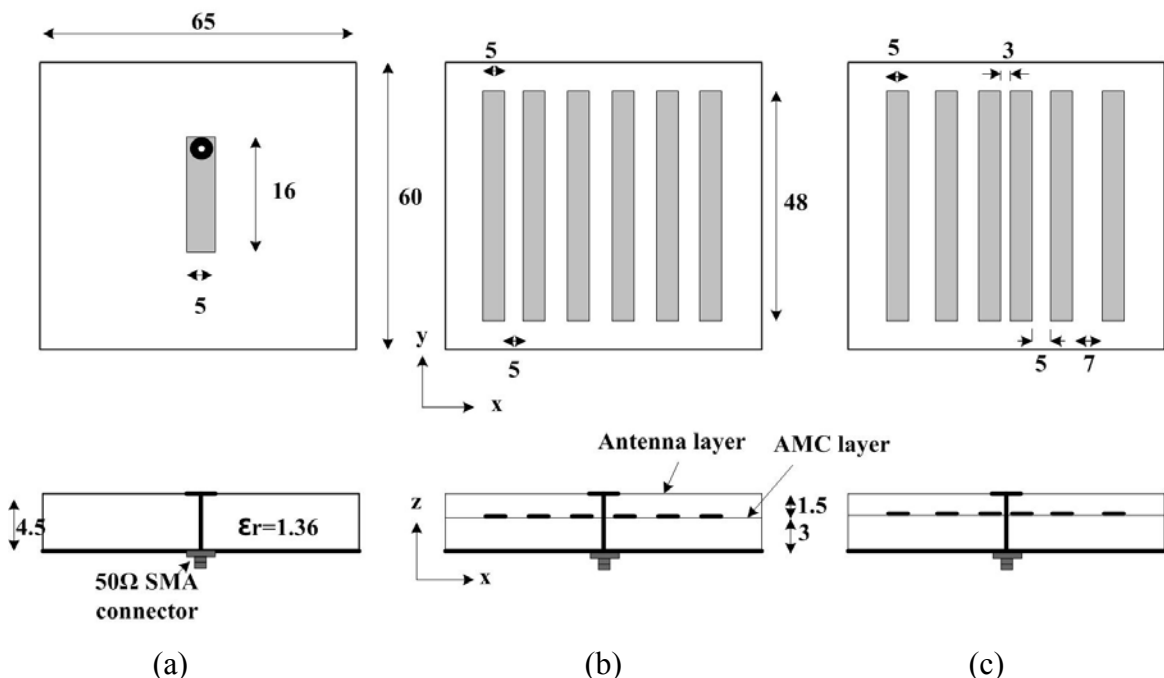
Figure 4-12 Design stages of low profile wearable inverted L antenna, top view and cross view.

(a) Inverted L shaped antenna without HIS, (b) inverted L antenna with uniform HIS (U-HIS), (c) inverted L antenna with non uniform HIS (NU-HIS).

Note: All dimensions in mm. Also in (b) and (c) the top antenna layer is hidden to show the HIS layer.

(a)   (b)
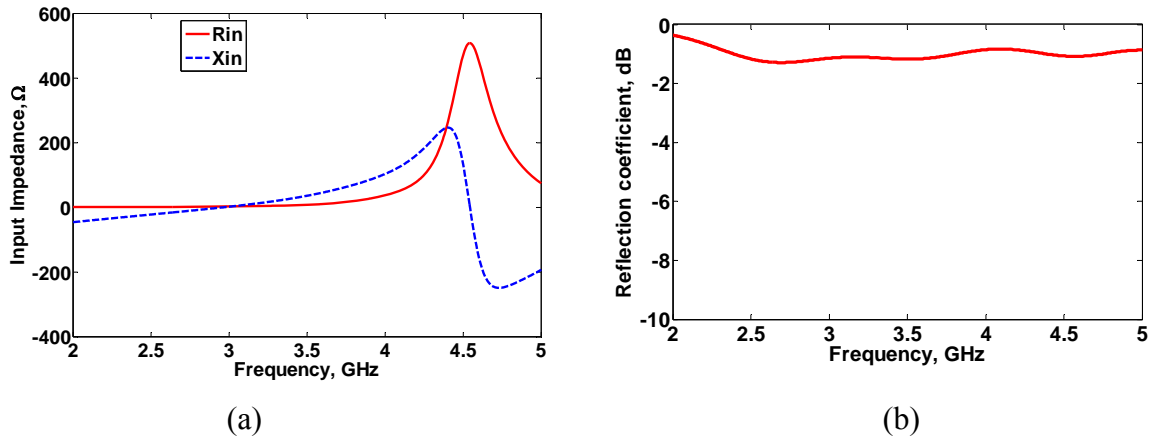
Figure 4-13 An Inverted L antenna above a PEC. (a) Input impedance, (b) Reflection coefficient (S$_{11}$).

The strip was fed at the end by the central pin of an SMA connector. The total size of the antenna PEC was made to be $65mm \times 60mm$. The simulated input impedance and reflection coefficient (S$_{11}$) results are shown in Figure 4-13. In the range of frequencies shown a first resonance occurs at $\approx$2.9GHz where the imaginary part of the input impedance (Xin) is zero, However since real part of the input impedance (Rin) is low the antenna, although resonant, may not be radiating. This is shown by S$_{11}$ result in Figure 4-13 (b) where the minimum S$_{11}$ is only -1.5dB. Also the peak input resistance is close to 500Ω which is quite high (see Figure 4-13 (a)). This shows that monopoles with low profiles (inverted L) have higher Q values which makes impedance matching difficult and results in narrow impedance bandwidth. At $\approx$ 4.6GHz a second resonance exists which is not useful for this thesis research.

A unit cell of the HIS was then optimised by simulation for zero degree reflection coefficient phase resonance. The results are shown in Figure 4-14.
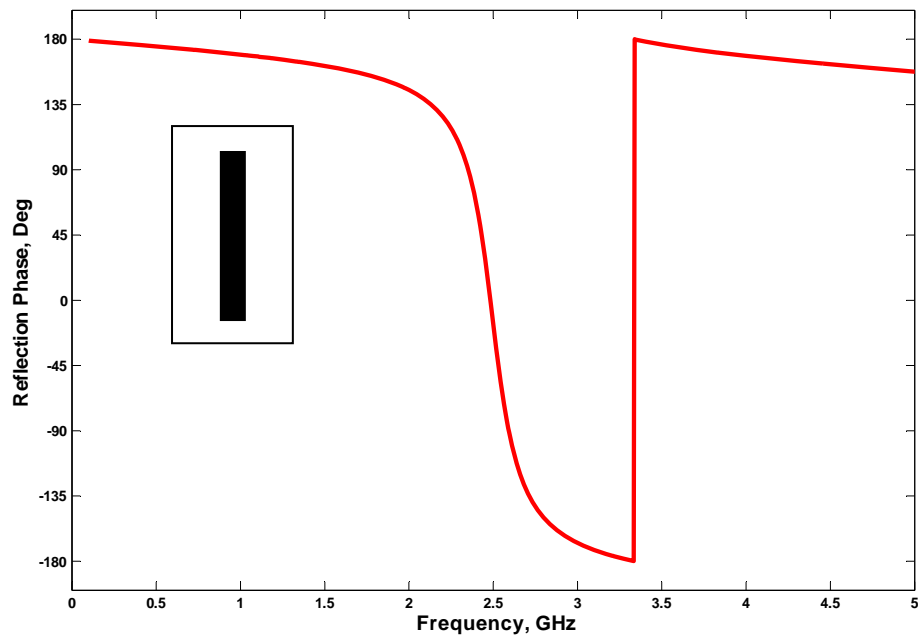
Figure 4-14 Reflection Coefficient phase of HIS unit cell.

The HIS resonant frequency is 2.5GHz where the reflection coefficient phase is zero. The HIS bandwidth (+90º to -90º) is from 2.35GHz to 2.58GHz.

An inverted L antenna above a uniform version of HIS is shown in Figure 4-12(b). Each of the six unit cells consists of a strip above a PEC supported by felt $\approx 0.027\lambda$ Thick (3mm). The optimised strips are $\approx 0.44\lambda$ long (48mm) and $\approx 0.04\lambda$ wide(5mm). Six unit cells were used with a spacing of $\approx 0.09\lambda$(10mm). The simulated reflection phase result for this finite size HIS structure is shown in Figure 4-15. The HIS resonant frequency was 2.4GHz which is not very different from the infinite HIS structure case.
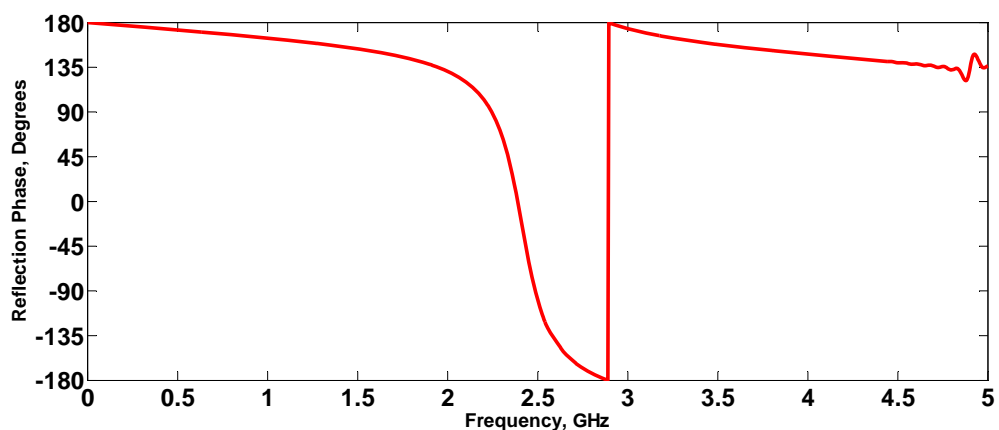
Figure 4-15 Reflection coefficient phase of 6 cell finite HIS structure.

 A further layer of felt (1.5mm)was then used to support the inverted L antenna above the HIS. Dimensions and the geometry are shown in Figure 4-12 (b).

The complete structure shown in Figure 4-12 (b) is simulated and the corresponding results for input impedance and S_{11} are shown in Figure 4-16 .

| (a) | (b) |
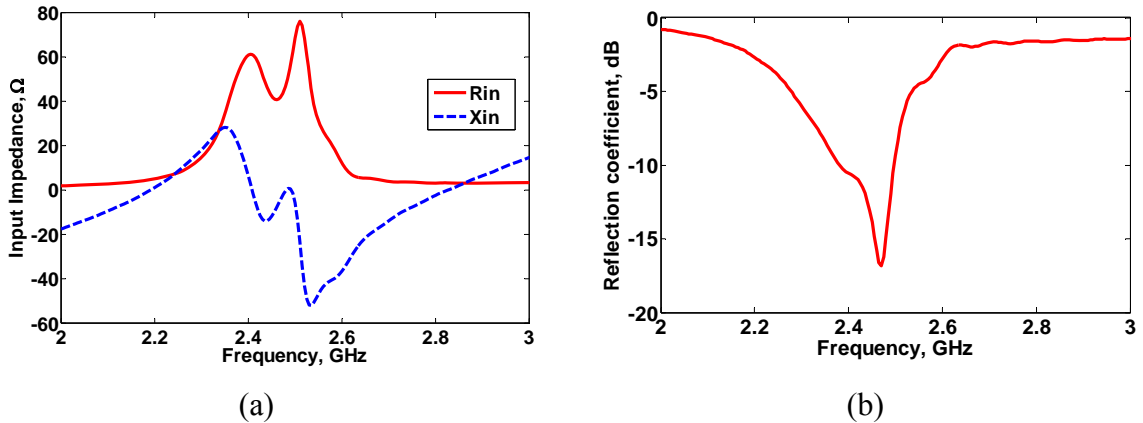
Figure 4-16 An Inverted L antenna above a uniform HIS. (a) Input Impedance, (b) Reflection coefficient (S_{11}).

These simulations show a resonant frequency at ≈2.47GHz. The impedance bandwidth for RL < -10dB is from 2.38GHz to 2.5GHz which is 4.9% of the centre operating frequency. It can be seen that the system has a relatively stable impedance. Also it is important to mention that peak input resistance is only 75Ω which is quite small as compared to the inverted L antenna without HIS surface. This clearly shows the enhancement introduced by the HIS surface to the impedance behaviour of low profile inverted L antenna.

In the next design cycle shown in Figure 4-12 (c) the design was modified using a tapered distribution for the gap between the unit cells. The spacing was reduced between the strips lying directly under the inverted L antenna. This spacing was then increased towards the edge of the substrate. The spacing taper was optimised for the best impedance bandwidth. The input impedance and S_{11} results for the optimised design are shown in Figure 4-17.
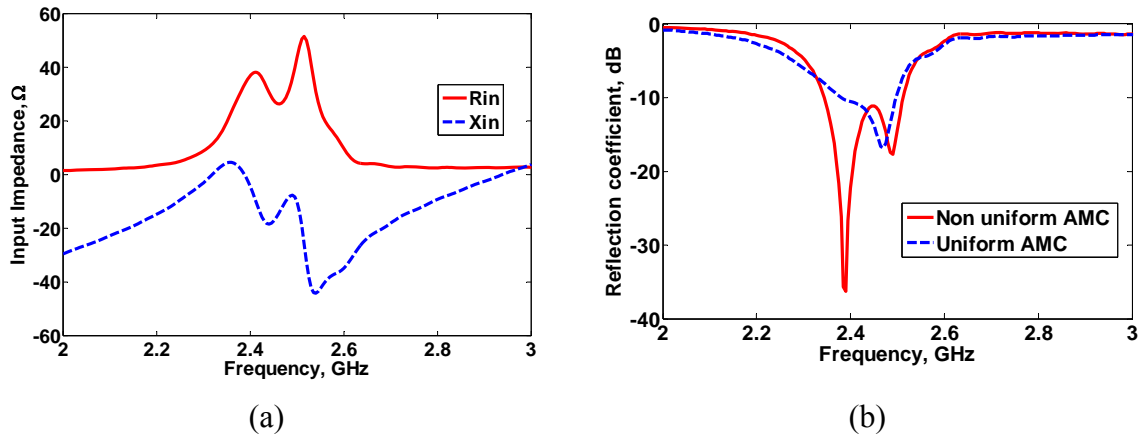
Figure 4-17 Inverted L antenna over Non uniform HIS. (a) Input Impedance, (b) Reflection coefficient (S$_{11}$).

The imaginary part of the input impedance is 0Ω at 2.39GHz while the real part is 32Ω at this frequency (see Figure 4-17(a)) . It is pertinent to mention that the peak value of the input resistance is further reduced as compared to the uniform HIS design. The minimum S$_{11}$ value is also reduced and it occurs at 2.4GHz. The input match bandwidth for S$_{11}$ < -10dB criteria is from 2.34GHz to 2.51GHz which is 7% of the centre operating frequency. For comparison the S$_{11}$ result of the uniform HIS was also plotted. It is clear from Figure 4-17 (b) that non-uniform HIS improves the input impedance bandwidth as compared to the uniform HIS structure. It is to be noted that original inverted L antenna was showing resonance at $\approx$2.9GHz (shown in Figure 4-13), but when integrated with the HIS the resonant frequency was seen to reduce to $\approx$2.4GHz. Thus for the same resonant frequency of 3GHz a small size antenna is needed after integrating HIS with the antenna. Thus HIS structure not only improves the input match of the antenna but helps in miniaturisation as well. Figure 4-18 shows the computed surface current distribution of the antenna at 2.44GHz. The maximum current is clamped at 10 (A/m) so that this distribution can be compared to the modified version of this antenna to be discussed in Section 4.4.
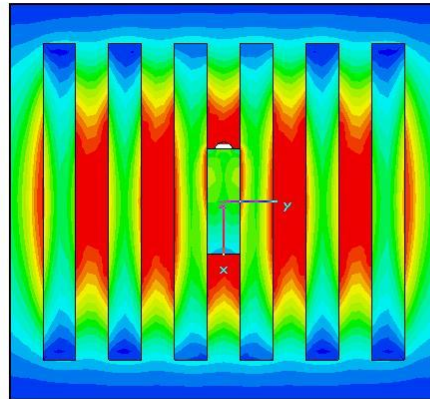
Figure 4-18 Computed surface current distribution of the antenna at 2.44GHz

4.3.2 Measured Results For an Inverted L Antenna Over a High Impedance Surface

A prototype of wearable inverted L antenna was constructed and is shown in Figure 4-19. The footprint of the antenna was targeted to be a square $\lambda/2$. However, since this one was made by hand a ±2mm margin of error is there. All conducting elements were made from the flexible textile discussed in Chapter 3. Elements of the HIS are concealed in Figure 4-19 and these were made using an etching process whereby copper coating was etched away according to a mask. The elements of the HIS therefore comprise conductive areas upon a thin textile section approximately 65×65mm.

(a)   (b)   (c)
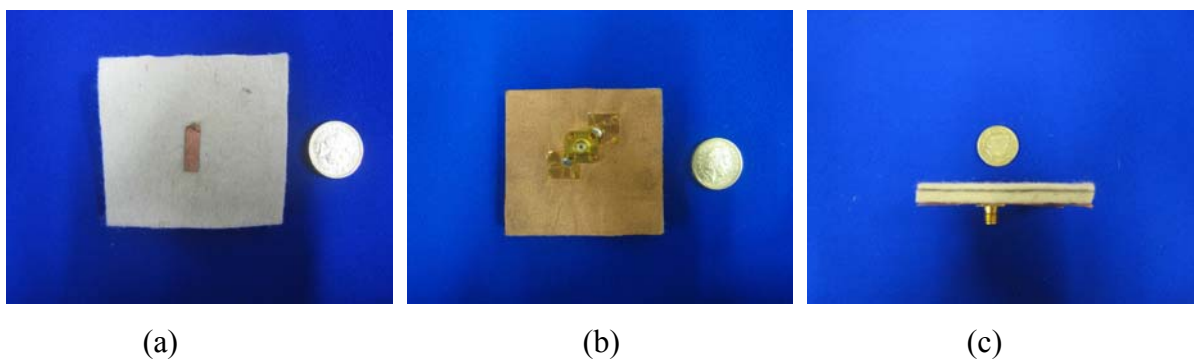
Figure 4-19 Prototype wearable inverted L antenna. (a) Top view, (b) Bottom view, (c) side view showing the hidden AMC layer.

The prototype antenna was connected to Vector Network Analyser (VNA) to measure its scattering parameters. The VNA was first calibrated up to the end of VNA coax cable to remove the effect of the cable on the measured results. The measured reflection coefficient (S_{11}) result along with the simulated value is shown in Figure 4-20.
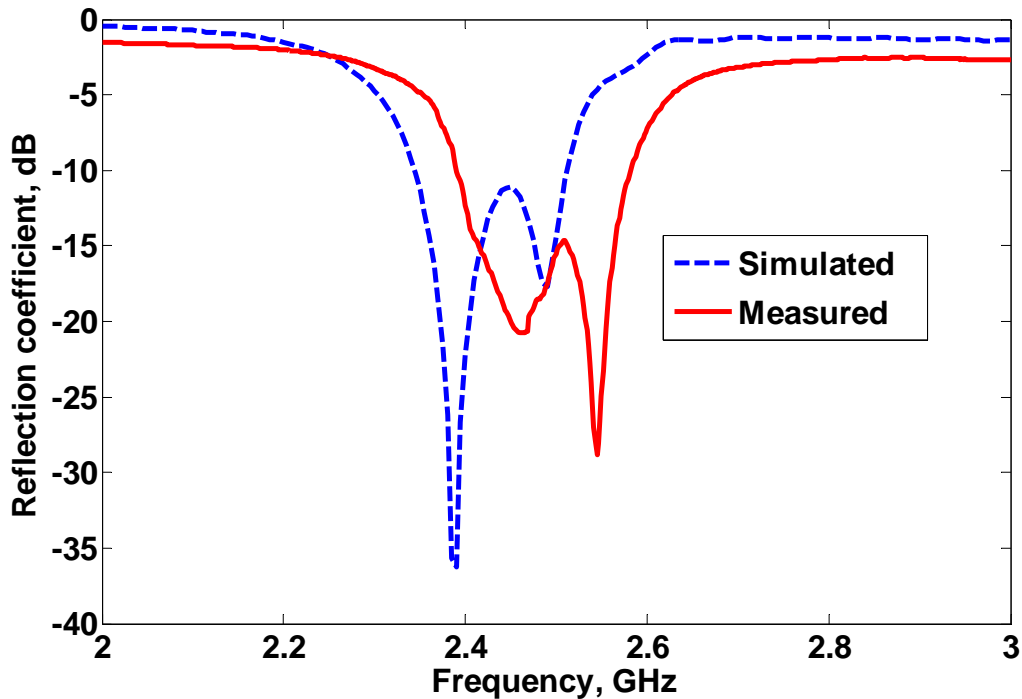
Figure 4-20 Measured and Simulated Reflection coefficient (S_{11}) of an inverted L antenna over a non-uniform HIS

It can been observed that measured S_{11} is shifted toward higher frequencies as compared to simulated results. There are two reasons for this drift. One there is an air gap between the two Felt layers which has not been considered in the simulation. Secondly adhesive spray was used to fixed two Felt layers as well as attaching the conductive fabric to the Felt. Again this has not been included in the simulation setup. However prototype antenna was still able to work in the WLAN band (2.4GHz-2.484GHz). The input match bandwidth for $S_{11} < -10$dB is about 4% at the centre operating frequency of 2.48GHz.

The radiation performance of this prototype antenna was measured in the Anechoic Chamber (Appendix B). The standard horn antenna was used as a reference antenna to find the gain and radiation pattern of prototype antenna. The measured radiation patterns in the E-plane and H- plane are shown in Figure 4-21.

E-Plane (yz Plane)

(a)

H-Plane (xz Plane)

(b)
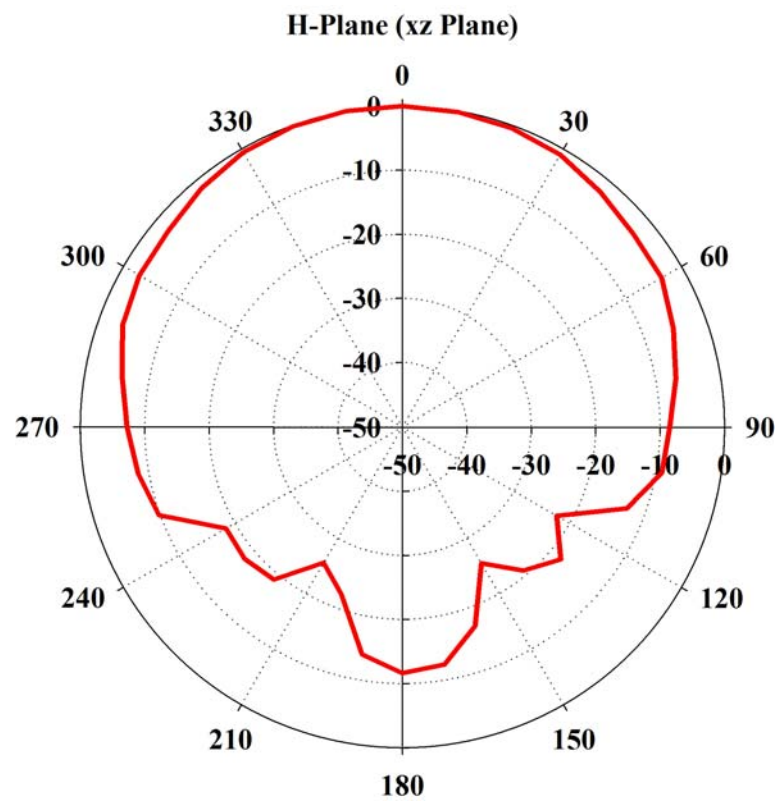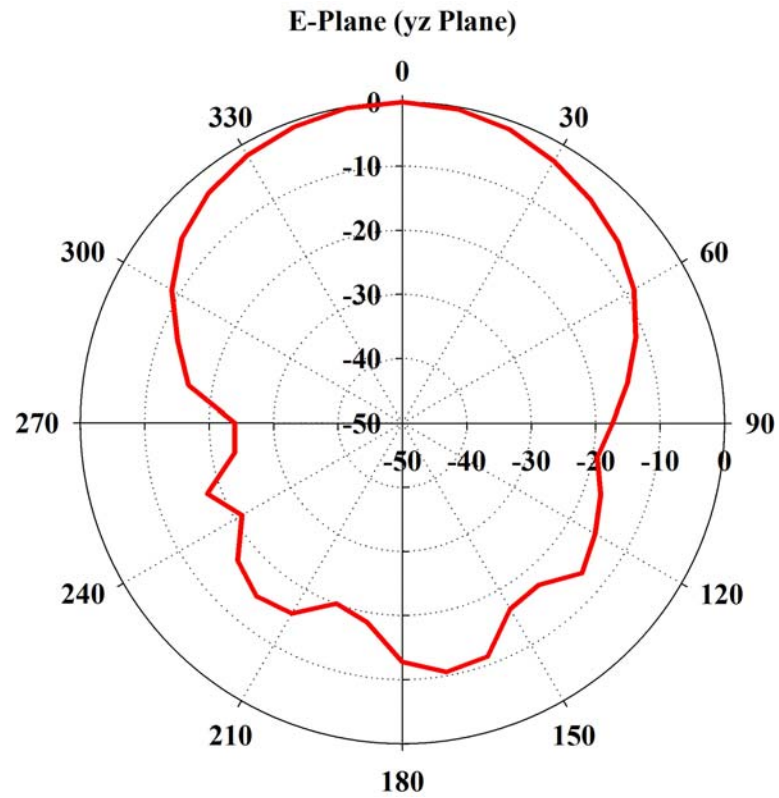
Figure 4-21 Measured Radiation patterns of wearable antenna. (a) E-plane, (b) H-Plane

The radiation patterns showed that the maximum radiation was towards broadside which is desirable for wearable antennas. The E-plane pattern was also more directive as compared to H plane. The Half Power Beam width (HPBW) is 50º in E-plane and 75º in H-plane.

The gain and radiation efficiency of antenna were also measured and results are plotted in Figure 4-22(a) and Figure 4-22(b) respectively. The average radiation efficiency is close to 55% while the highest efficiency across the operating range of frequency is about 60%. The gain has an average value of 5dBi with the maximum value of 5.5dBi. The front-to-back (F/B) ratio was -13dB which is quite exceptional for such a small size antenna.
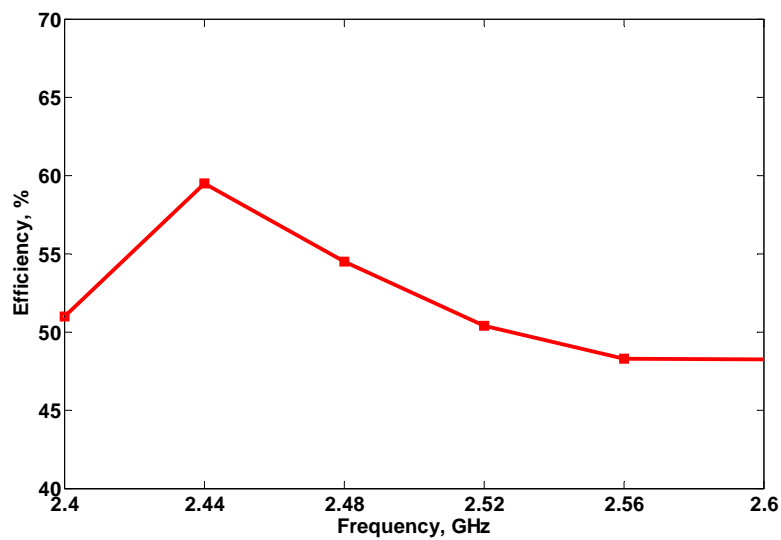
(a)
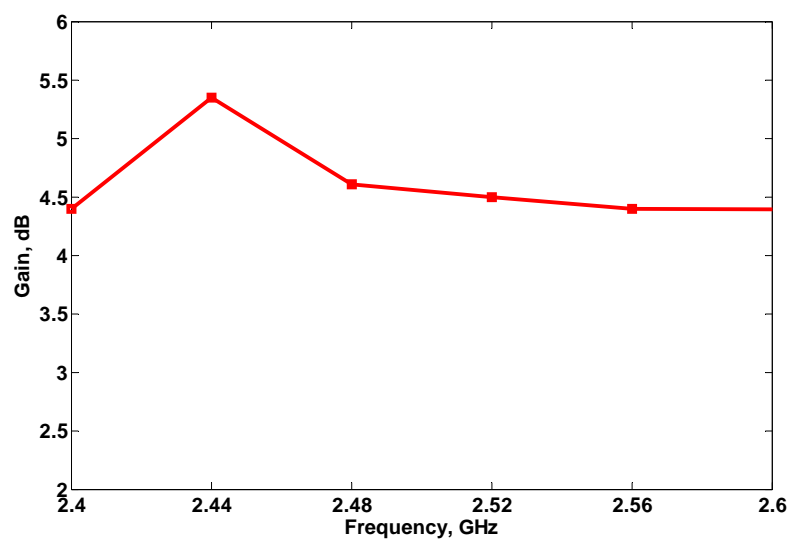
(b)

Figure 4-22 An inverted L antenna above an HIS. (a) Efficiency, (b) Gain.

4.4 A Low Profile Wearable Antenna for 2.4GHz WLAN

To simplify the fabrication process and also to further reduce the profile of wearable antenna the design shown in Figure 4-23 was also evaluated. It consisted of five metallic strips etched onto the conducting Polyester fabric. Only one layer of substrate was used and the radiating element was incorporated into the plane of the HIS elements. The total size of structure of this antennas was optimised to be 60×50×3(in millimetres) . The length and width of the strips was 48mm and 8mm respectively. For initial assessment of this HIS a uniform spacing between elements of 5mm was used. This topology is shown in Figure 4-23 and produced a phase return coefficient very similar to the one shown in Figure 4-15. In line with previous discussion (section 4.3) in order to improve impedance match bandwidth the element spacing distribution was now tapered by closing the more central elements and expanding the outer. The optimised structure for the HIS is shown in Figure 4-23 (b) along with the relevant dimensions.

In order to reduce the profile of the antenna to a greater degree than the iteration discussed in Section 4.3 the central element of the HIS was replaced by the radiating element, namely the inverted planar L antenna.

(a)   (b)   (c)
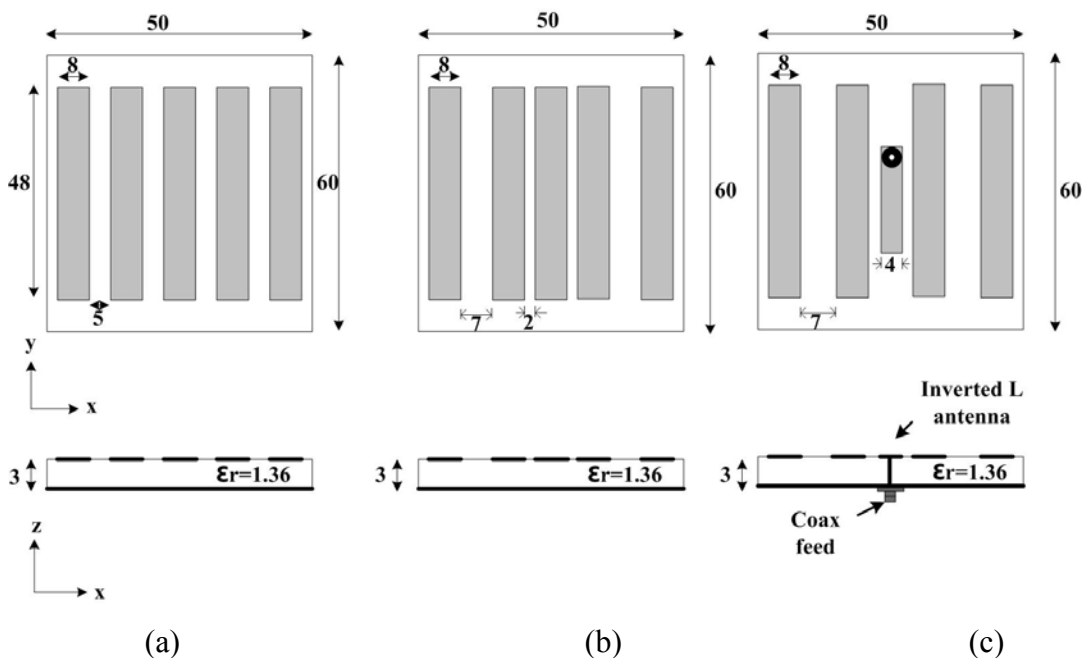
Figure 4-23 Design stages of modified low profile inverted L antenna Top view and Cross view. (a) Uniform strip AMC, (b) Non uniform strip AMC, (c) Inverted L antenna integrated with Non uniform strip AMC.

Note: All dimensions in mm.

4.4.1 Synthesis of an Inverted L Antenna Integrated into an HIS

Synthesis began with the simulation of inverted L antenna without any HIS strips. The length of the strip was set to 23mm while the width was kept 4mm. The simulated input impedance and S_{11} results are shown in Figure 4-24.

(a)   (b)
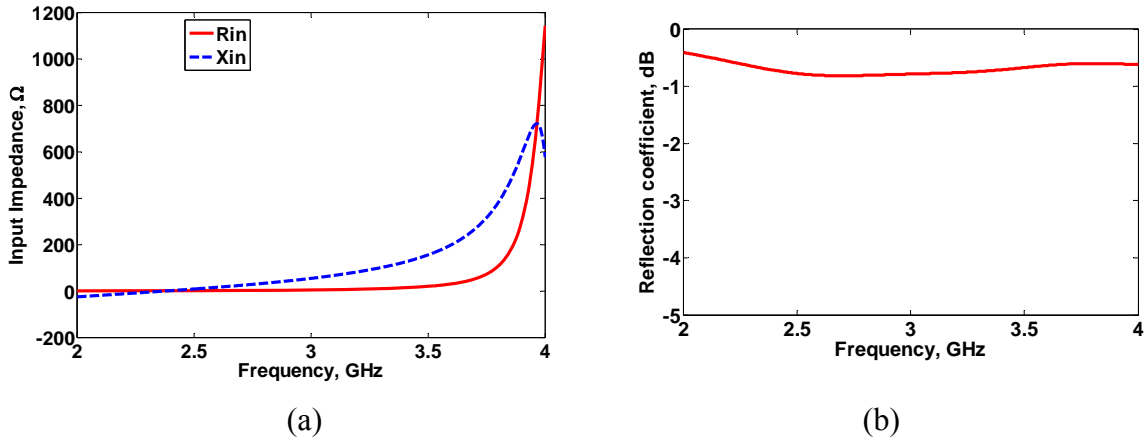
Figure 4-24 Inverted L antenna. (a) Input impedance. (b) Reflection coefficient (S_{11}).

The antenna is resonant at about 2.36GHz where the imaginary part of input impedance (Xin) is zero (see Figure 4-24 (a)). The real part of input impedance (Rin) is only 2Ω which is difficult to match to a 50Ω source feed. The S_{11} result shown in Figure 4-24 (b) clearly shows this behaviour as the minimum value of S_{11} is only -1dB at the resonant frequency. The peak value of input impedance is also very high $\cong 1200\Omega$.

Note that as discovered previously the addition of the HIS alters the properties of the inverted L antenna substantially. First a uniform HIS was modelled as shown in Figure 4-23 (b). The simulated input impedance and S_{11} results are shown in Figure 4-25.

(a)   (b)
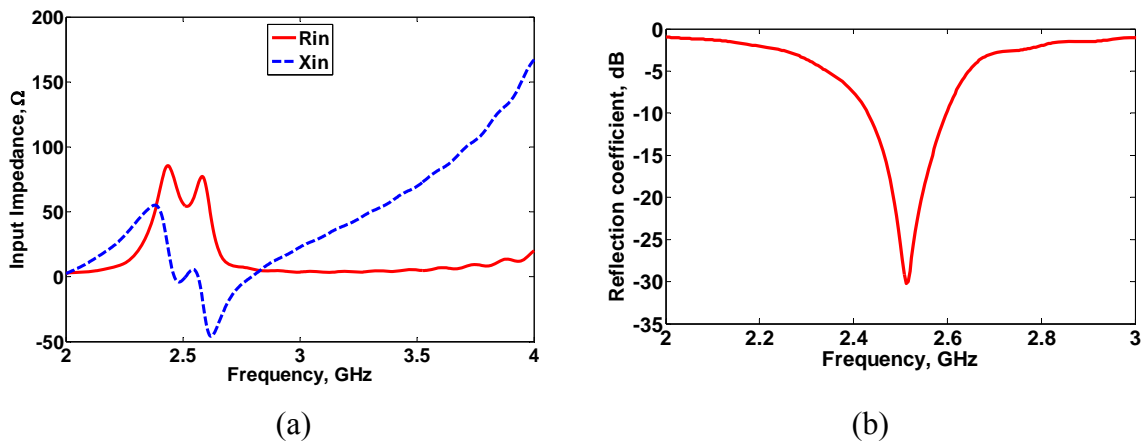
Figure 4-25 Inverted L antenna with uniform AMC. (a) Input Impedance. (b) Reflection coefficient (S_{11}).

The imaginary part of input impedance (Xin) is zero at 2.46GHz. The real part of the input impedance (Rin) is close to 75Ω at this frequency. The peak value of input resistance has been significantly reduced to about 150Ω as shown in Figure 4-25 (a). The input resistance does not vary sharply around the resonant frequency. Thus antenna can be easily impedance matched to a 50Ω source. The minimum S_{11} is -30dB at 2.5GHz as shown in Figure 4-25 (b). The impedance bandwidth using $S_{11} < -10$dB criteria is from 2.42GHz to 2.6GHz which is 7.0 % of the centre operating frequency.

In the final stage of design cycle the S_{11} was optimised by tapering the spacing between the elements of the HIS. For fair comparison between uniform and non uniform version of the design the overall dimension of the structure was kept the same. Figure 4-26 shows the simulated input impedance and S_{11} results for the non uniform HIS version of wearable inverted L antenna.

| (a) | (b) |
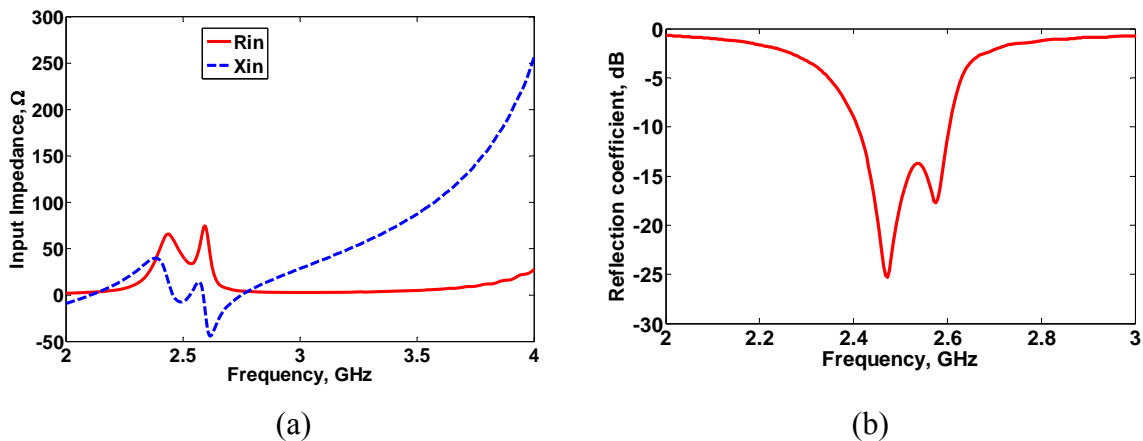
Figure 4-26 Inverted L with non uniform HIS. (a) Input impedance. (b) Reflection coefficient (S_{11}).

The imaginary part of input impedance (Xin) is zero at 2.45GHz and 2.52GHz while the real part of the input impedance (Rin) is 60Ω and 35Ω respectively. The input resistance variation is small around the resonant frequency. Due to dual resonance behaviour the input impedance bandwidth is increased as shown in Figure 4-26(b). The S_{11} value is about -25dB at 2.46GHz. The input match bandwidth for $S_{11} < -10$dB criteria is from 2.4GHz to 2.61GHz which is about 8.4% of the centre operating frequency. Hence non uniformity helps in increasing the input match bandwidth of this wearable antenna. Figure 4-27 shows the computed surface current distribution for this antenna at 2.44GHz. By comparing this current distribution with the previous antenna (Section 4.3) it can be seen that there is not

much difference in the current distribution of the two antennas. Thus radiation mechanism of both appears to be the same.
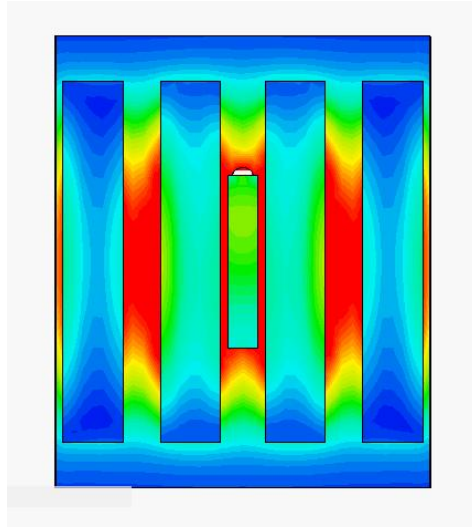
Figure 4-27 Computed surface current distribution of the antenna at 2.44GHz

4.4.2 Measured Results Discussion

The prototype of modified wearable inverted L antenna was fabricated in order to measure and verify its characteristics. The top and bottom views of fabricated antenna are shown in Figure 4-28. The etched conducting Polyester fabric was attached to the felt fabric using adhesive spray. The same procedure was used to attach conducting Polyester on the other side of felt substrate to work as ground plane. To feed the antenna an SMA connector was used. The measured and simulated S_{11} results are shown in Figure 4-29 .

(a)   (b)
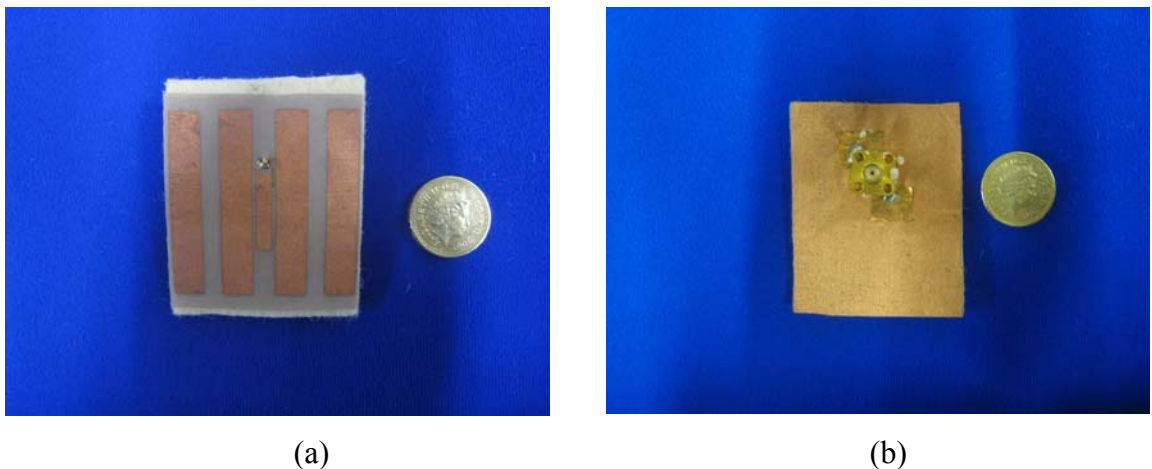
Figure 4-28 Prototype of modified wearable inverted L antenna. (a) Top view. (b) Bottom view.
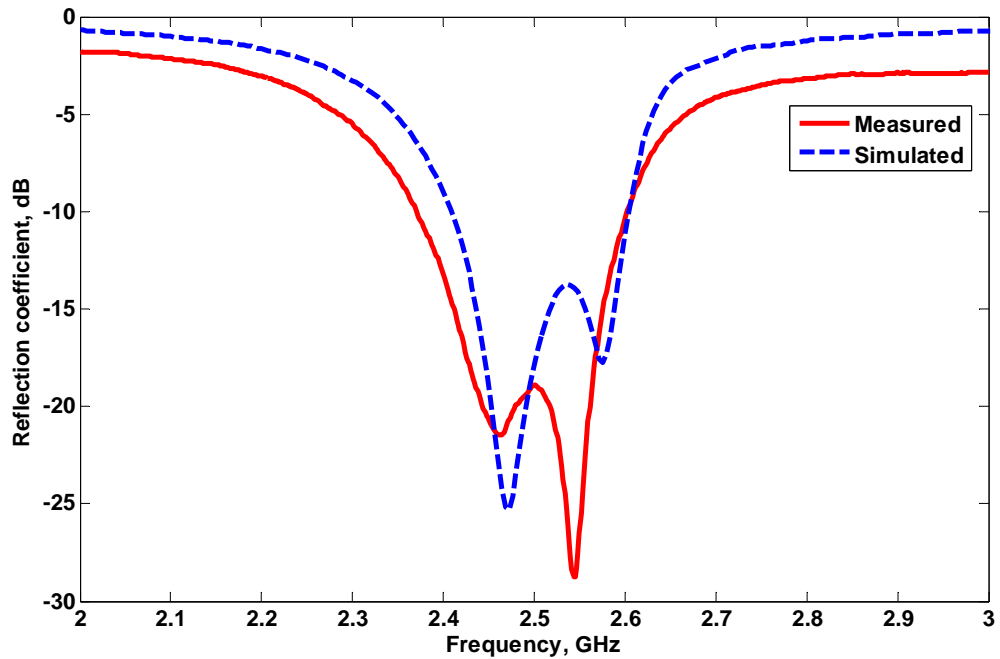
Figure 4-29 Measured and Simulated reflection coefficient (S_{11}) result for modified inverted L wearable antenna.

There is quite good agreement between the simulated and measured results when compared with the two substrate layer design discussed previously. The input impedance bandwidth is from 2.37GHz to 2.6GHz which is about 9.3% of the centre operating frequency.

The radiation characteristic of this antenna had been measured in an Anechoic Chamber. The measured E-plane and H-plane patterns are shown in Figure 4-30.

E-Plane (yz Plane)

(a)

H-Plane (xz Plane)

(b)
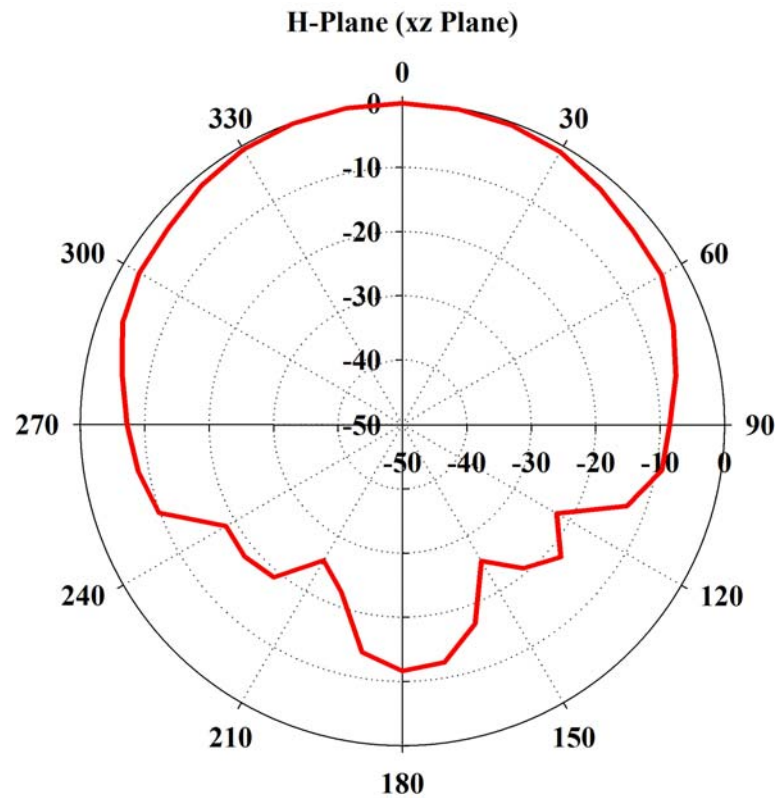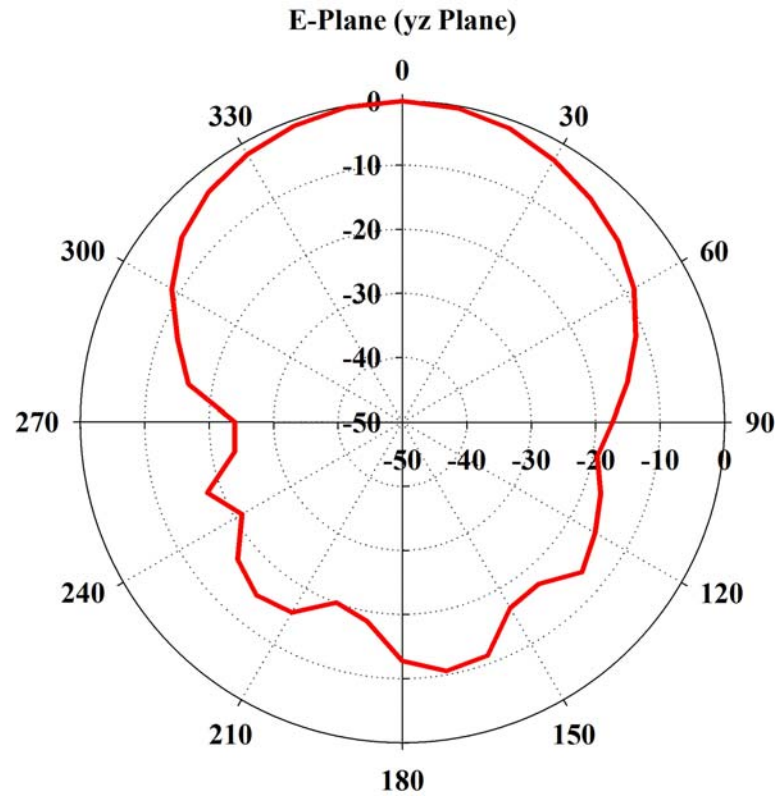
Figure 4-30 Measured radiation patterns of modified wearable inverted L antenna (a) E-Plane (b) H-Plane

As can be seen the main beam is broadside . The front-to-back (F/B) ratio is ≈13dB which is quite good for such a small size antenna. The E-Plane pattern is more directive than the H-plane. The half power beam width (HPBW) in E-Plane is 70 degrees while in H-plane it is ≈ 90 degrees. One possible reason for this is the longer dimension of antenna along the E-plane direction as compared to H-plane. The radiated efficiency and gain were also measured in Anechoic Chamber and results are plotted in Figure 4-31.
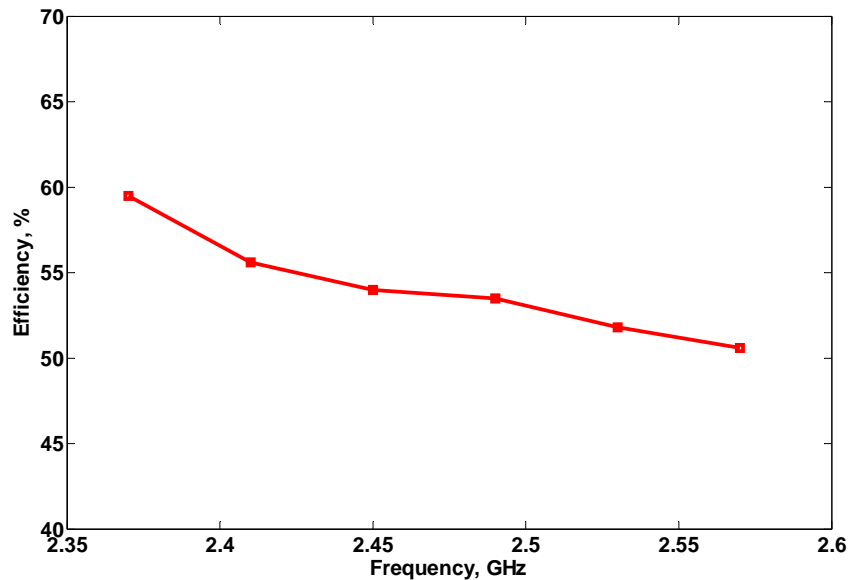
(a)
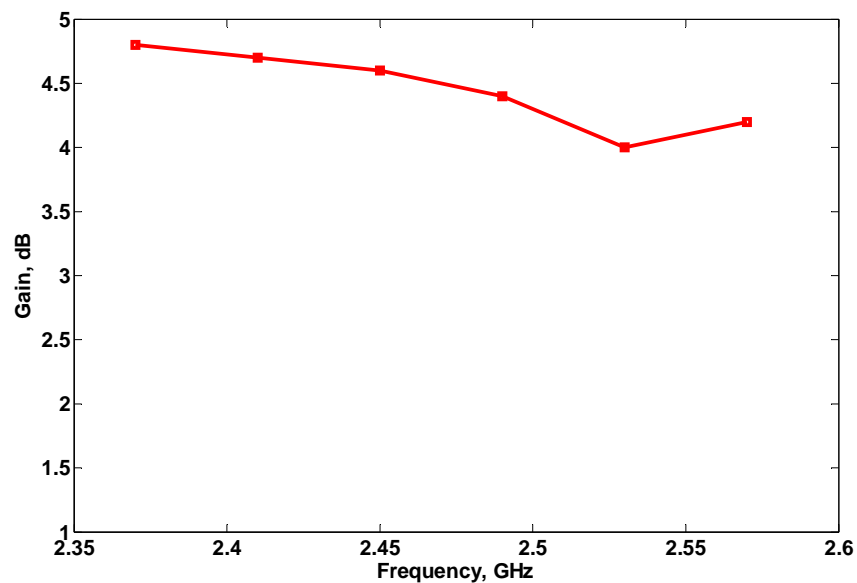
(b)

Figure 4-31 Measured radiation characteristics of modified inverted L antenna. (a) Efficiency, (b) Gain.

The average Radiation efficiency is around 55% and it remains more than 50% throughout the 2.4GHz WLAN band, The gain value remains above 4dB throughout the range. The maximum Gain is close to 4.8dBi.

4.5 Conclusions

In this chapter different wearable antenna designs employing high impedance surfaces (HIS) were investigated. For antennas a low profile is one of the important criteria for mass adaptation of wearable antennas. However some antennas, for example the horizontal antenna has poor efficiency when they are designed to be placed closer than $\lambda/4$ above a PEC. In this chapter the design of low profile wearable antenna based on the modified form of monopole antenna defined as inverted L antenna was proposed. The first wearable antenna discussed in this chapter is a two layer design with radiating element on top of a HIS. The input match bandwidth has been shown to be enhanced by introducing non uniformity in the periodic spacing of the HIS elements. This structure was then modified to a single substrate design. The radiating element was integrated in the same layer as the HIS structure elements. The thickness of this modified structure was thus reduced and was shown to have improved performance compared with non uniform HIS structure. After synthesis the prototypes were fabricated and measured. The reflection coefficient (S_{11}) results were in good agreement with the simulated results. The radiation patterns showed the broadside radiation behaviour of these wearable antennas which is important for on body placement of these antennas. The measured radiation efficiency and gain were also quite good for such a small size wearable antennas. The large F/B ratio of 13dB is desirable feature for on body antennas. In short. these compact and low profile wearable antennas can be successfully employed in wearable communication on body systems.

5 WEARABLE PATCH ANTENNAS OVER NON UNIFORM HIGH IMPEDANCE SURFACES

5.1 Introduction

When compared to small ceramic antennas for example dielectric resonator chip antennas, that have high dielectric constants, fabric antennas suitable for integration onto and into clothing tend to have low relative permittivity. Therefore the footprint of microstrip type antennas with their ground plane parallel to the body can be larger than desired particularly at lower frequencies. However, in the frequency ranges discussed in this research the thickness of a printed planar antenna is less of a problem since many garments can have thickness of up to typically 10mm depending on the use of the clothing. Another emerging trend among garments is their multi layer construction. These two factors provide exciting new opportunities for wearable antenna designs based on multilayer topology.

The microstrip patch antenna is a one type of an antenna that can benefit from the use of multilayer topology for wearable applications. Patch antennas have been used in wearable applications [9, 24]. These designs showed the viability of patch antennas using textile fabrics as components. However because of the effects of the body on antennas in close proximity, such as resonant frequency shift and power absorption, a relatively large ground plane may be required to reduce near field interaction. The use of High Impedance Surfaces (HIS) has been shown to mitigate these effects without requiring a large ground plane [137].

In chapter 4 enhancements in wearable antenna performance due to the use of non uniform High Impedance Surfaces (HIS) were discussed. In this chapter the same improvements to a flexible wearable patch antenna were applied. It started with the design and simulation of simple patch antenna for 2.4GHz WLAN band. Then using a multilayer design an HIS under the patch antenna was introduced. The performance enhancement related to

impedance bandwidth, gain and backward radiation will be discussed. It has been seen that loading of a flexible patch antenna by a HIS detunes the antenna by shifting the resonant frequency downward. This effect supports miniaturization of patch antennas.

Then in the final design stage the non uniformity in the HIS design and resultant changes in antenna performance will be discussed.

5.2 Wearable Patch Antenna for 2.4GHz WLAN Applications

Figure 5-1 shows the geometry of a textile antenna for WLAN band (2.4GHz to 2.484 GHz).
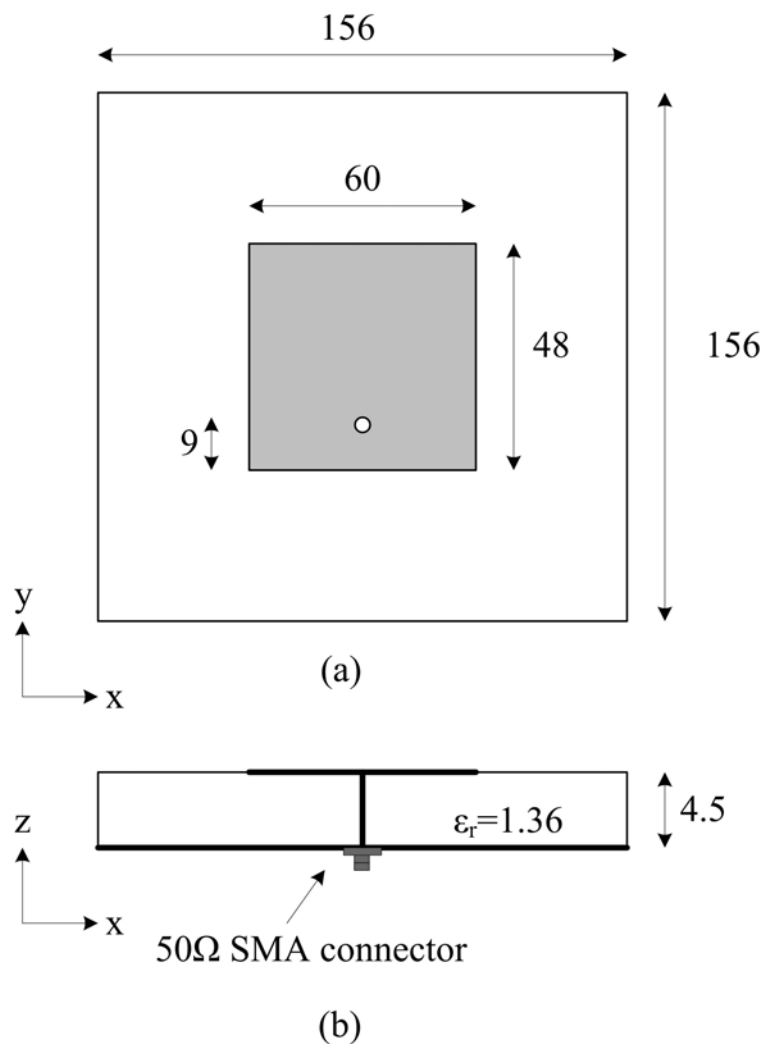
Figure 5-1 Wearable Patch Antenna. (a) Top view, (b) Cross view.

Note: All dimensions in millimetres (not to scale)

The ground plane size was $156mm \times 156mm$ and was chosen to accommodate 6 unit cells of HIS which would be integrated later in the design cycle. The patch antenna size was calculated to be $48mm \times 60mm$ for resonance at 2.4GHz WLAN band. The patch was modelled on a 4.5mm felt substrate. The patch was fed by probe. The feeding position was optimised for the best impedance match to 50Ω source. The simulated reflection coefficient (S_{11}) is shown in Figure 5-2.
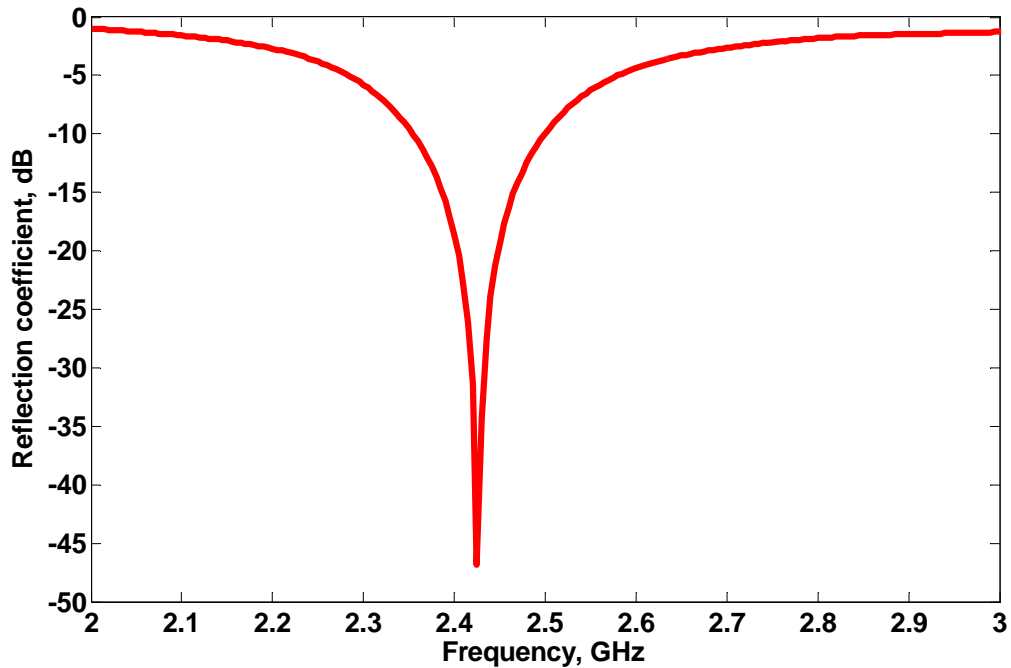
Figure 5-2 Wearable Patch antenna simulated reflection coefficient (S_{11}).

The antenna has the minimum S_{11} of -46dB at 2.42GHz. The impedance bandwidth for $S_{11} <$ -10dB is 140MHz from 2.35GHz to 2.49GHz. The simulated antenna gain was 8.9dBi and the back lobe was -19dB relative to the front lobe.

5.3 High Impedance Surface Using Square Patches

In the next High impedance surface (HIS) using square patches was designed and simulated. It started with the analysis of a single unit cell of patch HIS. The width of patch was 24mm while the gap was chosen 1mm. Thus total size of the unit cell was 26mm. Figure 5-3 showed the reflection phase of patch HIS (unit cell shown in inset).
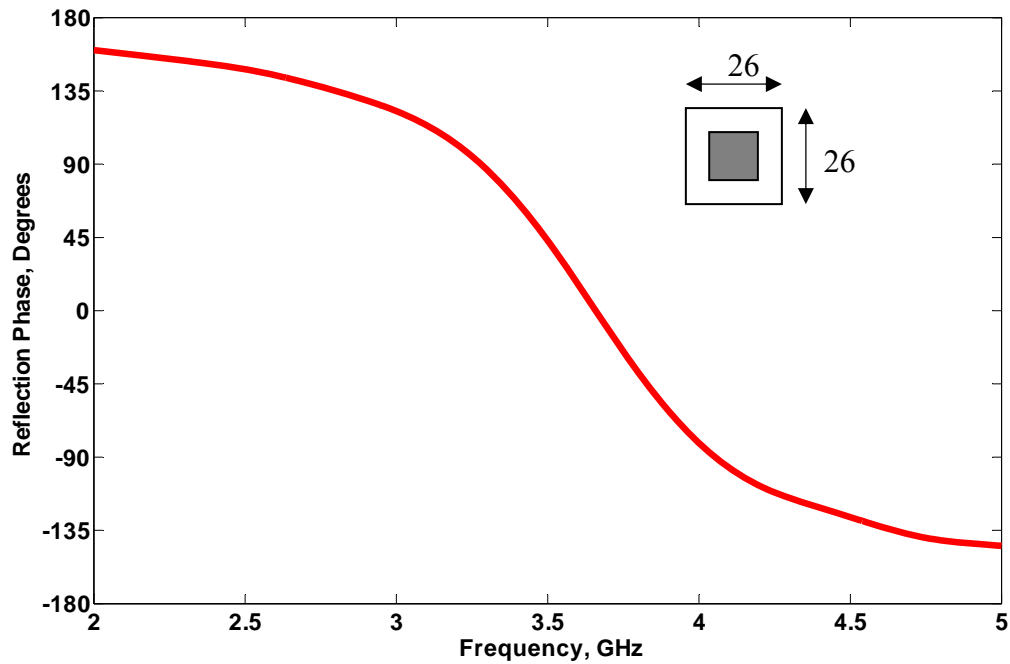
Figure 5-3 Square Patch HIS reflection phase with the unit cell shown in inset.

The zero degree reflection phase frequency is 3.5GHz. The ±90 degree bandwidth is from 3.2GHz to 4 GHz. The unit cell reflection phase result corresponds to infinite periodic structure however the behaviour of finite cell periodic structure was not much different from this as was demonstrated in chapter 4. The 6 unit cells of patch HIS (shown in Figure 5-4) were then combined to create a finite HIS to be integrated with the patch antenna discussed in the next section.

5.4 Wearable Antenna on Top of Patch Based Uniform HIS

The six unit cells of patch HIS were then integrated with the main rectangular patch antenna. For fair comparison the total thickness of the antenna was taken to be the same as for the conventional patch antenna discussed in section 5.2. For this purpose two layers were selected. The bottom layer was 3mm thick and 6 unit cells of patch HIS were modelled on this layer. The top layer was 1.5mm thick and rectangular patch antenna was modelled on this layer. The rectangular patch was fed by 50Ω SMA connector at the best impedance match point. The complete layout is shown in Figure 5-5.
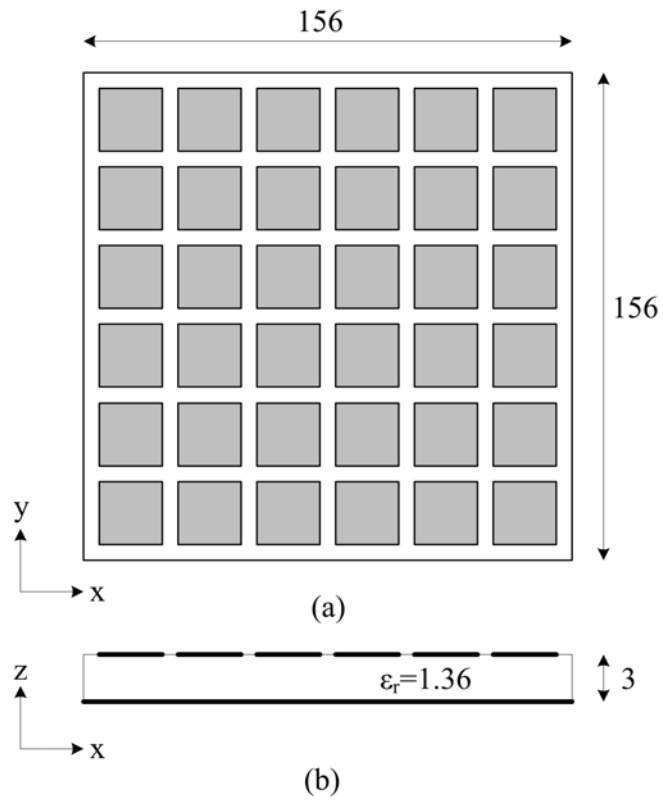
Figure 5-4 HIS consisting of six unit cells. (a) Top view, (b) Cross view.
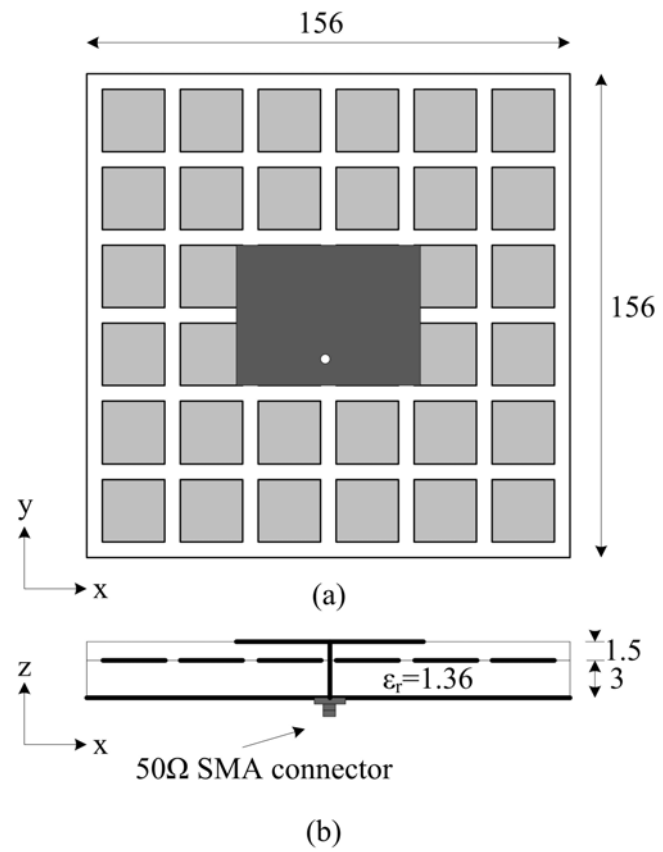
Figure 5-5 Patch antenna on top of HIS. (a) Top view, (b) Cross view.

The simulated reflection coefficient (S_{11}) result is shown in Figure 5-6. The antenna was resonant at 2.38GHz corresponding to minimum S_{11}. By integration of the HIS the resonant frequency has shifted down from 2.42GHz to 2.38GHz. The -10dB bandwidth was from 2.30GHz to 2.45GHz $\cong$144MHz. The simulated antenna gain was also increased from 8.9dBi to 9.4dBi while the backward radiation was decreased from -19.4dB to -21.2dB.
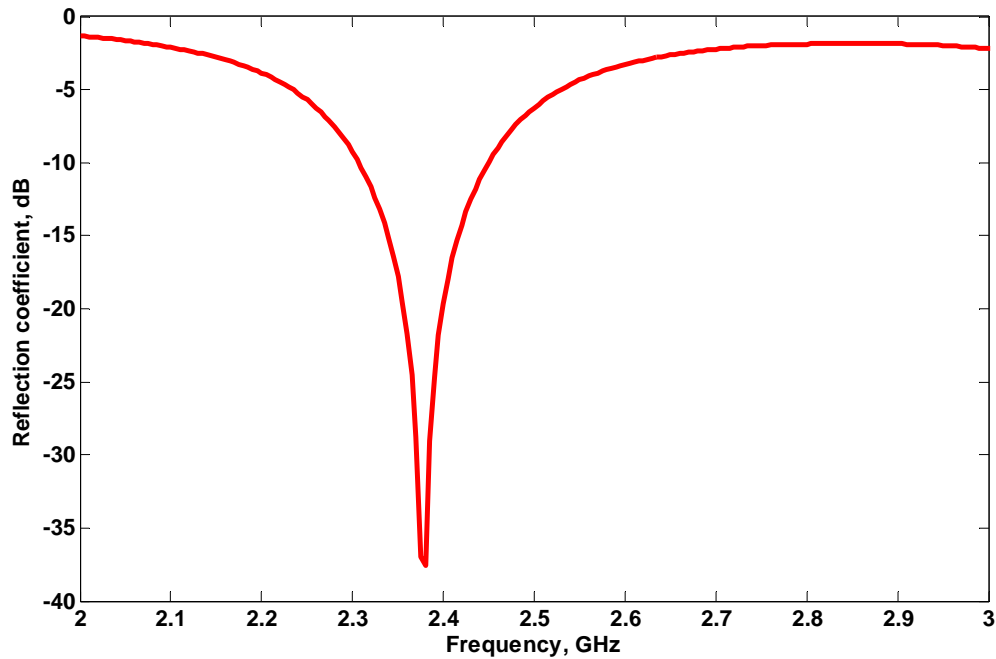
Figure 5-6 Simulated reflection coefficient (S_{11}) for wearable antenna over patch HIS.

The decrease in resonant frequency can be explained as follows. The impedance of patch antenna changes from capacitive below resonance to inductive above resonance as frequency increases [138]. While as discussed in Chapter 2 Section 2.4 HIS behaviour is equivalent to parallel LC circuit. So its impedance changes from inductive to capacitive as frequency increases. Below the resonant frequency the capacitive reactance of conventional patch antenna is compensated by the inductive reactance introduced by the nearby HIS. As a result the patch antenna resonates at a lower frequency. This decrease in resonate frequency can help in miniaturisation of patch antenna.

5.5 Wearable Antenna Over Non Uniform HIS

With the enhanced performance achieved using non uniformity concept in Chapter 2 non uniformity was applied to the patch HIS to see its effect on a patch antenna performance. The width of the patch was kept constant while the gap between the patches was varied from the centre towards the edge of the structure. The non uniform HIS layout is shown in the Figure 5-7.
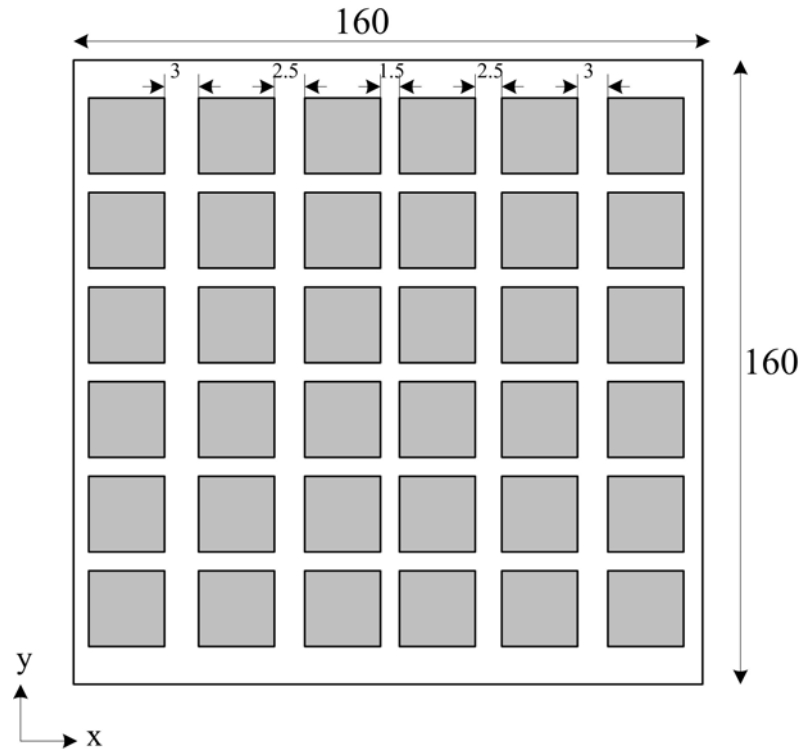
Figure 5-7 Non Uniform patch HIS using 6 unit cells.

Note: All dimension in millimetres (not to scale)

The non uniformity was introduced along one direction (x axis in Figure 5-7), only while the distance between the patches was the same along the y axis. The patch antenna was then simulated on the top of this non uniform HIS using the same design as in Figure 5-5. The parametric study was carried out on the gap between patches of HIS. The simulated S_{11} is shown in Figure 5-8 for the optimum gaps between the patches shown in Figure 5-7.

The antenna resonant frequency corresponding to minimum S_{11} was 2.34GHz which was lower as compared with the uniform HIS (2.38GHz). The -10dB bandwidth was from 2.26GHz to 2.41GHz. The simulated antenna gain was 9.5dBi while the backward

radiation was -21.2dB relative to front lobe. These results showed that non uniform HIS can help further reduce the resonant frequency of patch antenna and also marginally increase the gain.
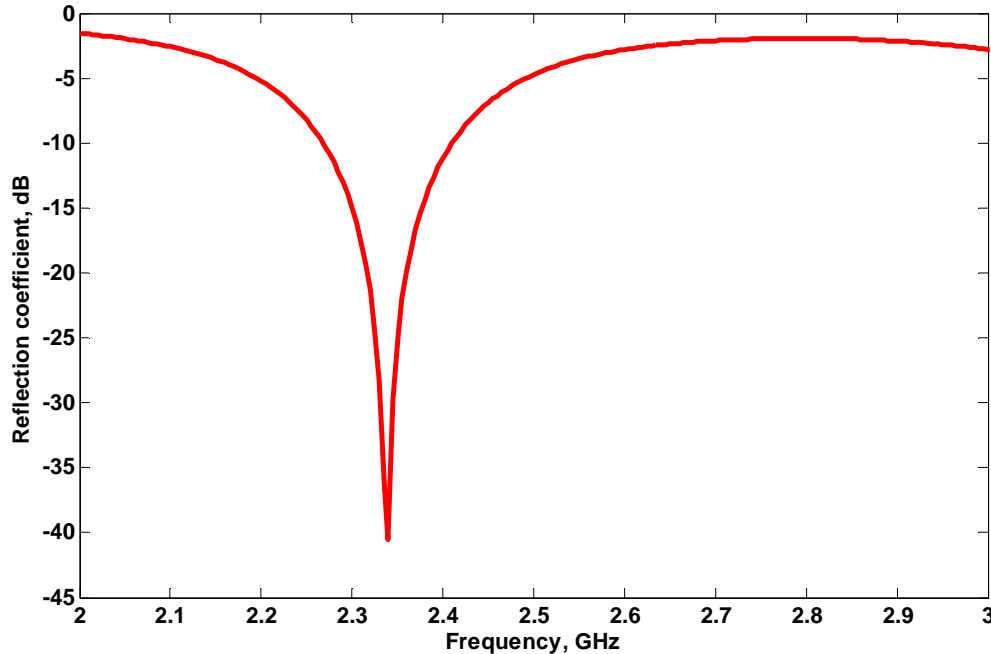
Figure 5-8 Simulated reflection coefficient (S$_{11}$) of wearable antenna over non uniform HIS.

5.5.1 Wearable Antenna Over Non Uniform HIS Using 4×4 Unit Cells

The total size of wearable antenna using 6×6 cells was 165mm×165mm. In order to reduce this size and also to confirm the validity of design idea 4×4 unit cells HIS was also designed. To show the comparison between antenna performance 3 designs were modelled: (1) Patch antenna without any HIS, (2) patch antenna with uniform HIS and (3) patch antenna with non uniform HIS.

The layout of uniform and non uniforms HIS using 4×4 unit cells is shown in Figure 5-9. The total size of both HIS designs was 130mm×130mm. The rectangular patch antenna 48mm×60mm was modelled on top of these HIS structures. The gap between patches for the uniform case was kept 2mm throughout. While for the non uniform HIS the gap between inner patches was kept 2mm while the gap between the outer patches was parametrically varied for the best result in terms of S$_{11}$.

The simulated S_{11} result for the three designs of wearable patch antenna (Figure 5-10) is shown in Figure 5-11.
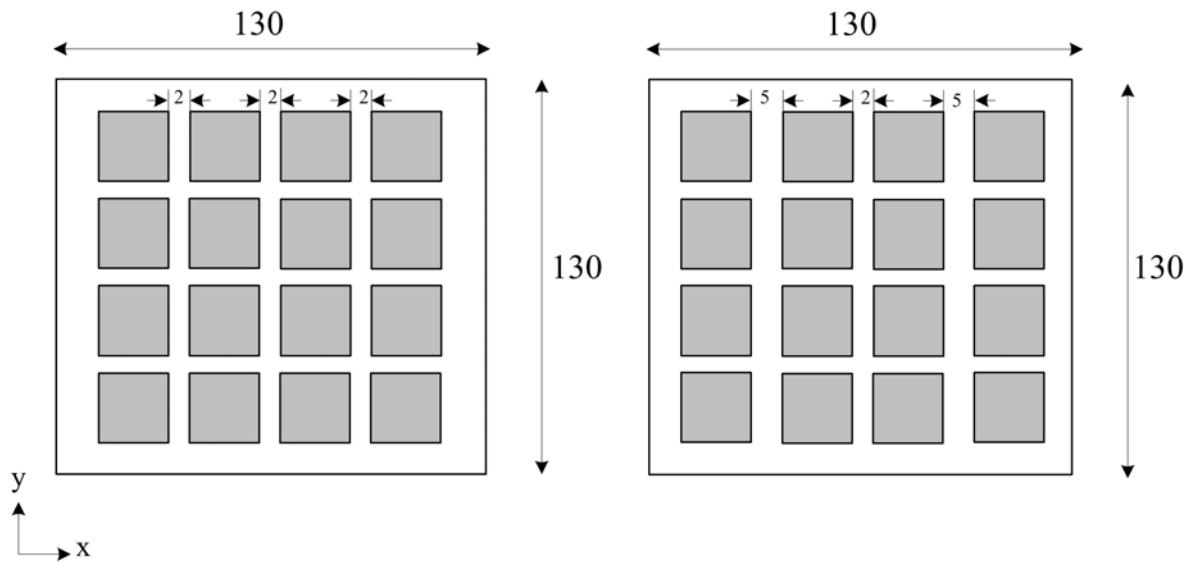
Figure 5-9 Reduced size 4×4 unit cell HIS. (a) uniform HIS, (b) non uniform HIS.

Note: All dimensions in millimetres (not to scale)
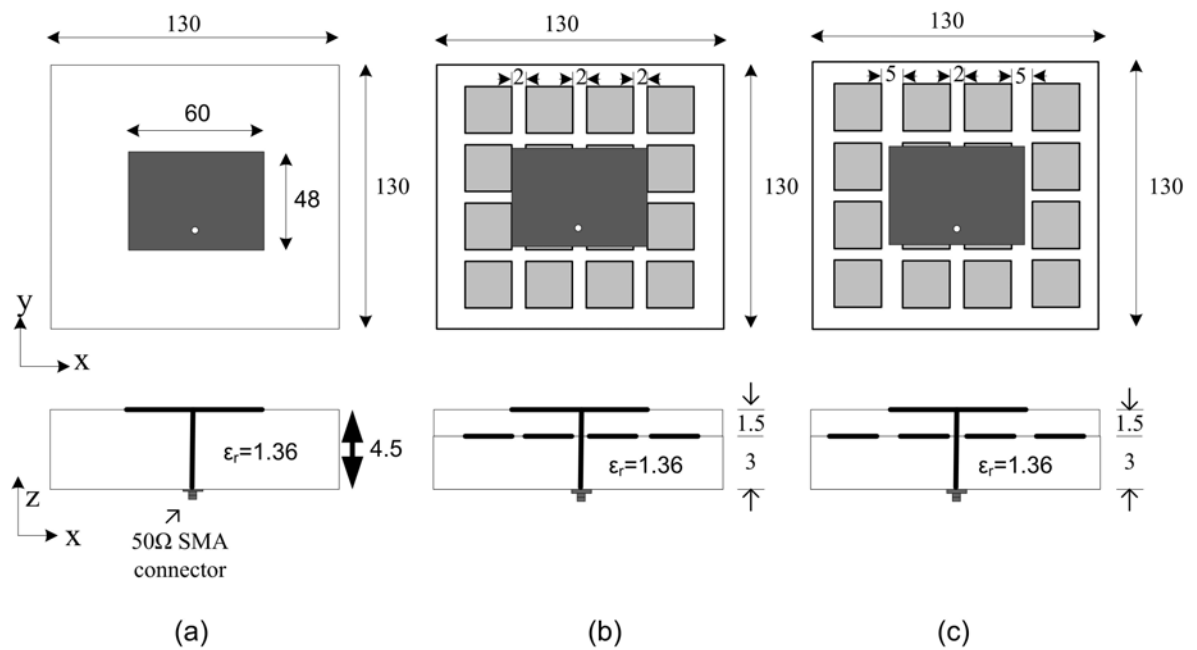
Figure 5-10 Wearable patch antenna layout. (a) Patch antenna only, (b) Patch over uniform HIS, (c) Patch over non uniform HIS.

Note: All dimensions in millimetres (not to scale).
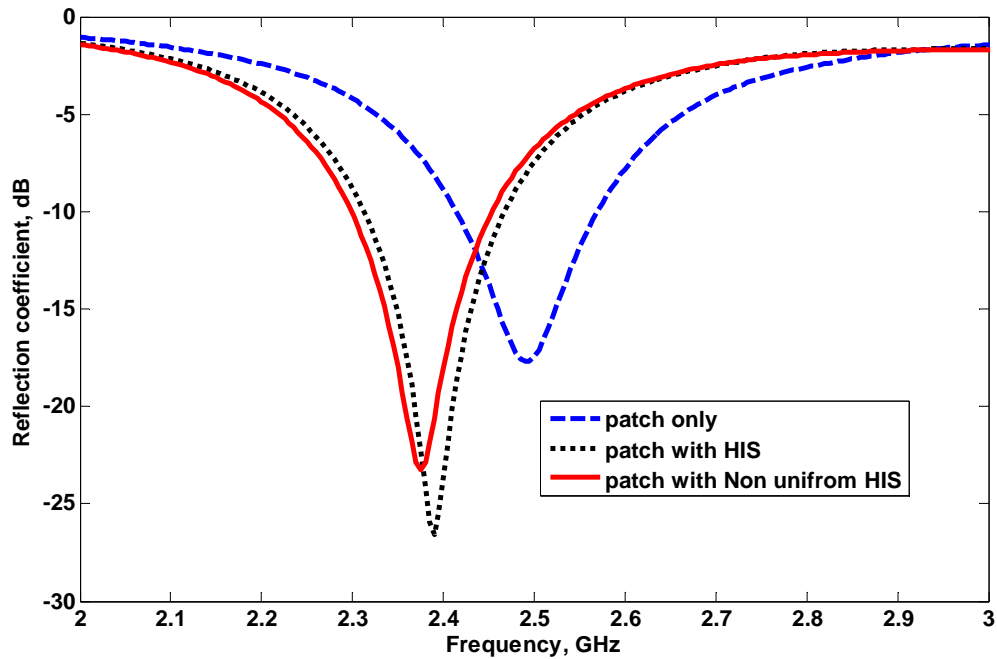
Figure 5-11 Simulated reflection coefficient (S$_{11}$) comparison of patch on different surfaces.

Due to reduced ground plane size the patch antenna without HIS resonates at a higher frequency as compared to that with larger ground plane [118]. The resonant frequency corresponding to minimum S$_{11}$ of patch without HIS was about 2.49GHz. The S$_{11}$ < -10dB bandwidth was 153MHz starting from 2.41GHz to 2.56GHz. The simulated gain at the centre frequency (2.49GHz) was 8.7dBi. The backward lobe was -19dB relative to front lobe.

For the patch antenna on top of uniform HIS the minimum S$_{11}$ frequency shifted down to 2.39GHz. The S$_{11}$ < -10DdB bandwidth was 155MHz starting from 2.31GHz to 2.46GHz. The simulated gain at the centre frequency (2.39GHz) was 9dB with backward lobe at -21.2dB relative to front lobe.

For the patch antenna on top of non uniform HIS the resonant frequency corresponding to minimum S$_{11}$ further shifted down to 2.36GHz. The impedance bandwidth corresponding to S$_{11}$ < -10dB was 155MHz starting from 2.28GHz to 2.44GHz. The simulated gain at 2.36GHz was 9.2dBi with backward lobe at -21.1dB relative to front lobe. In order for non uniform HIS based patch to resonate at the same frequency as the patch without HIS the

size of the patch has to be decreased to 44mm×56mm. This is about 15% reduction in size of patch antenna.

These observations showed that using HIS the resonant frequency can be manipulated without changing the main patch antenna dimension. Also by introducing non uniformity to the HIS the resonant frequency can be further shifted down without changing the overall size of the complete antenna. This feature can be used for reducing the size of the patch antenna for the same operational frequency. The gain of the antenna was also improved due to antenna interaction with the patch HIS. The backward lobe was also decreased which is desirable feature for wearable antennas.

5.6 Measured Characteristics of Wearable Patch Antenna Using Non Uniform HIS

5.6.1 Fabrication

To confirm the design idea the patch antenna along with non uniform HIS on polyester copper fabric (Taffeta) was fabricated. The conventional PCB etching technique was employed for this purpose as before. The non uniform HIS layer was fixed on top of 3mm thick felt substrate using adhesive spray. On the bottom side of this felt, polyester copper was attached to function as ground plane of antenna. Another felt substrate with 1.5mm thickness was then glued to the top of this structure. Finally the patch layer was attached to the 1.5mm felt. The 50Ω SMA connector was then soldered to this antenna structure to feed the antenna with the excitation source. The fabricated prototype wearable antenna is shown in Figure 5-12.

.   (a)   (b)

                           (c)   (d)
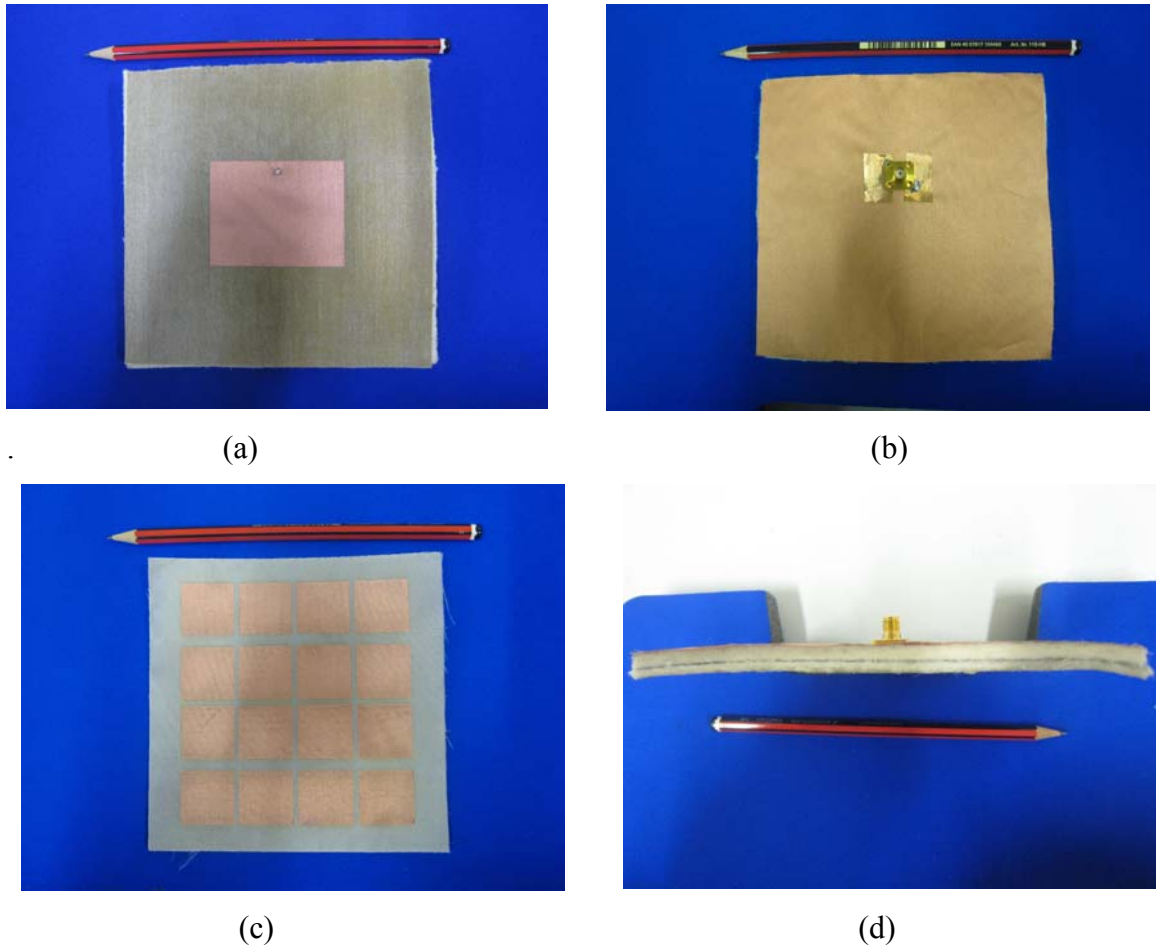
Figure 5-12 Prototype HIS based wearable patch antenna, (a) top view, (b) bottom view, (c) middle layer showing HIS patches, (d) side view.

5.6.2 Measured Reflection Coefficient (S_{11})

The fabricated antenna was connected to a calibrated VNA and measured along with simulated S_{11} results are shown in Figure 5-12. As can be seen the measured resonant frequency was shifted down to 2.46GHz as compared to the simulated resonant frequency of 2.5GHz. One possible reason for this discrepancy could be the small unavoidable air gap between the two layers when they are glued together. This also increased the overall thickness of the built antenna. These two factors along with fabrication tolerance and slight miss alignment between the two glued layers create slight shift in the S_{11} results.   The minimum S_{11} is at 2.46GHz. The input impedance bandwidth corresponding to $S_{11} < -10$dB is from 2.34GHz to 2.62GHz $\equiv$280MHz which covers the desired 2.4GHz WLAN operating band.
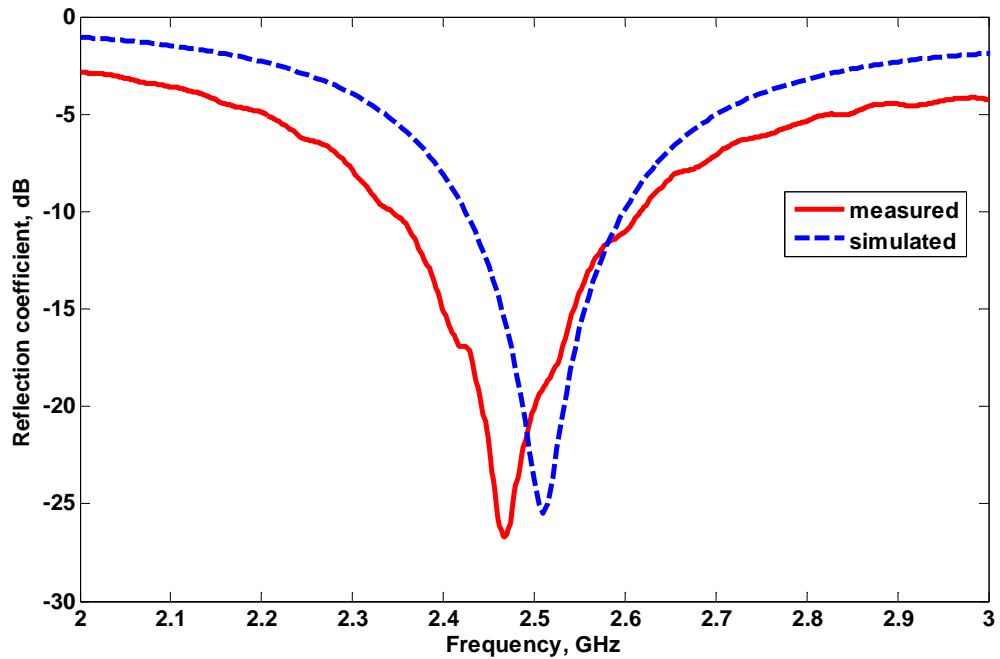
Figure 5-13 Measured and simulated reflection coefficient (S₁₁) of wearable HIS based wearable patch.

5.6.3   Measured Radiation Characteristics

The radiation performance of prototype antenna was measured in an anechoic chamber. The standard horn antenna was used as reference to measure the gain, efficiency and radiation patterns of prototype antenna. The measured E-plane (yz plane see Figure 5-10) and H-plane (xz plane see Figure 5-10) radiation patterns are shown in Figure 5-14.

The antenna has the desired maximum radiation in the broadside while minimum radiation in the backward direction. The 3dB half power beam width (HPBW) in E-plane is about 40º and the back lobe is at -20dB relative to the main lobe. The H-plane pattern also showed broadside maximum radiation however the 3dB HPBW is about 55º which is broader then E-plane. The back lobe is at -22dB relative to main lobe.

E-Plane (yz Plane)

(a)

H-Plane (xz Plane)

(b)
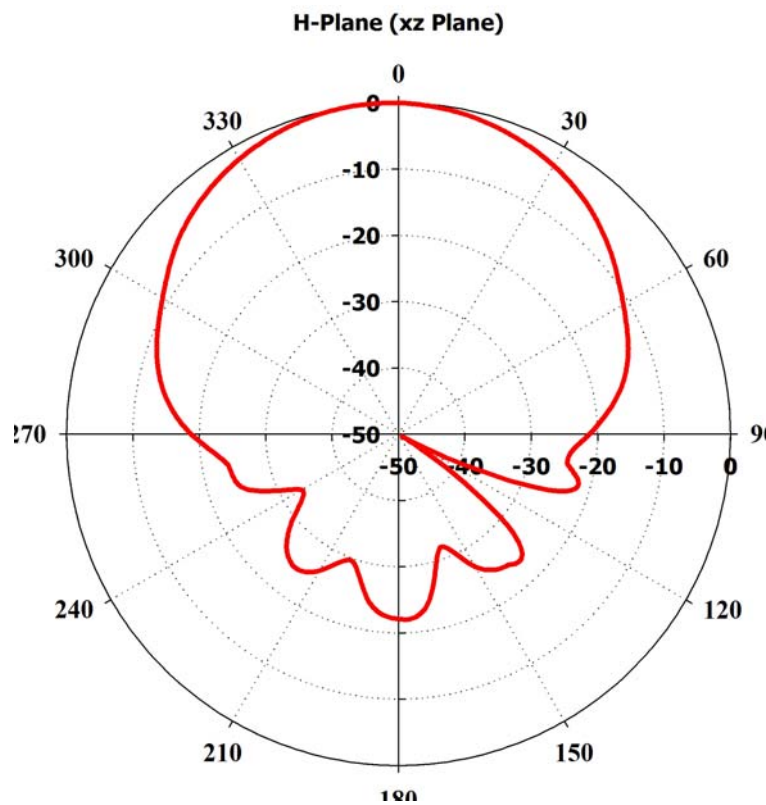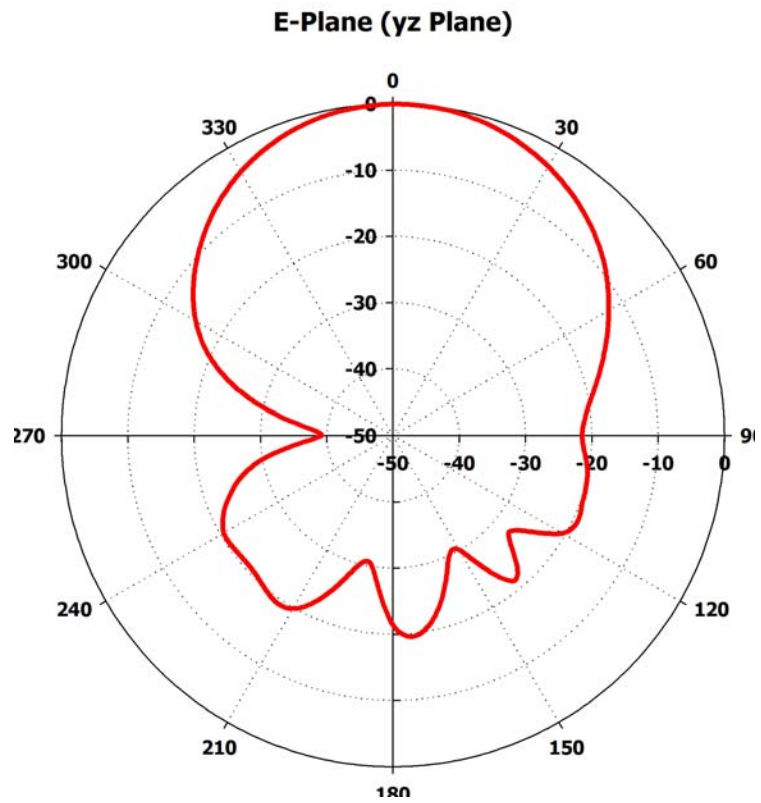
Figure 5-14 Measured radiation patterns of HIS based wearable patch antenna, (a) E-plane, (b) H-plane.

The gain and radiation efficiency were also measured over the operating frequency range. The measured results are shown in Figure 5-15.
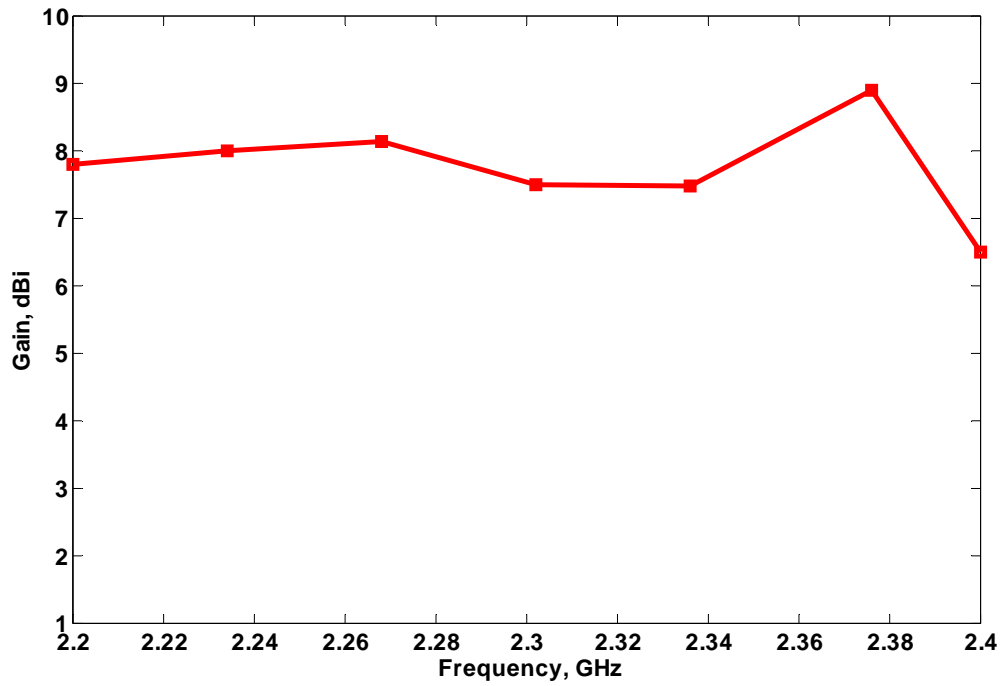
(a)
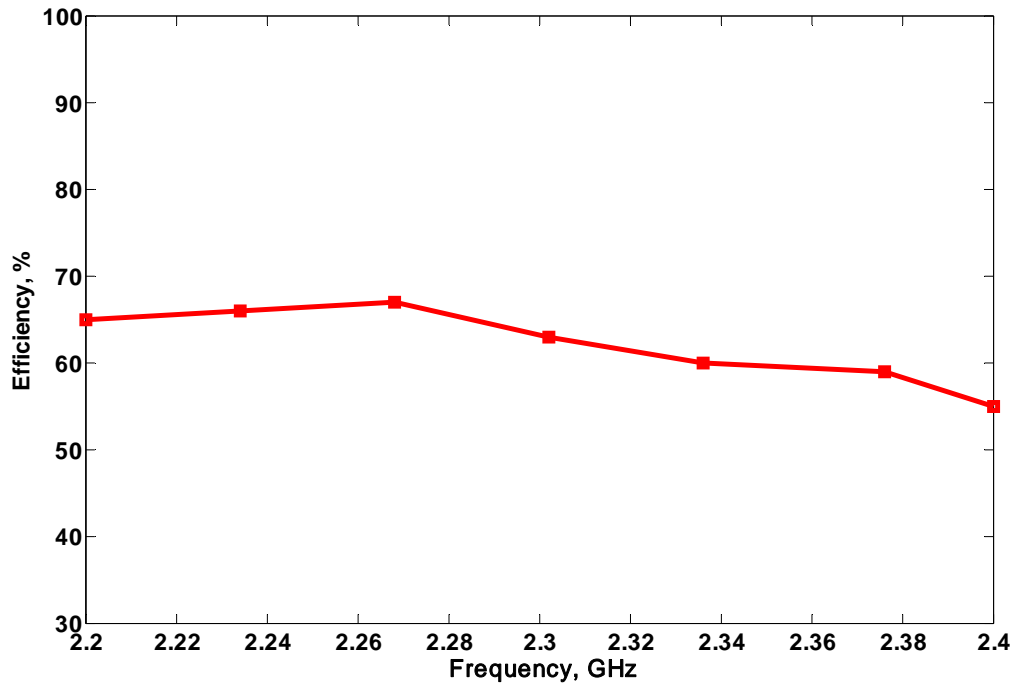
(b)

Figure 5-15 Measured radiation characteristics of HIS based wearable antenna. (a) Gain, (b) Efficiency.

The gain varies between 7.9dBi and 9dBi with an average gain of 8dBi over the operating frequency range. The efficiency is in between 55% to 68% over the same operating range.

5.7 Conclusions

In this chapter the integration of HIS with the rectangular patch antenna was investigated. The HIS was placed underneath the patch antenna. The close interaction between the patch and HIS desirably affects the performance of patch antenna. The patch antenna resonated at a lower frequency as compared to normal patch. This was due to the coupling between HIS patches and radiating patch that changed the impedance behaviour of antenna and shifted down its resonance. This fact can be used in miniaturization of patch antennas. The input match bandwidth was also enhanced as well as gain and backward radiation.

The concept of non uniformity to HIS structure was also applied to see its behaviour on patch antenna performance. It was observed that resonant frequency can be further reduced by introducing non uniform unit cells in the overall HIS structure. Non uniformity had been introduced only along one direction while keeping uniform cells along the other direction. The impedance bandwidth was also improved although not significantly.

Finally a prototype of wearable patch antenna using non uniform HIS structure was fabricated. The fabricated antenna was measured to validate the design concept. The measured results were observed to be in good agreement with the simulated ones.

6 WEARABLE ANTENNAS ON BODY PERFORMANCE

6.1 Introduction

The human body affects the antenna performance in the following way : (1) the lossy tissues absorb the radiated power and hence degrades radiation efficiency and gain, (2) the high permittivity of tissues changes the guided wavelength and hence detune the resonant frequency (3) due to proximity of human body the antenna input impedance changes and hence degrades the impedance matching achieved for free space design.

Apart from these detrimental effects occurring due to close interaction between antenna and human body there are some other factors that can affect the radiation performance of wearable antennas. Typically flexible antennas of the type discussed in this thesis will suffer some type of planar distortion in their dimensions due to conformability with the surface of the body. For example a wearable antenna may be placed on curved part of the body like arm or leg. Previously researchers have noted that bending can change the operating performance of an antenna [70, 70, 139].

To examine the wearable antenna performance on the dynamic body environment the wearable inverted L antennas (Chapter 4, Section 4.3 and Section 4.4) and wearable patch antenna (Chapter 5, Section 5.6) were measured for the effects of bending in two planes (E-plane and H-plane) and in close proximity to human body. The analysis will be focused on the input match variation under these dynamically changing situations. The radiation characteristics when these antennas are bent and when close to human body will also be discussed. These measurements will be discussed in detail for all the three wearable antennas designed in this research.

6.2 Wearable Inverted L Antenna Over HIS

The measured performance of wearable inverted L antenna over HIS was investigated in detail in Section 4.3 of Chapter 4. However the results assumed that antenna was always planar and there were no interfering objects in the vicinity of antenna. In other words the results were valid for free space environment. In this section antenna under real life situations will be tested for their performance. Specifically the reflection coefficient (S_{11}) result under bending condition for both E-plane and H-plane bending as well as on human body will be presented. The radiation pattern shape under bending condition will be explored to observe the change in radiation performance and the limitation for any bending plane.

6.2.1 Input Match Results Under Bending Conditions

For these experiments two polystyrene foam cylinders with diameters of 70mm and 140mm were used. These dimensions are typical of the human body arm and leg respectively. Since the permittivity of polystyrene foam is close to that of free space and that the size of the cylinders was large compared to the AUT it is reasonable to assume that results showed effect of bending in isolation. For linearly polarized antennas the effect on antenna performance is different depending, along which of the two principal planes namely E-plane and H-plane, the antenna is bent [70]. So the input matching and impedance bandwidth were measured for bending along both of these planes. Figure 6-1 shows the measurement setup for antenna bending using foam cylinders. The whole setup was placed inside the lab where it was insured that there were no interfering objects in front of the antenna. The height of the antenna from the ground was also quite high to reduce the effect of the ground on antenna performance. As the measurements were carried out in the same place for all test scenarios it is reasonable to assume that if there was any interference its effect would have been observed on all measurements. So any change in measured values would be due to the effect of bending. The antenna measured was the inverted L antenna integrated with HIS on a felt substrate. The total dimension of antenna was 65mm × 65mm×4.5mm. Cello tape was used to fix antenna conformably on the foam cylinder. As a result the edges of the antenna were deformed slightly. The results are therefore valid for the worst possible bending on the cylinder diameters used in this setup.

Figure 6-1 Measurement setup for bending condition. (a) H-plane bending, (b) E-plane bending

The E-plane and H-plane bending results along with the non bending results for comparison purpose are shown in Figure 6-2. As can be seen the bending in general reduced the input match bandwidth.
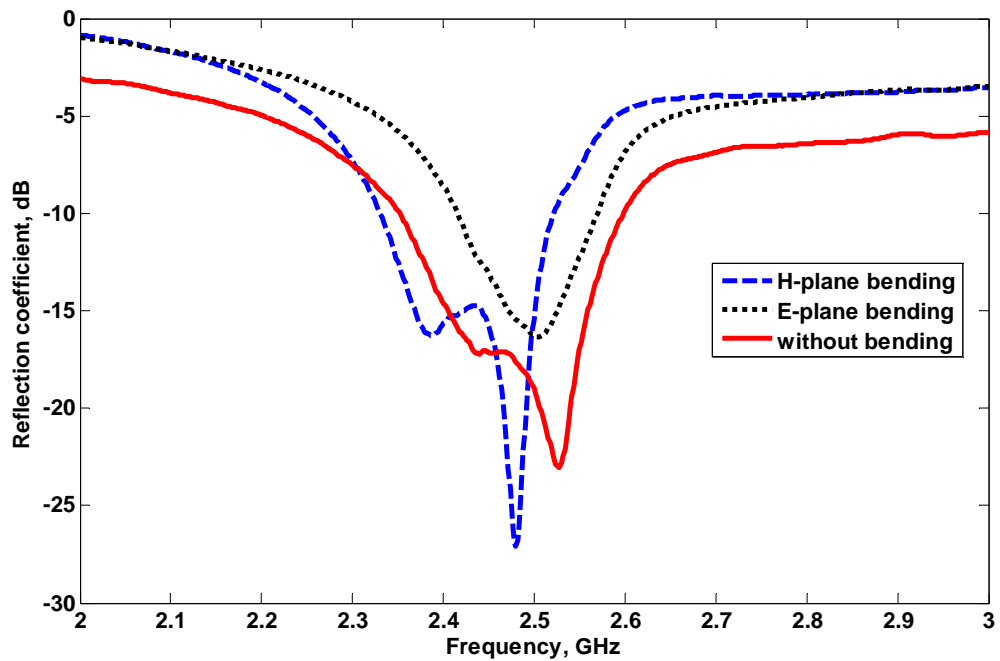
(a)
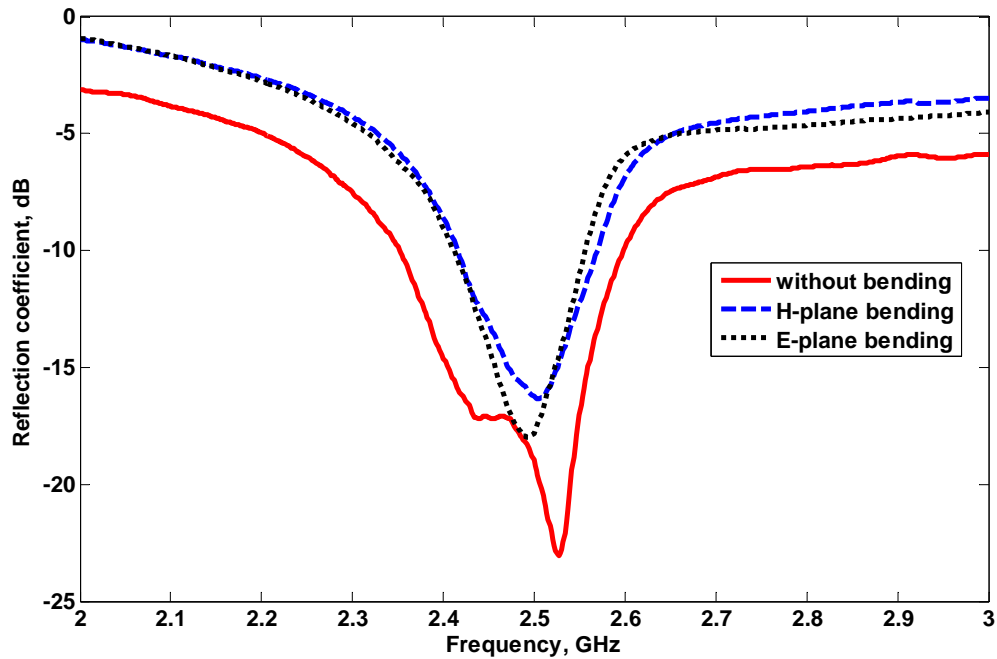
(b)

Figure 6-2 Measured reflection coefficient (S_{11}) results for inverted L over HIS wearable antenna bending on (a) 140mm cylinder (b) 70mm cylinder

The upward shift in operating frequency band for E-plane bending while downward shift for H-plane bending was observed on 140mm foam cylinder. The input match bandwidth was reduced from 2.35GHz-2.6GHz for the unbend case to 2.33GHz-2.52GHz for H-plane bending and 2.41GHz-2.57GHz for E-plane bending. Thus the E-plane bending is more significant for correct behaviour of this wearable antenna. When the antenna was bent around a smaller diameter 70mm cylinder the effect on input match due to E-plane and H-plane bending is almost the same. The H-plane bending input match was 2.4GHz-2.57GHz while E-Plane bending was 2.4GHz-2.55GHz

One possible reason for worst E-plane bending effect on input match is due to the fact that E-plane bending affects the antenna's resonant length. The more the antenna is bent the more the resonant length is reduced and thus adversely affects the antenna's matching. It is important to mention that this antenna was still able to operate in the desired 2.4GHz WLAN band even under bending conditions. This proves the reliability of this wearable antenna when conformed to any curved surface.

6.2.2 Input Match Results on Body

To see the affect of body on input match characteristics of wearable antenna it was measured by placing it close to human body. The measurement setup is shown in Figure 6-3.

Figure 6-3 Measurement setup for on body effect on input match behaviour of inverted L over HIS wearable antenna.

Due to probe fed connector the antenna was placed conformably in the region between arm and chest with the VNA cable coming from behind. Again it was ensured that no other interfering object was there other than the human body.

The measured results for both on body and in free space are shown in Figure 6-4. As can be seen the input match bandwidth has been slightly reduced from 2.35GHz-2.6GHz to 2.4GHz-2.57GHz. Even though the minimum S_{11} at the resonant frequency of 2.5GHz has been improved to -29dB as compared to –23dB for without body case. It is important to mention however that antenna was still able to work in the desired 2.4GHz WLAN band.
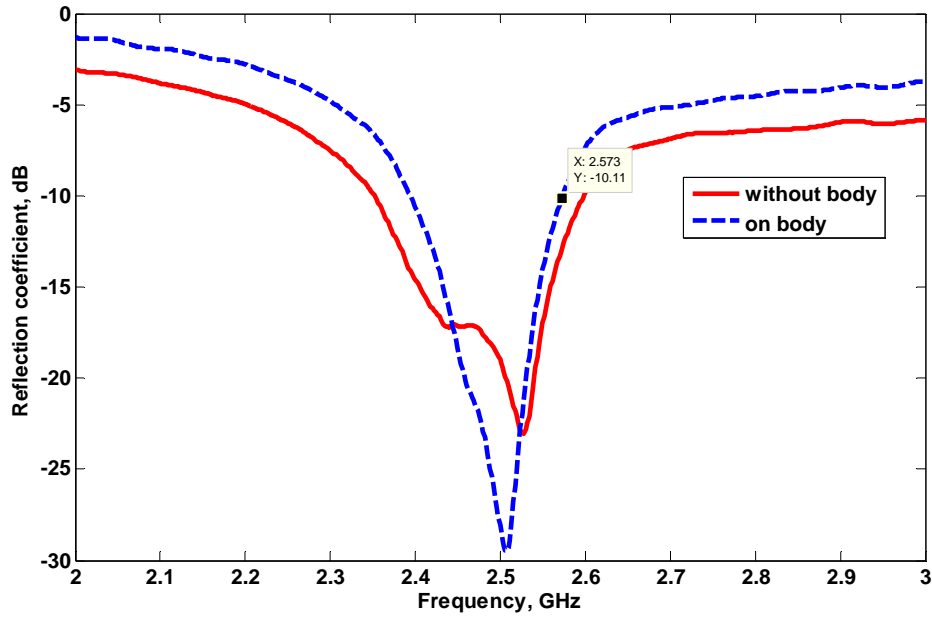
Figure 6-4 Measured reflection coefficient (S_{11}) of inverted L over HIS wearable antenna with and without body

6.2.3 Radiation Pattern Under Bending Conditions

The radiation characteristics under bending conditions were measured in an Anechoic Chamber (Appendix B). The standard AUT (antenna under test) positioner setup in the chamber was modified for this purpose. The 140mm and 70mm diameter polystyrene foams were attached to the positioner using paper tape. A hole was drilled in the cylinders to make space for the connecting cable coming from the VNA. The antenna was then conformably fixed on the cylinders using cello tape. The measurement setup is shown in Figure 6-5.

           (a)   (b)
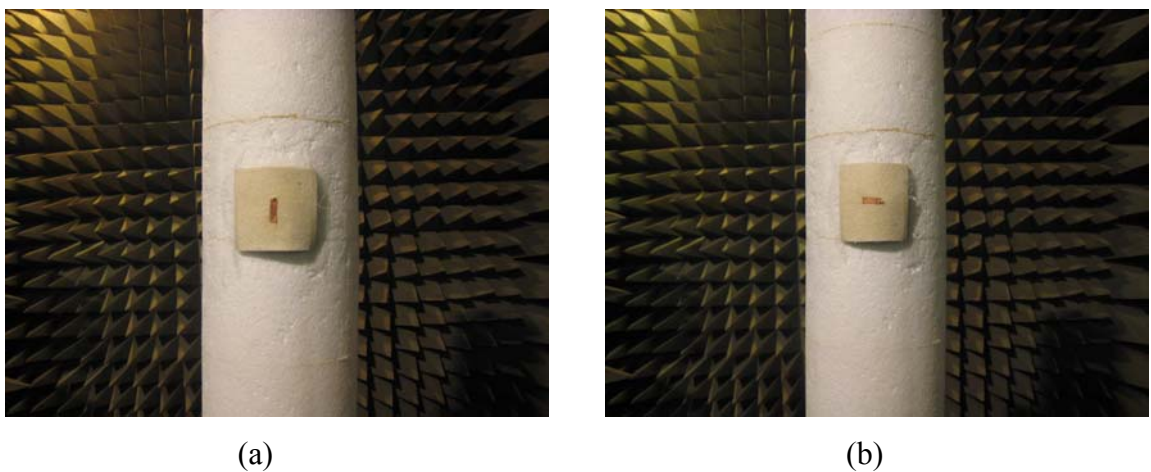
Figure 6-5 Measurement setup in an Anechoic Chamber for radiation characteristics under bending condition. (a) H-plane bending, (b) E-plane bending.

(a)   (b)

Figure 6-6 Measured radiation pattern for H-plane bending. (a) E-plane, (b) H-plane.

(a)   (b)

Figure 6-7 Measured radiation patterns for E-plane bending. (a) E-plane, (b) H-plane.

115

The radiation patterns were measured for two orthogonal bending planes (E-plane and H-plane). The measured pattern cuts in E-plane and H-plane for these two bending positions on 140mm and 70mm foam cylinders are shown in Figure 6-6 and Figure 6-7 respectively. The patterns for the unbending case are also plotted to compare the variation in pattern shape. The results show that antenna bending has remarkable effect on radiation characteristics, i.e., radiation pattern shape and gain. It is intuitively clear that antenna bending broadens the radiation pattern in the bending plane which results in a drop of gain. For bending on smaller 70mm diameter this effect is more obvious. For H-plane bending there was not much deviation in pattern shape in relation to the unbending case for both E-plane and H-plane cuts. The antenna maintained its broadside radiation performance under bending condition. Also the 3dB HPBW in H-plane cut was broader as compared to E-plane as was the case without bending. The front-to-back ratio (F/B) in E-plane remained at 10dB while in H-plane it reduced to 8dB on 140mm cylinder and 6dB on 70mm cylinder. Also for H-plane cut under E-plane bending the radiation pattern seemed to be changing to omni directional which is not desirable for on body antennas. It can therefore be concluded that this antenna functions normally under bending condition in general. However, bending along E-plane should be avoided as it affects the directional characteristics of antenna.

6.3 Wearable Inverted L Antenna Integrated with HIS

The measured performance of wearable inverted L antenna integrated with HIS in the same plane was investigated in detail in Section 4.4 of Chapter 4. However the results assumed that antenna was always planar and there were no interfering objects in the vicinity of antenna. In other words the results were valid for free space environment. In this section antenna was tested under real life situations. Specifically the reflection coefficient (S_{11}) result under bending condition for both E-plane and H-plane bending as well as on human body will be presented. The radiation pattern shape under bending condition will be explored to observe the change in radiation performance and the limitation for any bending plane.

6.3.1 Input match results under bending condition

The effect of bending on the S_{11} characteristics of integrated HIS inverted L wearable antenna was also measured. The experimental setup is shown in Figure 6-8. This was the same setup as was used before. Again both E-plane and H-plane bending conditions were measured on 140mm and 70mm foam cylinders. The measured results are shown in Figure 6-9.

(a)   (b)

Figure 6-8 Measurement setup for HIS integrated inverted L wearable antenna. (a) E-plane bending, (b) H-plane bending.

The measured results are given in Figure 6-9 for bending along two different diameters cylinders. The input match bandwidth for S_{11} < -10dB reduced in general compared with the unbending case. The H-plane bending shifted the operating frequency band 2.40GHz-2.61GHz to 2.3GHz-2.55GHz while the E-plane bending was again significant reducing the frequency band even further to 2.3GHz-2.55GHz.

For bending along smaller 70mm diameter the behaviour was not much different. The H-plane bending reduced the input match frequency band to 2.36GHz-2.58GHz while E-plane bending to 2.42GHz-2.57GHz. As observed with the previous antenna the E-plane bending was again most significant. And the reason is the same shortening of resonant length when antenna is bent along E-plane. Overall antenna was able to function in its desired 2.4GHz WLAN band apart from some drift for E-plane bending along smaller

70mm cylinder. These observations suggest that when placing antenna on body its better to align E-plane along the planar part of the body surface.
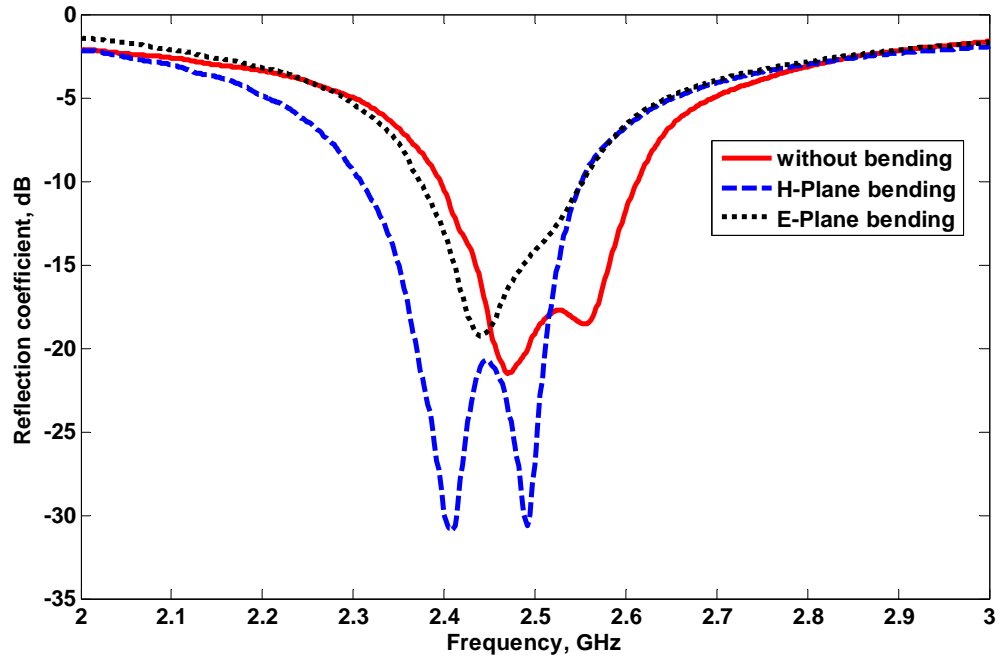
(a)
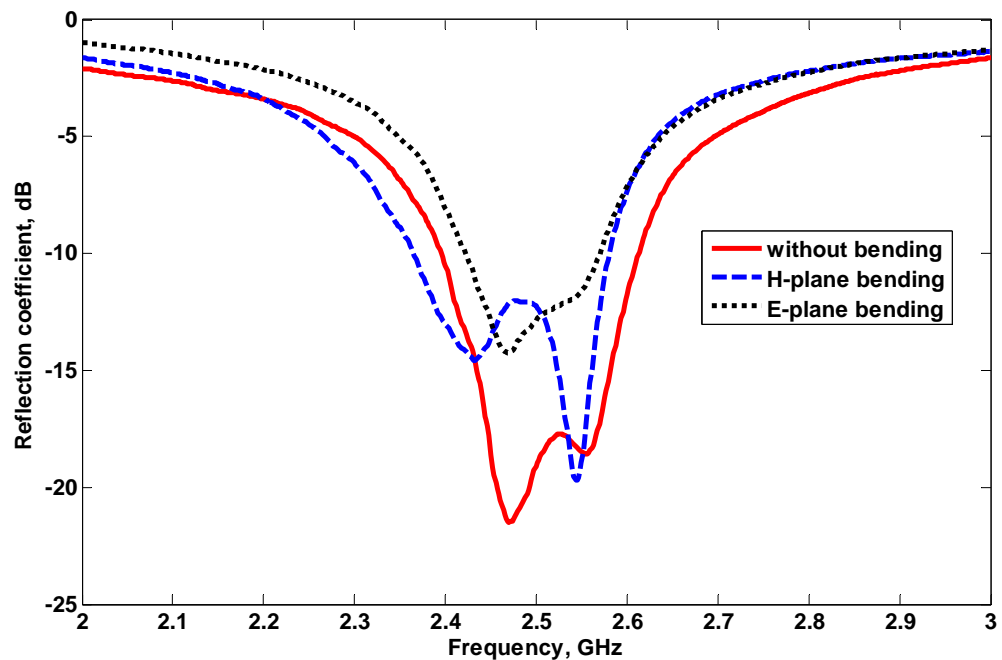
(b)

Figure 6-9 Measured reflection coefficient (S$_{11}$) results for wearable inverted L antenna integrated with HIS bending on (a) 140mm cylinder, (b) 70mm cylinder

6.3.2 Input Match Results on Body

To measure the on body performance of wearable inverted L antenna integrated with HIS the antenna was placed on the human body. The measurement setup is shown in Figure 6-10 while the measured reflection coefficient (S_{11}) behaviour is shown along with the free space result in Figure 6-11.

Figure 6-10 Measurement setup for on body test of wearable inverted L antenna integrated with HIS.
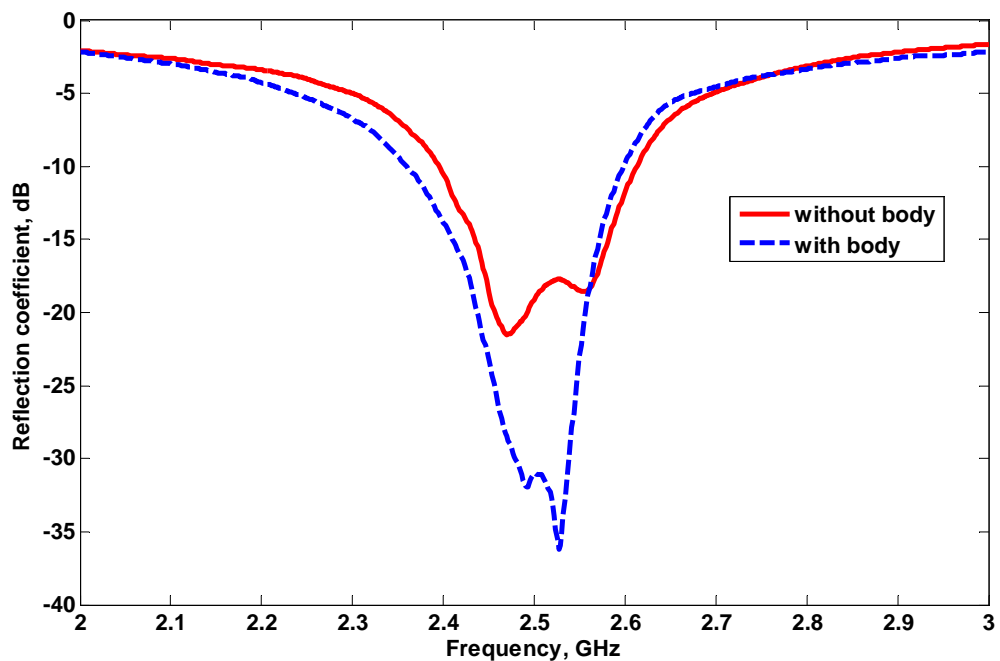
Figure 6-11 Measured reflection coefficient (S_{11}) of HIS integrated inverted L antenna with and without body

As can be seen the S_{11} was slightly affected by the presence of human body. However the input match bandwidth corresponding to $S_{11} < -10$ dB was almost the same as for without the body. The minimum S_{11} value has also improved by almost 15dB. This demonstrates the effectiveness of this design to be insensitive to the presence of human body a desirable feature for wearable antennas.

6.3.3 Radiation Pattern Under Bending condition

The bending measurement setup used for measuring radiation pattern in Anechoic Chamber was the same as before and is shown in Figure 6-12. The antenna was again fixed to the cylinder using cello tape. As a result there was some deforming of antenna at the edges. So the results are valid for the worst scenario bending on the diameter considered. Both orthogonal planes bending were measured. The measured radiation patterns under bent condition along with the normal patterns under unbent condition are shown in Figure 6-13 and Figure 6-14 for H-plane and E- plane bending respectively.

(a)   (b)
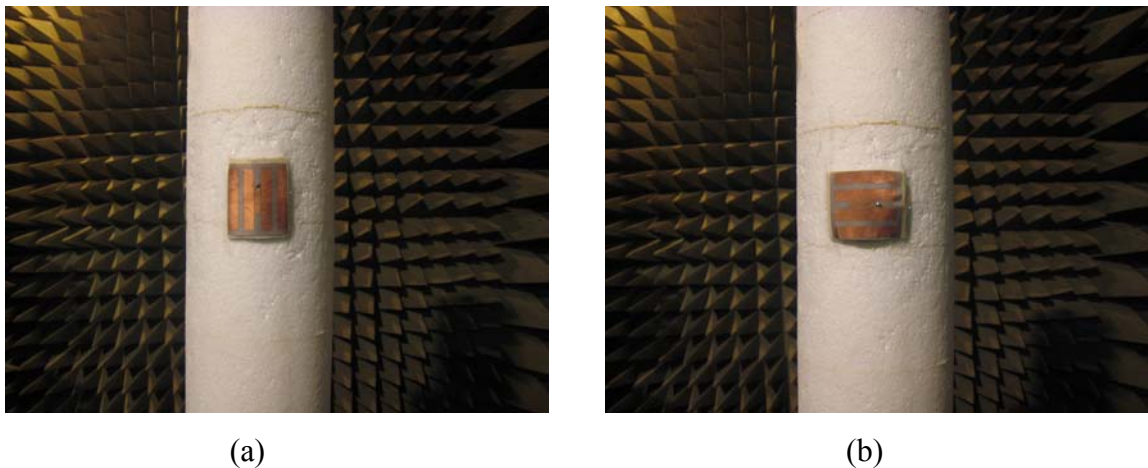
Figure 6-12 Measurement setup in Anechoic Chamber for radiation characteristics of HIS integrated inverted L antenna under bending condition. (a) H-plane bending, (b) E-plane bending.

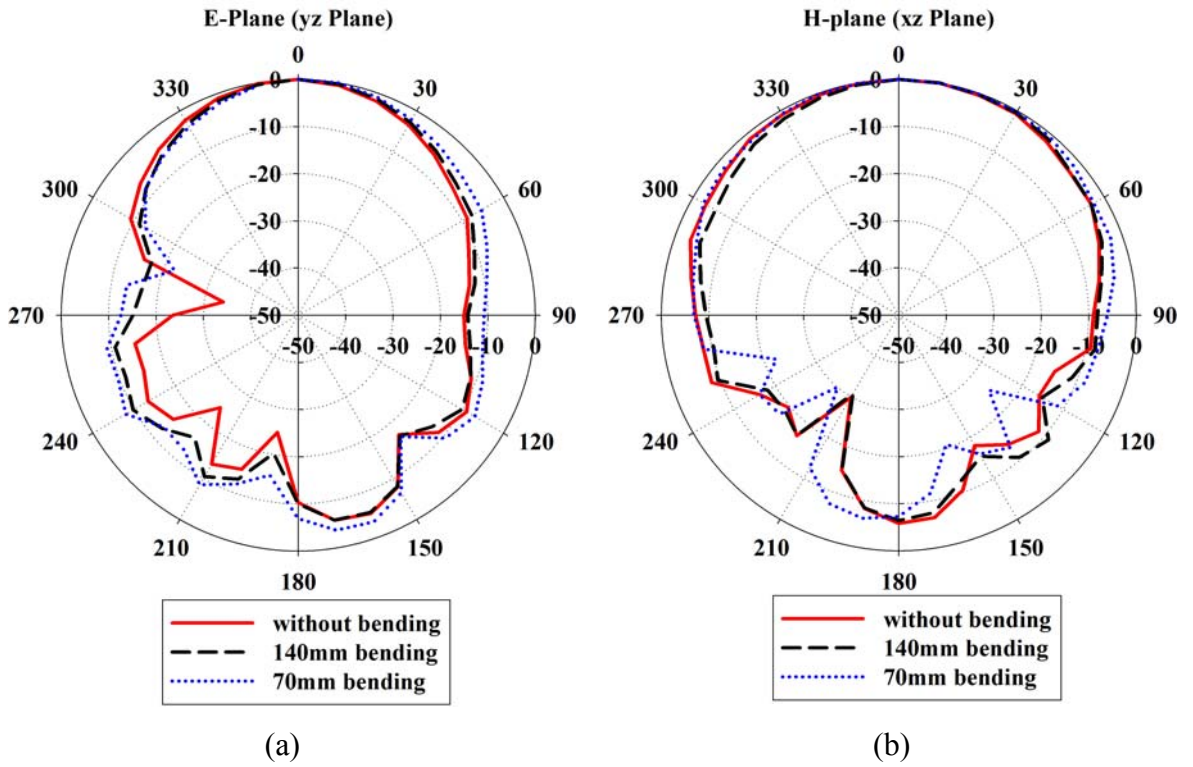(a)   (b)
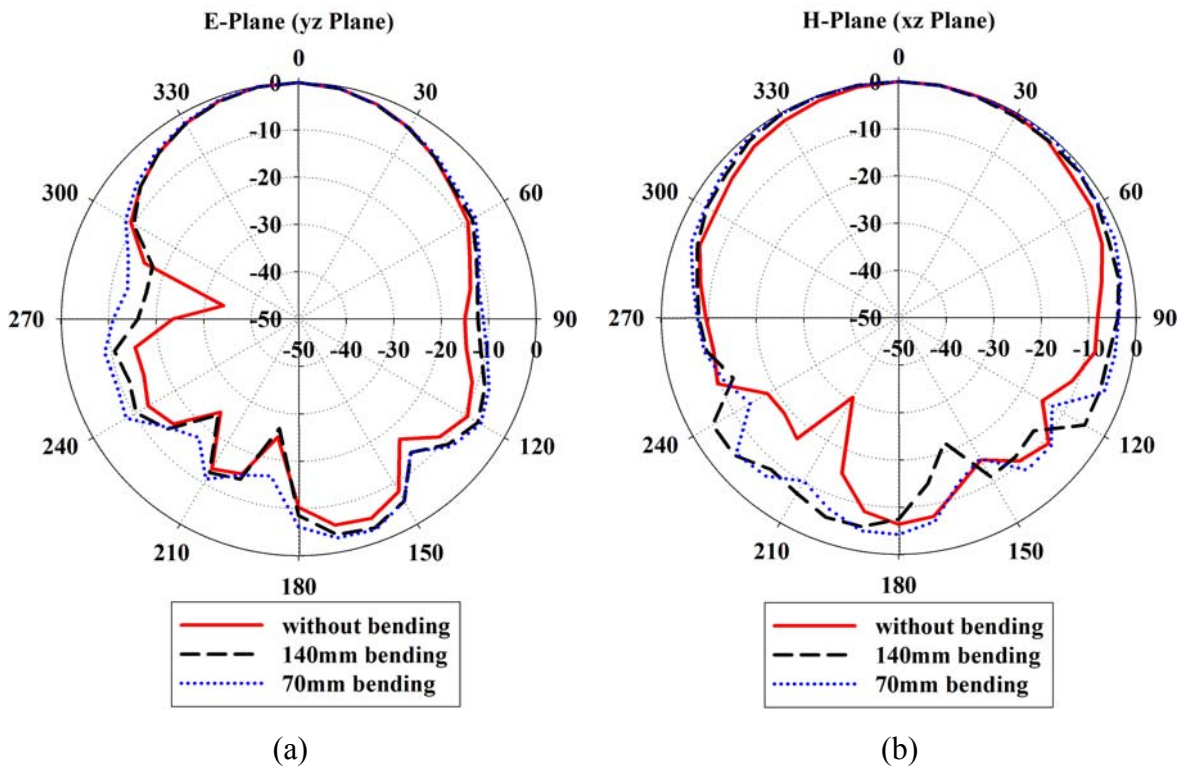
Figure 6-13 Measured radiation patterns for H-plane bending. (a) E-plane, (b) H-plane

(a)   (b)

Figure 6-14 Measured radiation patterns for E-plane bending. (a) E-plane, (b) H-plane

The antenna continued radiating towards the bore site direction in general. There was not much change in the radiation pattern for H-plane bending except the H-plane pattern on 70mm cylinder which became more omni directional. The front-to-back ratio (F/B) remained at 10dB. For the E-plane bending the backward radiation was increased for E-plane cut and F/B ratio dropped to 5dB. For H-plane cut the pattern showed omni directional behaviour. These observations showed that this wearable antenna was able to maintain its good radiation characteristics under bending conditions with the exception of E-plane cut under E-plane bending and H-plane cut under H plane bending on 70mm cylinder. Thus, it can be concluded that E-plane bending puts a limit on the performance of this antenna and for better results it must be ensured that antenna is not bent too much along E-plane.

6.4 Wearable Patch Antenna Over HIS

The measured performance of HIS integrated wearable patch antenna was investigated in detail in Chapter 5 . However the results assumed that antenna was always planar and there were no interfering objects in the vicinity of antenna. In other words the results were valid for free space environment. In this section antenna under real life situations was tested. Specifically the input match result under bending condition for both E-plane and H-plane bending as well as on human body will be presented. The radiation pattern shape under bending condition will be explored to observe the change in radiation performance and the limitation for any bending plane.

6.4.1 Input Match Results Under Bending Condition

The same measurement setup which was discussed previously was employed to find the performance of wearable patch antenna integrated with HIS using 70mm and 140mm foam cylinders. The measurement setup is shown in Figure 6-15.

(a)   (b)
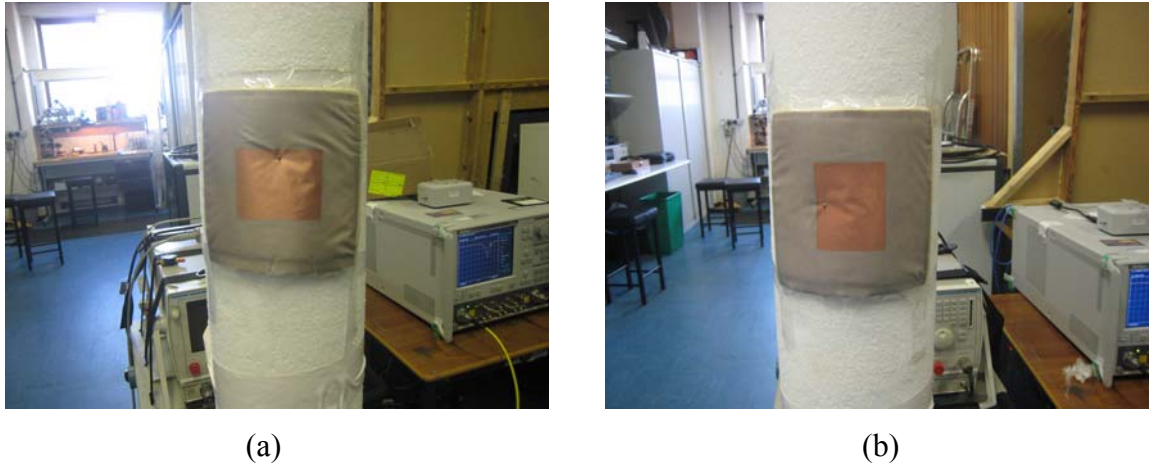
Figure 6-15 Measured setup for HIS integrated wearable patch antenna. (a) E-plane bending, (b)H-plane bending.

The effect on input match was observed for both E-plane and H- plane bending using 70mm and 140mm foam cylinders. The measured results are shown in Figure 6-16.
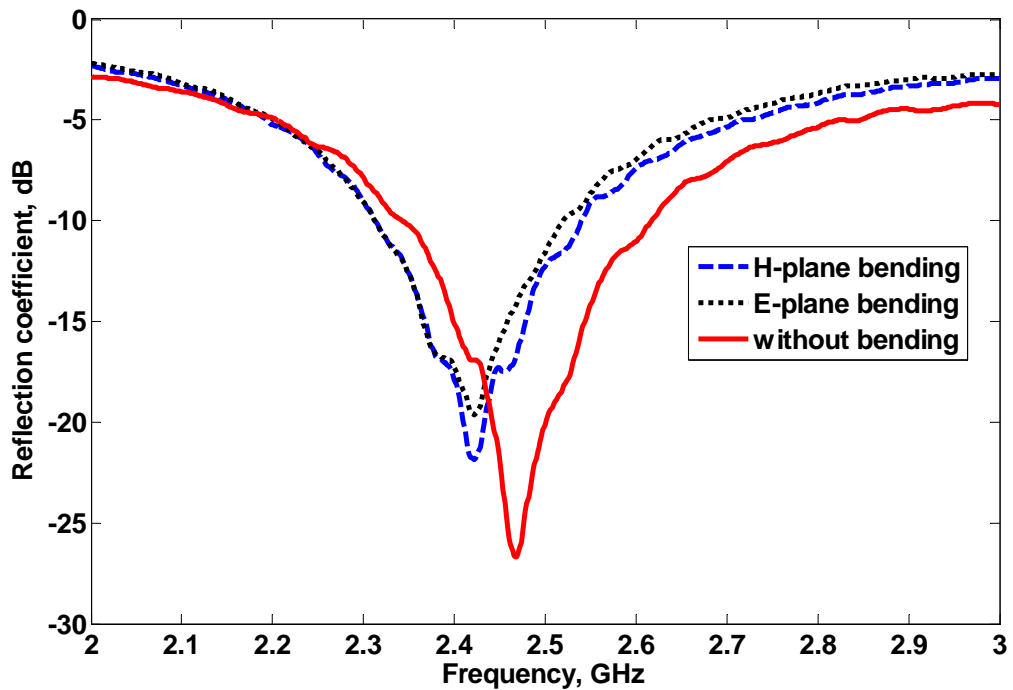

(a)
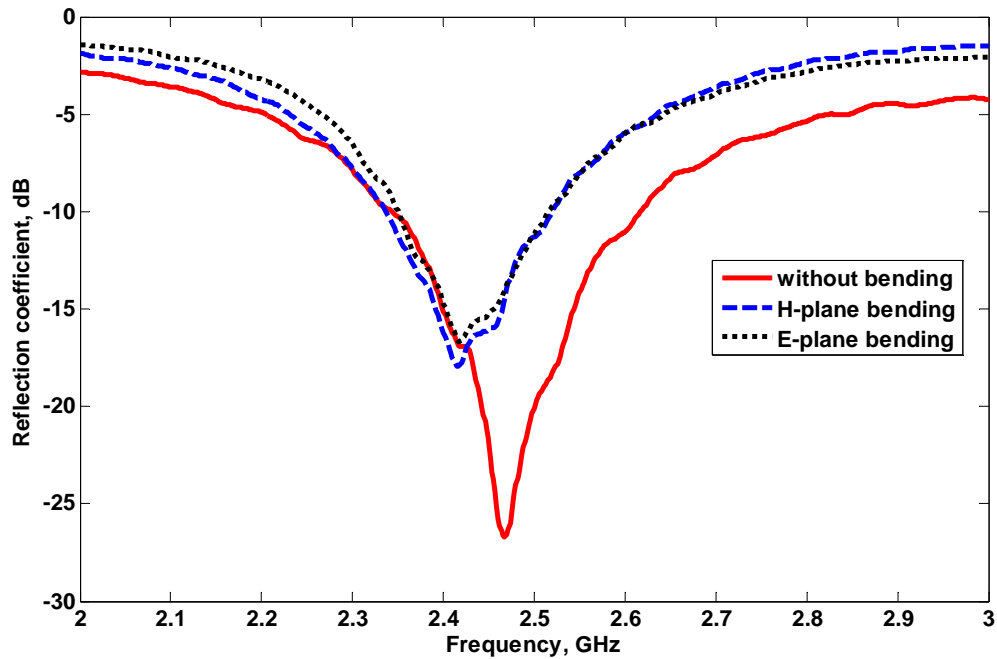
(b)

Figure 6-16 Measured reflection coefficient (S$_{11}$) results for antenna bending on. (a) 140mm cylinder, (b) 70mm cylinder.

The bending in general reduced the input match bandwidth related with S$_{11}$ < -10dB for both E-plane and H-plane bending on both foam cylinders. The input match bandwidth for unbent case was 2.34GHz-2.6GHz. H-plane bending on 140mm cylinder shifted down the matching band to 2.31GHz-2.54GHz, while E-plane bending on 140mm diameter cylinder changed it to 2.31GHz-2.52GHz. So there is not much difference in behaviour in two orthogonal plane bending using large diameter cylinder. When antenna was bent by placing it on 70mm foam the H-plane bending input match bandwidth was measured to be 2.35GHz-2.52GHz while for E-plane bending it was found to be 2.33GHz-2.52GHz. So bending has quite limited effect on the input match performance of this antenna. However the input match bandwidth is slightly reduced but it was still able to function in the desired 2.4GHz WLAN band.

6.4.2 Input Match Results on Body

Finally the human body effect on input matching was measured by placing the antenna on the human body. The measurement setup is shown in Figure 6-17.

124

Figure 6-17 Measurement setup for HIS integrated wearable patch antenna.

As can be seen the patch was placed in an area around arm and chest. The connecting cable not shown was feeding the antenna from behind through VNA. The measured result on human body along without body are shown in Figure 6-18.
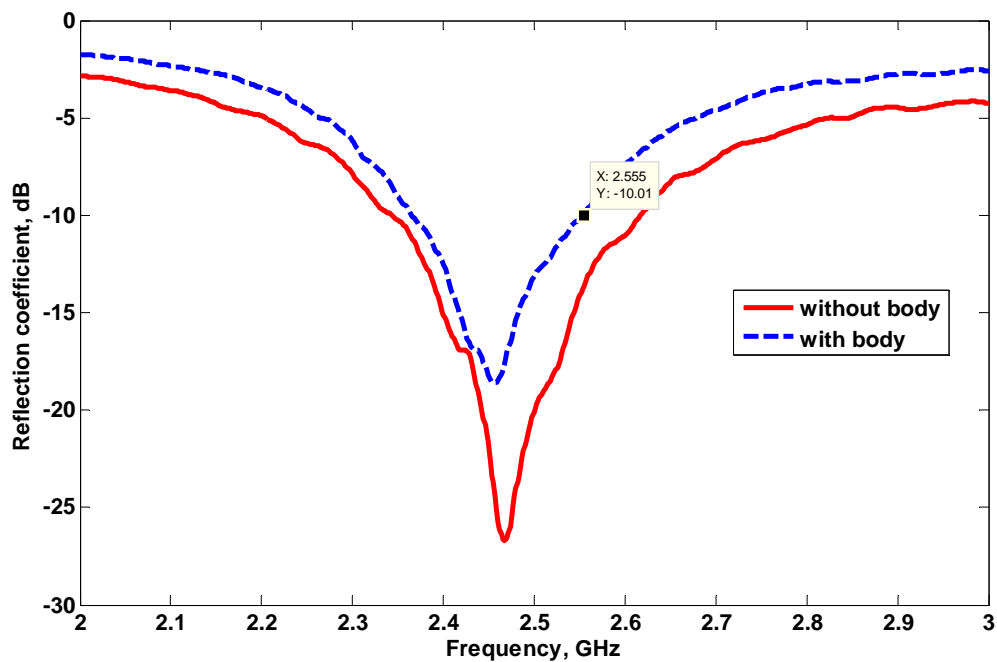
Figure 6-18 Measured reflection coefficient (S_{11}) of HIS integrated wearable patch antenna with and without body

The human body presence did not change the reflection coefficient behaviour significantly. There was a slight shift in the operating frequency range. Also the input match bandwidth was reduced slightly from 2.34GHz-2.6GHz to 2.36GHz-2.55GHz. Despite this reduction

in bandwidth antenna was still able to operate in the desired WLAN band. Thus this antenna is a good candidate for future on body antenna systems.

6.4.3 Radiation Pattern Under Bending Condition

Again the same measurement setup shown in Figure 6-19 was used for measuring bending radiation characteristics of this wearable antenna. The E-plane and H-plane pattern cuts are shown in Figure 6-20 and Figure 6-21 for two orthogonal bending planes. As can be seen the antenna was able to maintain its broadside radiation characteristic under bending conditions. For H-plane bending there is hardly any change in the radiation pattern shape on 140mm cylinder from the reference pattern of planar antenna. however H-plane cut on 70mm showed omni directional behaviour. Also in H-plane cut the pattern became wider which is intuitively obvious. The F/B ratio remained at 20dB for this plane bending for both plane cuts.

For E-plane bending a change in pattern shape was observed in both E-plane and H-plane cuts specially on 70mm cylinder. The pattern got broader in E-plane cut which resulted in decrease of directivity and gain. Also the F/B was reduced to 15dB in E-plane for 140mm cylinder and 10dB for 70mm cylinder.

From these observations it can be concluded that this antenna can perform well under bending conditions. However E-plane bending has significant effects on F/B ratio. So if possible its better to avoid E-plane bending.

| (a) | (b) |
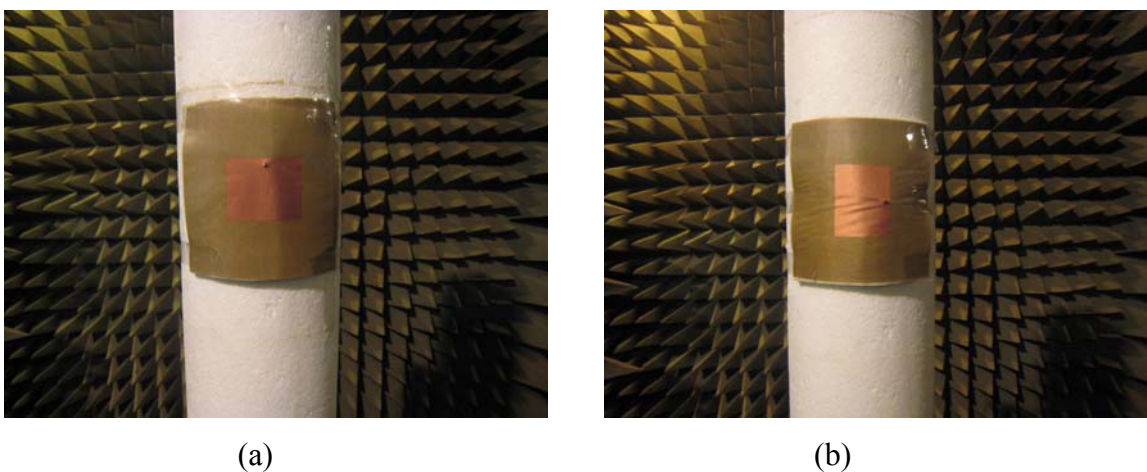
Figure 6-19 Measurement setup in Anechoic Chamber for radiation characteristics under bending condition. (a) H-plane bending, (b) E-plane bending.

(a)   (b)
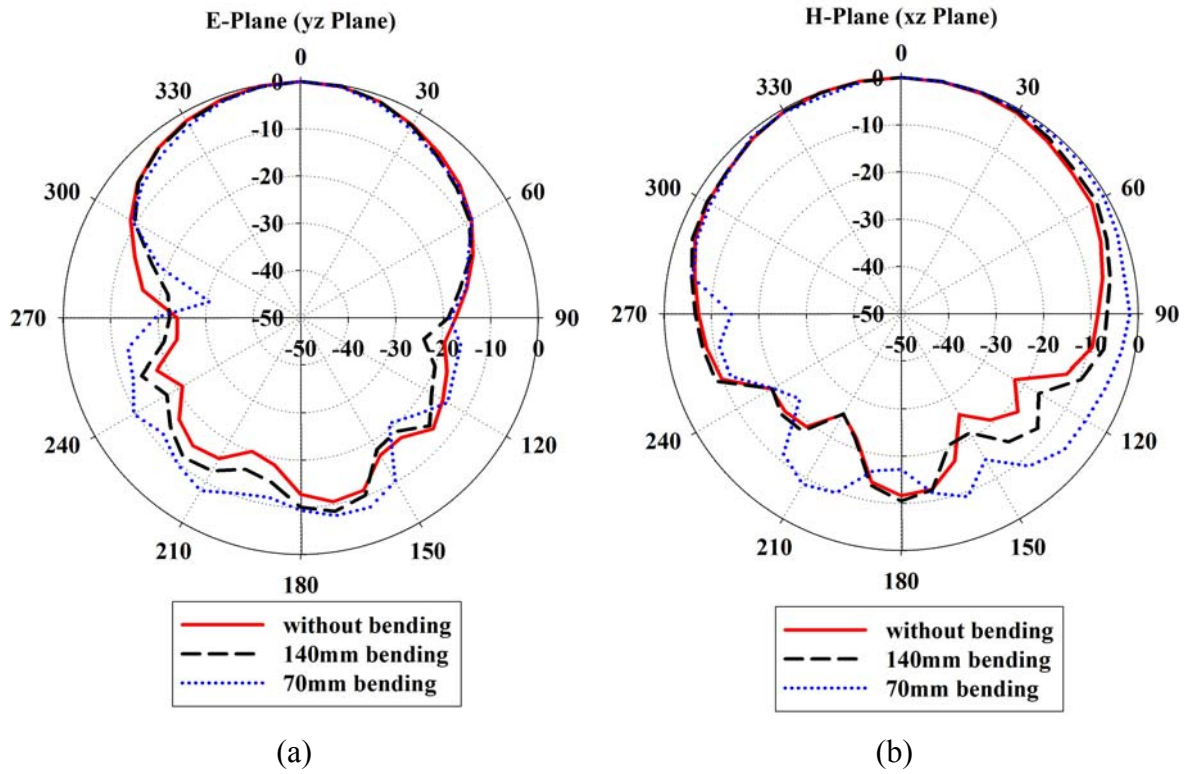
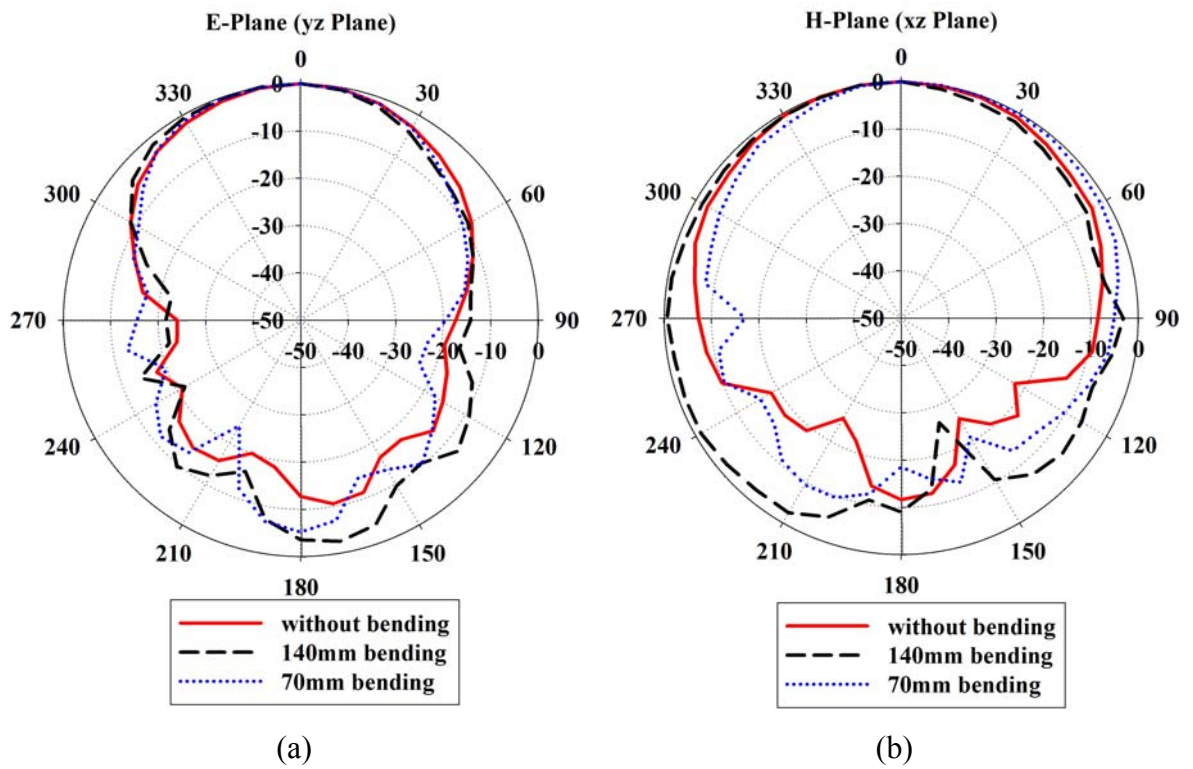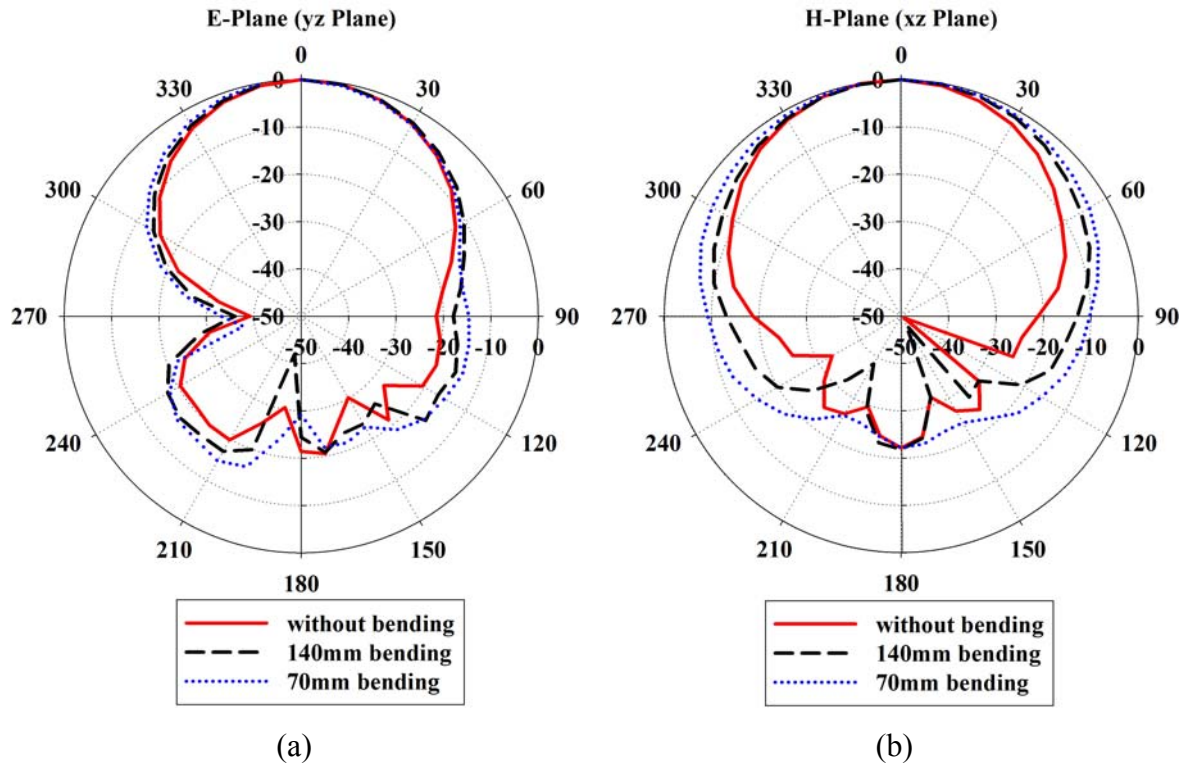**Figure 6-20 Measured radiation pattern for H-plane bending (a) E-plane (b) H-plane**

(a)   (b)
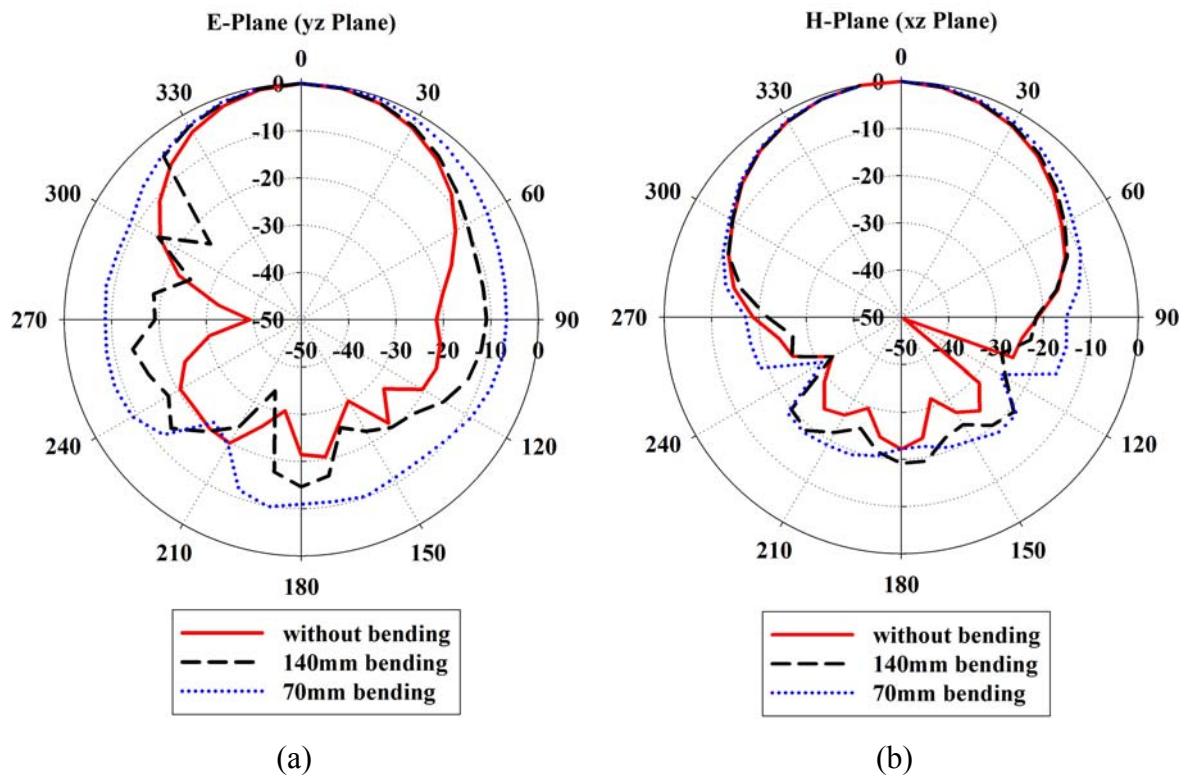
Figure 6-21 Measured radiation patterns for E-plane bending (a) E-plane (b) H-plane

6.5 Conclusions

In this chapter focused was on studying the effect of bending and human body proximity on resonant frequency shift and input match bandwidth. The radiation patterns under bending conditions have also been discussed. For antenna bending study two polystyrene foams with 70mm and 140mm diameters were constructed. These dimensions are typical for the human arm and leg respectively. For the complete study antennas were bent along two orthogonal planes to observe its effect on antenna performance. The reflection coefficient (S_{11}) measurements showed that resonant frequency shifts up in general when antenna is bent while the input match bandwidth is also reduced. The bending along the E-plane has more effect on antenna performance as the antenna's effective resonant length is varied for this plane bending. Therefore it was concluded that E-plane bending should be avoided by placing this dimension along the straight part. However it was observed that designed wearable antennas resonated in the designed frequency band even when they were bent. To study the effect of human body on the wearable antenna they were measured in close proximity to human body. Due to HIS the effect of body on antenna input match bandwidth is not significant. And the antenna is well isolated from the detrimental effects of lossy human body tissues. These encouraging measured results proved that HIS based wearable antennas will increasingly find applications in future communications systems specially on body wearable systems.

7 CONCLUSIONS AND FUTURE WORK

7.1 Summary of Research

This thesis has studied the design and fabrication of fully textile wearable antennas integrated with novel high impedance surfaces (HIS). This thesis covered the entire design cycle of wearable antennas including suitable material selection, electromagnetic characterisation of wearable materials, HIS synthesis, integration of HIS with wearable antennas and finally measurement of radiation performance of overall antenna system. It has been shown that performance of wearable antennas can be improved by HIS integration. In this chapter, summary of main research work of thesis, it's significance and conclusions based on the results will be presented. Finally suggestions for future work that can be done in this area will be given.

The literature review of previous work relevant to this thesis was provided in Chapter 1. In that Chapter it was determined that with the rapid growth and use of wireless communication systems more and more people are taking advantage of portable computing systems on daily basis. Also with the advancement in electronic industry new and sophisticated wireless devices have come up which are being used closed to human body. For user convenience there is an increasing need for integrating antennas on or in the clothing. The conventional antennas being rigid and obtrusive to user movements have limitations. It was spotted that there is a clear need of antennas made of flexible textile materials that can be part of user clothing defined as wearable antennas. Also the use of these wireless devices in proximity to human body has a profound effect on antenna performance. This has necessitated the need for efficient, low profile, compact and light weight antennas that are immune to human body proximity. The use of emerging high impedance surfaces (HIS) has shown significant performance advantages when integrated with wearable antennas. As these structures had not been fully exploited in wearable antenna applications, this was set as research objective of this thesis . Goal was set on non uniform HIS structures which have not been used before in wearable applications.

In Chapter 2 some useful concepts, terminology and definitions extensively used throughout this thesis were introduced. It specifically discussed the effect of perfect electric conductor (PEC) ground plane on low profile antenna performance. The out of phase reflection from PEC was shown to short the antenna and resulted in poor input match and radiation efficiency. The use of Perfect Magnetic Conductor (PMC) was shown to improve the matching but it is of no practical use as it does not exist in nature. However the existing artificially engineered PMC defined as high impedance surface (HIS) was shown to provide the desirable performance enhancement to low profile antennas. The unique electromagnetic properties of in-phase reflection and surface wave suppression offered by HIS were then highlighted. The equivalent circuit model of HIS and its operation mechanism was also explained in detail. The limitation of uniform HIS for oblique incident waves radiated by antenna was highlighted. The concept of non uniform HIS and its benefit for oblique incidence waves was demonstrated using equivalent circuit model. Also the performance improvement of simple dipole over non uniform HIS was shown to validate the design concept.

In chapter 3 the importance of selection of suitable materials for wearable antenna construction was highlighted. The electromagnetic characteristics of any material to be used in antenna fabrication has to be known for any design idea. Different methods that are currently used for electromagnetic characterisation of materials were explained in detail. The cavity method was selected because of its ease of analysis and accuracy. The split post dielectric resonator (SPSR) that worked on cavity method was then used to measure different fabric samples. Felt was chosen because of its daily use and cheap and ready availability. For making complete fabric antenna it was decided to use electro textiles as conducting part of antenna designs. Different electro textiles were tested by fabricating simple patch antennas and then selected pure polyester copper fabric as the conducting part of wearable antenna because of its better input match performance.

For etching metal parts of antenna on electro textile a novel fabrication method was proposed for these thin conducting fabrics. A modification was introduced to the conventional PCB fabrication technique. It can be claimed this is the first time such technique has been used to fabricate wearable antennas. This improves etching accuracy and more complex design can be fabricated.

In Chapter 4 the design stages of a novel wearable inverted L antenna were shown. It started with a simple low profile inverted L antenna which showed poor input match performance due to small separation between radiator and PEC ground plane. In the next stage HIS was introduced below inverted L antenna and it improved the input match of antenna significantly using the same separation between the PEC ground plane and antenna. In the final stage of design non uniformity in HIS design was introduced and it further widened the input match bandwidth due to its stable response for oblique incident waves radiated by the antenna. A modified design was proposed by integrating HIS in the same layer as antenna. This further reduced the profile of antenna without deteriorating the improved match performance achieved with the two layer design.

The prototype antennas were fabricated and input match and radiation characteristics were measured. There was a good agreement between simulated and measured results. The wearable antennas had desired broadside radiation pattern with an average gain of 5dBi and about 60% radiation efficiency.

In chapter 5 the idea of HIS was extended in the design of wearable patch antenna. The integration of HIS lowered down the resonant frequency of the conventional patch antenna. Also the input match bandwidth was also improved under the influence of HIS. By introducing non uniformity in the design improved antenna performance in terms of input match bandwidth and gain was shown. The fabricated prototype was measured and showed good agreement with the simulated results. The desired broadside radiation performance was achieved with the complete fabric patch antenna. The average gain was about 8dBi and radiation efficiency was about 70%.

The wearable antenna should perform equally well when place on body. Also planar surfaces cannot be provided on human body in general. In chapter 6 the performance of prototype wearable antennas was shown under bending and on human body situations. The bending conditions for arm and leg were simulated by fabricating two polystyrene foam cylinders. The antennas were bended in two orthogonal planes and change in input match characteristics were observed. The input match bandwidth was reduced in general for both bending conditions. Specifically the E-plane bending effect was to shift the resonant frequency up. However prototype antennas were able to function in the desired frequency

band. The on body measurement tests also showed the isolation of antenna from the detrimental effects of human body due to HIS.

In short low profile and compact wearable antennas were successfully designed that showed improved performance due to HIS integration into the design. The antennas conducting and non conducting parts were all made of fabric material . They can be easily integrated within felt clothing or sewn on top of any other fabric. They can be conveniently worn by people without hindering their movement. These wearable antennas can withstand the dynamically changing operating environment like bending or human body placement.

7.2 Conclusions

The research in this thesis concerns designing and fabricating fully textile wearable antennas integrated with novel HIS. The selection of materials and their characterisation for wearable antenna design has received limited attention in scientific journals. In this thesis full classification of different techniques available for characterising electromagnetic properties of materials was given. The advantages and disadvantages of different methods clearly mentioned. It was concluded that cavity method was best due to its accuracy and non destructive nature. The split post dielectric resonator (SPDR) working on the principle of cavity method and used in this research was demonstrated. Different fabric samples as potential wearable antenna substrates were then measured for the first time using SPDR. The accuracy of this device was verified with the values of the published results.

To date wearable antennas were fabricated using copper tape or electro textiles using conventional knife cutting or laser ablation [73]. In this research a novel technique was employed to fabricate wearable antennas using electro textile. The traditional printed circuit board (PCB) etching method was modified for the thin electro textiles. It was claimed this is the first time such a technique has been implemented in wearable antenna design. This method allows rapid prototyping with industry standard accuracy. Also this opens a new possibility of complex wearable antenna design shapes that were never designed before. This has major implications for wearable computing industry as well.

The use of HIS with antenna has been studied in detail in past. However majority of HIS structures reviewed are uniform with unit cell repeating itself uniformly over the whole periodic structure. There is a variation of uniform HIS known as non uniform HIS in which the parameters of unit cell varies from one cell to other cell. By introducing non uniformity the performance of some types of antenna had been shown enhanced in relation to input match bandwidth and F/B ratio. This design concept was modified to wearable form factor and successfully design low profile and compact non uniform HIS based wearable antennas in this research. This study has demonstrated the potential of HIS in wearable antenna performance enhancement .

The effect of bending on wearable antenna characteristics has demonstrated that E-plane bending has a major effect on resonant frequency stability. The reason being the antenna's effective resonant length lies along the E-plane. The more the antenna is bent along E-plane, the more the resonant length is reduced and thus resonant frequency shifts up. Therefore it can be concluded that for on body placement like arm the HIS based wearable antenna performs better when its E-plane is aligned along the sleeve length.

7.3 Future Work Suggestions

This thesis has investigated wearable antenna design cycle and proposed some new wearable antenna design concepts however any new design leads to more questions and future study that has not been carried out as part of this research. There is still an enormous amount of research and development that needs to be performed in this exciting area of wearables.

First of all, all designs fabricated in this research used coax probe for feeding. This feeding method makes it slightly inconvenient and difficult for antenna on body placement. In future probe fed can be replaced by more convenient microstrip feed or co planar waveguide (CPW) feed. Also the effect of different feeding methods on the overall performance can be carried as a future research idea.

Secondly, to feed antennas commonly used metallic SMA connectors were employed. These connectors are large in size and heavy in weight specially for wearable applications. In future new types of connectors can be proposed that are small and light weight.

Thirdly, conventional soldering method was used to connect SMA connectors to the conducting fabric. The heat generated by soldering machine is prone to burn out the thin conducting fabric. Also the soldered connection between metal connector and conducting fabric is brittle and tend to break easily if some force is applied. Rather then using conventional soldering method some new solder less techniques can be proposed in future study to avoid this problem.

Fourthly, different materials were tested for wearable antenna substrates and then felt was selected in this research. There is still need for study on material selection. There are variety of textile materials available that need to be studied for their viability and suitability in wearable antenna designs. Also more attention needs to be paid to the firmness and drapability of fabric in the final selection of materials.

Fifthly, wearable antennas designed in this research are not tested under wet conditions. So this topic can be explored in future studies. Also if performance deterioration under wet conditions is to be avoided then search needs to be carried out on water proof materials for future wearable communication designs.

Lastly, the specific absorption rate (SAR) is an important parameter to be measured for any antenna design. This parameter shows the rate of energy absorption by the human body tissue when exposed to fields radiated by the antenna. The SAR is potentially important to any wearable antenna as they are placed in very close proximity to the body. There is no specific legislation which considers wearable devices, however minimization of SAR is a sensible design goal. For this reason the SAR characteristics of wearable antennas designed in this research could be carried as future work.

Appendix A

Conducting Fabric Etching   Process

A novel method was used to fabricate textile wearable antennas to avoid inaccuracy involved in hand cutting the metallic parts of wearable antennas. The steps involved in design cycle are similar to a traditional Printed Circuit Board (PCB) etching however because of very small thickness of conducting copper fabric some modifications were introduced to the design process. These novel steps helped to avoid the undesirable etching out of the copper pattern on the other side of the conducting fabric.

The design cycle of wearable antenna etching should involve the following steps:

➢ Prepare artwork using a standard PCB CAD application. The output should be Gerber plot files. If the element is symmetrical about an axis then you need only one Gerber file plotted twice. If the element is not symmetrical, then there should be two plot files, one ordinary, and one mirrored. This is because, for maximum definition in the finished element, the emulsion of the plotted film should always be in contact with the photosensitive layer when exposed.

➢ Plot and develop the master artworks films. If negative photo-resist is being used then the plotter is set to produce a negative master (black areas are etched, clear areas are not). Both films are then taped together in register to form the complete artwork.

➢ Coat both sides of a suitable piece of conducting fabric using heat bonded dry film photo resist. Apply each side as a separate action to avoid wrinkles after removing the dull protective film.

➢ Place the coated cloth between the two artwork films and expose to Ultra Violet (UV) light for 35 seconds per side, but this will vary depending on the type and

power of the exposure unit. The areas to be etched will now be in a different colour to those to be left as metal which enables inspection.

➢ Remove the second protective coating from the dry film photo resist on both sides of the cloth. This is the protective coating with the glossy surface (compared to the one with the dull surface, which was removed earlier).

➢ Develop the conducting cloth thoroughly using the recommended dry film developing solution and then etch away the unwanted metal coating on the conducting fabric. This is best done in a tray, rather than the spray develop and etch tanks, as it only takes a little longer and is a much more controlled environment, with the process taking place under user continuous view.

➢ The remaining photo resist must be removed after the etching process using a resist stripper solution specific to the dry film process. Organic strippers, such as acetone, will not remove the resist.

Appendix B

Experimental Measurement Facilities

The measurements that were carried out during this research can be classified into three categories.:

1. Material parameters measurement
2. HIS evaluation
3. Antenna Characteristics measurement

The purpose of material evaluation was to find out the electromagnetic properties of the flexible material and choose the optimal performance material for this research wearable antennas. The split post dielectric resonator (SPDR) was employed for this purpose. The theoretical description and experimental setup for material evaluation was discussed in Chapter 3. The HIS evaluation is carried out to find the bandgap position. For this purpose a suspended microstrip line was fabricated. The antenna measurements involved finding S parameters and radiation characteristics like radiation pattern, Gain and efficiency.

All these measurements involved the use of Vector Network Analyser (VNA). While radiation characteristics were measured in Anechoic Chamber. Below is the general description of the VNA and Anechoic chamber used in this research.

➢ HP 8753D VNA

The HP 8753D is a high performance VNA for measuring Scattering Parameters (S-parameters). It has a working frequency range from 30kHz to 6GHz which was enough for this research study. For accurate measurements the VNA was calibrated up to the terminating SMA connector before every measurement. This removed the errors introduced by the connecting coax cables on measurement data. The reflection coefficient (S_{11}) of antenna is measured by using only one port of the VNA. While for transmission parameters both ports were used. One acted as a source while other port was terminated with a matched load.

➢ Anechoic Chamber

Indoor Anechoic chambers have been developed for far field measurements as an alternative to outdoor testing of radiation performance. There are two basic shapes, depending on the frequency of operation: rectangular chambers and tapered chambers. The antennas are placed in the middle line of the chamber with the reference source antenna and the antenna under test (AUT) placed across from each other at a fixed distance. The conducting walls of the chamber are covered with RF absorbers to create a reflection-less free space environment and allow all weather antenna measurements in a controlled laboratory environment. The radiation patterns, Directivity, Gain, Radiation efficiency which are used to characterise antenna performance are measure on the surface of constant radius sphere. Since the distance between the two antennas is fixed, only two angular coordinates (θ,φ) are varied to measure the three dimensional radiation pattern as well as two dimensional pattern cuts of an antenna.

The chamber used during the course of this research was a rectangular chamber of dimension $3m \times 3m \times 7m$. The setup consisted of positioner which rotated the AUT in azimuth and elevation plane. The transmitting antenna was on a fixed positioner. A linearly polarized standard gain horn antenna (900MHz-18GHz) was employed as the transmitting antenna. Both the antennas were connected to HP 8753D VNA with a frequency range of 30KHz to 6GHz. During the measurement the AUT positioner was automatically controlled by the software to rotate it through full 360º in both azimuth and elevation planes. The frequency markers were defined at the start of measurement. The measured data was recorded by the network analyser as a function of frequency and angles. The data was then transferred to the computer to plot the 2D pattern cuts and directivity, Gain and radiation efficiency were computed. For symmetrical pattern the AUT was positioned at the centre of positioner rotation circle.

References

[1] C. Baber, J. Knight, D. Haniff and L. Cooper, "Ergonomics of wearable computers," *Mobile Networks and Applications,* vol. 4, pp. 15-21, 03/01. 1999.

[2] T. G. Zimmerman, "Personal area networks: Near-field intrabody communication," *IBM Syst J,* vol. 35, pp. 609, 09. 1996.

[3] P. S. Hall and Y. Hao, *Antennas and Propagation for Body-Centric Wireless Communications (Artech House Antennas and Propagation Library).* Artech House, 2006, pp. 314.

[4] P. Salonen, Y. Rahmat-Samii and M. Kivikoski, "Wearable antennas in the vicinity of human body," in *IEEE Antennas and Propagation Society Symposium 2004 Digest Held in Conjunction with: USNC/URSI National Radio Science Meeting,* 2004, pp. 467-470.

[5] P. Salonen, L. Sydanheimo, M. Keskilammi and M. Kivikoski, "A small planar inverted-F antenna for wearable applications," in *Wearable Computers, 1999. Digest of Papers. the Third International Symposium on,* 1999, pp. 95-100.

[6] F. Gemperle, C. Kasabach, J. Stivoric, M. Bauer and R. Martin, "Design for wearability," in *Wearable Computers, 1998. Digest of Papers. Second International Symposium on,* 1998, pp. 116-122.

[7] M. Klemm, I. Locher and G. Troster, "A novel circularly polarized textile antenna for wearable applications," in *Conference Proceedings- 34th European Microwave Conference,* 2004, pp. 137-140.

[8] C. Hertleer, A. Tronquo, H. Rogier, L. Vallozzi and L. Van Langenhove, "Aperture-Coupled Patch Antenna for Integration Into Wearable Textile Systems," *Antennas and Wireless Propagation Letters, IEEE,* vol. 6, pp. 392-395, 2007.

[9] I. Locher, M. Klemm, T. Kirstein and G. Troster, "Design and characterization of purely textile patch antennas," *IEEE Transactions on Advanced Packaging,* vol. 29, pp. 777-788, 2006.

[10] J. Lebaric and Ah-Tuan Tan, "Ultra-wideband RF helmet antenna," *MILCOM 2000. 21st Century Military Communications Conference Proceedings,* vol. 1, pp. 591-594 vol.2, 2000.

[11] J. Lebaric and Ah-Tuan Tan, "Ultra-wideband conformal helmet antenna," *Microwave Conference, 2000 Asia-Pacific,* pp. 1477-1481, 2000.

[12] J. E. Lebaric, R. W. Adler and M. E. Limbert, "Ultra-wideband, zero visual signature RF vest antenna for man-portable radios," *Military Communications Conference, 2001. MILCOM 2001. Communications for Network-Centric Operations: Creating the Information Force. IEEE,* vol. 2, pp. 1291-1294 vol.2, 2001.

References

[13] R. Abramo, R. Adams, F. V. Canez, H. Pace and P. Haglind, "Fabrication and testing of the COMWIN vest antenna," *MILCOM 2000. 21st Century Military Communications Conference Proceedings,* vol. 1, pp. 595-598 vol.2, 2000.

[14] E. C. Kohls, A. Abler, P. Siemsen, J. Hughes, R. Perez and D. Widdoes, "A multi-band body-worn antenna vest," *Antennas and Propagation Society International Symposium, 2004. IEEE,* vol. 1, pp. 447-450 Vol.1, 2004.

[15] E. C. Fear, S. C. Hagness, P. M. Meaney, M. Okoniewski and M. A. Stuchly, "Enhancing breast tumor detection with near-field imaging," *Microwave Magazine, IEEE,* vol. 3, pp. 48-56, 2002.

[16] P. Salonen and L. Hurme, "A novel fabric WLAN antenna for wearable applications," in *Antennas and Propagation Society International Symposium, 2003.IEEE,* 2003, pp. 700-703 vol.2.

[17] C. Hertleer, H. Rogier, L. Vallozzi and F. Declercq, "A Textile Antenna based on High-Performance Fabrics," *Antennas and Propagation, 2007. EuCAP 2007. the Second European Conference on,* pp. 1-5, 2007.

[18] P. Salonen, Y. Rahmat-Samii, H. Hurme and M. Kivikoski, "Dual-band wearable textile antenna," in *IEEE Antennas and Propagation Society Symposium 2004 Digest Held in Conjunction with: USNC/URSI National Radio Science Meeting,* 2004, pp. 463-466.

[19] R. Langley and Shaozhen Zhu, "Dual band wearable antenna," *Antennas and Propagation Conference, 2008. LAPC 2008. Loughborough,* pp. 14-17, 2008.

[20] Yuehui Ouyang and W. Chappell, "Distributed Body-worn Transceiver System with the Use of Electro-textile Antennas," *Microwave Symposium, 2007. IEEE/MTT-S International,* pp. 1229-1232, 2007.

[21] Federal Communications Commission. Http://www.fcc.gov/oet/rfsafety/dielectric.html.

[22] P. J. Massey, "Mobile phone fabric antennas integrated within clothing," in *Antennas and Propagation, 2001.Eleventh International Conference on (IEE Conf.Publ.no.480),* 2001, pp. 344-347 vol.1.

[23] P. Salonen and L. Sydanheimo, "Development of an S-band flexible antenna for smart clothing," in *2002 IEEE Antennas and Propagation Society International Symposium,* 2002, pp. 6-9.

[24] M. Tanaka and J. Jang, "Wearable microstrip antenna," in *2003 IEEE International Antennas and Propagation Symposium and USNC/CNC/URSI North American Radio Science Meeting,* 2003, pp. 704-707.

[25] A. Jafargholi, "VHF-LB Vest Antenna Design," *Antenna Technology: Small and Smart Antennas Metamaterials and Applications, 2007. IWAT '07. International Workshop on,* pp. 247-250, 2007.

[26] C. Cibin, P. Leuchtmann, M. Gimersky, R. Vahldieck and S. Moscibroda, "A flexible wearable antenna," in *Antennas and Propagation Society International Symposium, 2004.IEEE,* 2004, pp. 3589-3592 Vol.4.

[27] J. Slade, J. Teverovsky, B. Farrell, J. Bowman, M. Agpaoa-Kraus and P. Wilson, "Textile based antennas," in *Electronics on Unconventonal Substrates--Electrotextiles and Giant-Area Flexible Circuitse,* 2003, pp. 91-97.

[28] C. Cibin, P. Leuchtmann, M. Gimersky and R. Vahldieck, "Modified E-shaped PIFA antenna for wearable systems," in *URSl Lntemational Symposium an Electromagnetic Theory,* 2004,

[29] B. Sanz-Izquierdo, F. Huang, J. C. Batchelor and M. Sobhy, "Compact antenna for WLAN on body applications," in *Microwave Conference, 2006.36th European,* 2006, pp. 815-818.

[30] B. Sanz-Izquierdo, F. Huang and J. C. Batchelor, "Covert dual-band wearable button antenna," *Electron. Lett.,* vol. 42, pp. 668-670, 2006.

[31] B. Sanz-Izquierdo and J. C. Batchelor, "Wlan Jacket Mounted Antenna," *Antenna Technology: Small and Smart Antennas Metamaterials and Applications, 2007. IWAT '07. International Workshop on,* pp. 57-60, 2007.

[32] T. Kellomaki, J. Heikkinen and M. Kivikoski, "Wearable antennas for FM reception," in *European Conference on Antennas and Propagation: EuCAP 2006,* 2006, pp. 6.

[33] Yuehui Ouyang and W. Chappell, "Measurement of electrotextiles for high frequency applications," *Microwave Symposium Digest, 2005 IEEE MTT-S International,* pp. 4 pp., 2005.

[34] D. Cottet, J. Grzyb, T. Kirstein and G. Troster, "Electrical characterization of textile transmission lines," *Advanced Packaging, IEEE Transactions on,* vol. 26, pp. 182-190, 2003.

[35] Yuehui Ouyang and W. J. Chappell, "High Frequency Properties of Electro-Textiles for Wearable Antenna Applications," *Antennas and Propagation, IEEE Transactions on,* vol. 56, pp. 381-389, 2008.

[36] Yuehui Ouyang, E. Karayianni and W. J. Chappell, "Effect of fabric patterns on electrotextile patch antennas," *Antennas and Propagation Society International Symposium, 2005 IEEE,* vol. 2B, pp. 246-249 vol. 2B, 2005.

[37] P. Salonen, Y. Rahmat-Samii, H. Hurme and M. Kivikoski, "Effect of conductive material on wearable antenna performance: A case study of WLAN antennas," in *Antennas and Propagation Society International Symposium, 2004.IEEE,* 2004, pp. 455-458 Vol.1.

[38] R. Shaw, B. R. Long, D. H. Werner and A. Gavrin, "The radio frequency characterization of conductive textile materials: a preliminary step for accurate antenna modeling," *Antennas and Propagation Society International Symposium, 2005 IEEE,* vol. 4B, pp. 431-434 vol. 4B, 2005.

[39] E. Yilmaz, D. P. Kasilingam and B. M. Notaros, "Performance analysis of wearable microstrip antennas with low-conductivity materials," *Antennas and Propagation Society International Symposium, 2008. AP-S 2008. IEEE,* pp. 1-4, 2008.

[40] P. Salonen, Y. Rahmat-Samii, M. Schaffrath and M. Kivikoski, "Effect of textile materials on wearable antenna performance: A case study of GPS antennas," in *Antennas and Propagation Society International Symposium, 2004.IEEE,* 2004, pp. 459-462 Vol.1.

[41] A. Tronquo, H. Rogier, C. Hertleer and L. Van Langenhove, "Robust planar textile antenna for wireless body LANs operating in 2.45 GHz ISM band," *Electron. Lett.,* vol. 42, pp. 21-22, 2006.

[42] P. Salonen, J. Kim and Y. Rahmat-Samii, "Dual-band E-shaped patch wearable textile antenna," in *Antennas and Propagation Society International Symposium, 2005 IEEE,* 2005, pp. 466-469 Vol. 1A.

[43] C. Hertleer, H. Rogier and L. Van Langenhove, "A TEXTILE ANTENNA FOR PROTECTIVE CLOTHING," *Antennas and Propagation for Body-Centric Wireless Communications, 2007 IET Seminar on,* pp. 44-46, 2007.

[44] L. Vallozzi, W. Vandendriessche, H. Rogier, C. Hertleer and M. Scarpello, "Design of a protective garment GPS antenna," *Microwave Opt Technol Lett,* vol. 51, pp. 1504-1508, 2009.

[45] A. Tronquo, H. Rogier, C. Hertleer and L. Van Langenhove, "Applying textile materials for the design of antennas for wireless body area networks," in *European Conference on Antennas and Propagation: EuCAP 2006,* 2006, pp. 5.

[46] H. J. Visser and A. C. F. Reniers, "Textile Antennas, a Practical Approach," *Antennas and Propagation, 2007. EuCAP 2007. the Second European Conference on,* pp. 1-8, 2007.

[47] L. Januszkiewicz, S. Hausman, T. Kacprzak, M. Michalak, J. Bilska and I. Krucinska, "Textile body-worn exponentially tapered Vee antenna," *Microwaves, Radar and Wireless Communications, 2008. MIKON 2008. 17th International Conference on,* pp. 1-4, 2008.

[48] L. Yang, L. Martin, D. Staiculescu, C. P. Wong and M. M. Tentzeris, "Design and development of compact conformal RFID antennas utilizing novel flexible magnetic composite materials for wearable RF and biomedical applications," *Antennas and Propagation Society International Symposium, 2008. AP-S 2008. IEEE,* pp. 1-4, 2008.

[49] Jung-Yong Park and Jong-Myung Woo, "Microstrip Line Monopole Antenna for the Wearable Applications," *Microwave Conference, 2008. EuMC 2008. 38th European,* pp. 1277-1279, 2008.

[50] A. Galehdar and D. V. Thiel, "Flexible, light-weight antenna at 2.4GHz for athlete clothing," *Antennas and Propagation Society International Symposium, 2007 IEEE,* pp. 4160-4163, 2007.

References

[51] Y. Ouyang and W. J. Chappell, "Diversity characterization of body-worn textile antenna system at 2.4 GHz," in *Antennas and Propagation Society International Symposium 2006, IEEE,* 2006, pp. 2117-2120.

[52] J. G. Santas, A. Alomainy and Yang Hao, "Textile Antennas for On-Body Communications: Techniques and Properties," *Antennas and Propagation, 2007. EuCAP 2007. the Second European Conference on,* pp. 1-4, 2007.

[53] L. Vallozzi, H. Rogier and C. Hertleer, "Dual Polarized Textile Patch Antenna for Integration Into Protective Garments," *Antennas and Wireless Propagation Letters, IEEE,* vol. 7, pp. 440-443, 2008.

[54] L. Ma, R. M. Edwards, S. Bashir and M. I. Khattak, "A wearable flexible multi-band antenna based on a square slotted printed monopole," *Antennas and Propagation Conference, 2008. LAPC 2008. Loughborough,* pp. 345-348, 2008.

[55] C. A. Balanis, *Modern Antenna Handbook: V. 1 & 2.* WileyBlackwell, 2008, pp. 1680.

[56] T. F. Kennedy, P. W. Fink, A. W. Chu, N. J. Champagne, G. Y. Lin and M. A. Khayat, "Body-Worn E-Textile Antennas: The Good, the Low-Mass, and the Conformal," *Antennas and Propagation, IEEE Transactions on,* vol. 57, pp. 910-918, 2009.

[57] I. Oppermann, *UWB: Theory and Applications.* WileyBlackwell, 2004, pp. 248.

[58] M. Klemm and G. Troester, "Textile UWB Antennas for Wireless Body Area Networks," *Antennas and Propagation, IEEE Transactions on,* vol. 54, pp. 3192-3197, 2006.

[59] B. Sanz-Izquierdo, J. C. Batchelor and M. Sobhy, "UWB wearable button antenna," in *European Conference on Antennas and Propagation: EuCAP 2006,* 2006, pp. 4.

[60] B. Sanz-Izquierdo, J. C. Batchelor and M. I. Sobhy, "Compact UWB wearable antenna," in *LAPC 2007: 3rd Loughborough Antennas and Propagation Conference,* 2007, pp. 121-124.

[61] D. Sievenpiper, Lijun Zhang, R. F. J. Broas, N. G. Alexopolous and E. Yablonovitch, "High-impedance electromagnetic surfaces with a forbidden frequency band," *Microwave Theory and Techniques, IEEE Transactions on,* vol. 47, pp. 2059-2074, 1999.

[62] Fan Yang and Y. Rahmat-Samii, "Curl antennas over electromagnetic band-gap surface: a low profiled design for CP applications," *Antennas and Propagation Society International Symposium, 2001. IEEE,* vol. 3, pp. 372-375 vol.3, 2001.

[63] Fan Yang and Y. Rahmat-Samii, "Reflection phase characterization of an electromagnetic band-gap (EBG) surface," *Antennas and Propagation Society International Symposium, 2002. IEEE,* vol. 3, pp. 744-747, 2002.

[64] Fan Yang and Y. Rahmat-Samii, "Applications of electromagnetic band-gap (EBG) structures in microwave antenna designs," *Microwave and Millimeter Wave Technology,*

2002. Proceedings. ICMMT 2002. 2002 3rd International Conference on, pp. 528-531, 2002.

[65] Fan Yang and Y. Rahmat-Samii, "Microstrip antennas integrated with electromagnetic band-gap (EBG) structures: a low mutual coupling design for array applications," *Antennas and Propagation, IEEE Transactions on,* vol. 51, pp. 2936-2946, 2003.

[66] Fan Yang and Y. Rahmat-Samii, "Reflection phase characterizations of the EBG ground plane for low profile wire antenna applications," *Antennas and Propagation, IEEE Transactions on,* vol. 51, pp. 2691-2703, 2003.

[67] F. R. Yang, R. Coccioli, Y. Qian and T. Itoh, "PBG-assisted gain enhancement of patch antennas on high-dielectric constant substrate," *Antennas and Propagation Society International Symposium, 1999. IEEE,* vol. 3, pp. 1920-1923 vol.3, 1999.

[68] P. Salonen, M. Keskilammi and L. Sydanheimo, "A low-cost 2.45 GHz photonic band-gap patch antenna for wearable systems," *Antennas and Propagation, 2001. Eleventh International Conference on (IEE Conf. Publ. no. 480),* vol. 2, pp. 719-723 vol.2, 2001.

[69] P. Salonen, F. Yang, Y. Rahmat-Samii and M. Kivikoski, "WEBGA - wearable electromagnetic band-gap antenna," in *IEEE Antennas and Propagation Society Symposium 2004 Digest Held in Conjunction with: USNC/URSI National Radio Science Meeting,* 2004, pp. 451-454.

[70] P. Salonen and Y. Rahmat-Samii, "Textile Antennas: Effects of Antenna Bending on Input Matching and Impedance Bandwidth," *Aerospace and Electronic Systems Magazine, IEEE,* vol. 22, pp. 18-22, 2007.

[71] Shaozhen Zhu, Luyi Liu and R. Langley, "Dual Band Body Worn Antenna," *Antennas and Propagation Conference, 2007. LAPC 2007. Loughborough,* pp. 137-140, 2007.

[72] S. Zhu and R. Langley, "Dual-band wearable antennas over EBG substrate," *Electronics Letters,* vol. 43, pp. 141-142, 2007. 2007.

[73] Shaozhen Zhu and R. Langley, "Dual-Band Wearable Textile Antenna on an EBG Substrate," *Antennas and Propagation, IEEE Transactions on,* vol. 57, pp. 926-935, 2009.

[74] M. Hosseini, A. Pirhadi, R. Fallahi and M. Hakkak, "Bandwidth Enhancement of a Low Profile Antenna by Applying non-Uniformity to its High Impedance Ground Plane," *Mathematical Methods in Electromagnetic Theory, 2006 International Conference on,* pp. 202-204, 2006.

[75] M. Hosseini, A. Pirhadi and M. Hakkak, "Design of a Non-Uniform High Impedance Surface for a Low Profile Antenna," *Journal of Electromagnetic Waves and Applications,* vol. 20, pp. 1455-1464, 2006.

[76] M. Hosseini and S. Bashir, "Circularly polarized radiation by a dipole antenna over an innovative artificial ground plane," *Antennas and Propagation Conference, 2008. LAPC 2008. Loughborough,* pp. 453-456, 2008.

[77] S. Bashir, M. Hosseini, R. M. Edwards, M. I. Khattak and L. Ma, "Bicep mounted low profile wearable antenna based on a non-uniform EBG ground plane - flexible EBG inverted-l (FEBGIL) antenna," *Antennas and Propagation Conference, 2008. LAPC 2008. Loughborough,* pp. 333-336, 2008.

[78] J. R. James and P. S. Hall, *Handbook of Microstrip Antennas (IEE Electromagnetic Waves).* Institution of Engineering and Technology, 1989, pp. 1350.

[79] J. D. Kraus and R. J. Marhefka, *Antennas for all Applications.* ,Third ed.New York: McGraw-Hill, 2002,

[80] Y. Rahmat-Samii, "EBG structures for low profile antenna designs: What have we learned," in *European Conference on Antennas and Propagation, EuCAP 2007,* 2007,

[81] W. L. Stutzman and G. A. Thiele, *Antenna Theory and Design.* ,2nd ed.New York ; Chichester: Wiley, 1998,

[82] C. A. Balanis, *Advanced Engineering Electromagnetics.* New York ; London: Wiley, 1989,

[83] C. A. Balanis, *Antenna Theory : Analysis and Design.* ,3rd ed.Hoboken, NJ: John Wiley, 2005, pp. 1117.

[84] R. E. Collin and IEEE Antennas and Propagation Society, *Field Theory of Guided Waves.* ,2nd ed.New York: IEEE Press, 1991, pp. 851.

[85] D. Sievenpiper, L. Zhang and E. Yablonovitch, "High-impedance electromagnetic ground planes," *Microwave Symposium Digest, 1999 IEEE MTT-S International,* vol. 4, pp. 1529-1532 vol.4, 1999.

[86] D. Pozar and D. Schaubert, "Scan blindness in infinite phased arrays of printed dipoles," *Antennas and Propagation, IEEE Transactions on,* vol. 32, pp. 602-610, 1984.

[87] Y. Rahmat-Samii, "Electromagnetic band-gap structures: classification, characterization, and applications," *Antennas and Propagation, 2001. Eleventh International Conference on (IEE Conf. Publ. no. 480),* vol. 2, pp. 560-564 vol.2, 2001.

[88] R. Coccioli, Fei-Ran Yang, Kuang-Ping Ma and T. Itoh, "Aperture-coupled patch antenna on UC-PBG substrate," *Microwave Theory and Techniques, IEEE Transactions on,* vol. 47, pp. 2123-2130, 1999.

[89] R. Gonzalo, P. De Maagt and M. Sorolla, "Enhanced patch-antenna performance by suppressing surface waves using photonic-bandgap substrates," *Microwave Theory and Techniques, IEEE Transactions on,* vol. 47, pp. 2131-2138, 1999.

[90] D. Sievenpiper, "High Impedance Electromagnetic Surfaces," *PhD Dissertation at University of California, Los Angeles,* 1999.

[91] M. Rahman and M. A. Stuchly, "Transmission line-periodic circuit representation of planar microwave photonic bandgap structures," *Microwave Opt Technol Lett,* vol. 30, pp. 15-19, 2001.

[92] S. Maci, M. Caiazzo, A. Cucini and M. Casaletti, "A pole-zero matching method for EBG surfaces composed of a dipole FSS printed on a grounded dielectric slab," *Antennas and Propagation, IEEE Transactions on,* vol. 53, pp. 70-81, 2005.

[93] C. R. Simovski, P. de Maagt and I. V. Melchakova, "High-impedance surfaces having stable resonance with respect to polarization and incidence angle," *Antennas and Propagation, IEEE Transactions on,* vol. 53, pp. 908-914, 2005.

[94] F. Yang, Y. Qian and T. Itoh, "Low-profile cavity-backed slot antenna using UC-PBG substrate," in 2000, pp. 1796-1799 vol.3.

[95] C. C. Chiau, X. Chen and C. G. Parini, "A multi-period EBG structure for microstrip antennas," *Antennas and Propagation, 2003. (ICAP 2003). Twelfth International Conference on (Conf. Publ. no. 491),* vol. 2, pp. 727-730 vol.2, 2003.

[96] S. Tse, B. S. Izquierdo, J. C. Batchelor and R. J. Langley, "Reduced sized cells for high impedance (HIP) ground planes," *Antennas and Propagation, 2003. (ICAP 2003). Twelfth International Conference on (Conf. Publ. no. 491),* vol. 2, pp. 473-476 vol.2, 2003.

[97] Ang Yu and Xuexia Zhang, "A low profile monopole antenna using a dumbbell EBG structure," *Antennas and Propagation Society International Symposium, 2004. IEEE,* vol. 2, pp. 1155-1158 Vol.2, 2004.

[98] A. P. Feresidis, G. Goussetis and J. C. Vardaxoglou, "Metallodielectric arrays without vias as artificial magnetic conductors and electromagnetic band gap surfaces," *Antennas and Propagation Society International Symposium, 2004. IEEE,* vol. 2, pp. 1159-1162 Vol.2, 2004.

[99] P. K. Kelly, J. G. Maloney, B. L. Shirley and R. L. Moore, "Photonic band structures of finite thickness: theory and experiment," *Antennas and Propagation Society International Symposium, 1994. AP-S. Digest,* vol. 2; 2, pp. 718-721 vol.2, 1994.

[100] Fei-Ran Yang, Kuang-Ping Ma, Yongxi Qian and T. Itoh, "A novel TEM waveguide using uniplanar compact photonic-bandgap (UC-PBG) structure," *Microwave Theory and Techniques, IEEE Transactions on,* vol. 47; 47, pp. 2092-2098, 1999.

[101] H. -. D. Yang, Reonghee Kim and D. R. Jackson, "Design consideration for modeless integrated circuit substrates using planar periodic patches," *Microwave Theory and Techniques, IEEE Transactions on,* vol. 48, pp. 2233-2239, 2000.

[102] B. A. Munk, *Frequency Selective Surfaces: Theory and Design (Wiley-Interscience).* WileyBlackwell, 2000, pp. 416.

[103] G. Goussetis, A. P. Feresidis and J. C. Vardaxoglou, "FSS printed on grounded dielectric substrates: resonance phenomena, AMC and EBG characteristics," *Antennas and*

Propagation Society International Symposium, 2005 IEEE, vol. 1B, pp. 644-647 vol. 1B, 2005.

[104] D. J. Kern, D. H. Werner, A. Monorchio, L. Lanuzza and M. J. Wilhelm, "The design synthesis of multiband artificial magnetic conductors using high impedance frequency selective surfaces," *Antennas and Propagation, IEEE Transactions on,* vol. 53, pp. 8-17, 2005.

[105] F. Yang, A. Aminian and Y. Rahmat-Samii, "A novel surface-wave antenna design using a thin periodically loaded ground plane," *Microwave Opt Technol Lett,* vol. 47, pp. 240-245, 2005.

[106] G. Goussetis, A. P. Feresidis and J. C. Vardaxoglou, "Tailoring the AMC and EBG characteristics of periodic metallic arrays printed on grounded dielectric substrate," *Antennas and Propagation, IEEE Transactions on,* vol. 54, pp. 82-89, 2006.

[107] A. Aminian, F. Yang and Y. Rahmat-Samii, "In-phase reflection and EM wave suppression characteristics of electromagnetic band gap ground planes," *Antennas and Propagation Society International Symposium, 2003. IEEE,* vol. 4, pp. 430-433 vol.4, 2003.

[108] M. fan, R. Hu, Q. Hao, X. Zhang and Z. Feng. (Apr. 2003., Advance in 2D-EBG structures research. *Joumal of Infrared and Milimeter Waves*

[109] Long Li, Xiaojie Dang, Linnian Wang, Bin Li, Haixia Liu and Changhong Liang, "Reflection phase characteristics of plane wave oblique incidence on the mushroom-like electromagnetic band-gap structures," *Microwave Conference Proceedings, 2005. APMC 2005. Asia-Pacific Conference Proceedings,* vol. 3, pp. 4 pp., 2005.

[110] C. R. Simovski, P. de Maagt, S. A. Tretyakov, M. Paquay and A. A. Sochava, "Angular stabilisation of resonant frequency of artificial magnetic conductors for TE-incidence," *Electron. Lett.,* vol. 40, pp. 92-93, 2004.

[111] F. Yang and Y. Rahmat-Samii, "A low-profile circularly polarized curl antenna over an electromagnetic bandgap (EBG) surface," *Microwave Opt Technol Lett,* vol. 31, pp. 264-267, 20 Nov. 2001.

[112] F. Tavakkol-Hamedani, L. Shafai and G. Z. Rafi, "Comparison of PBG and perfect magnetic conductor surface effects on the performance of finite micros," *Antennas and Propagation Society International Symposium, 2002. IEEE,* vol. 3, pp. 748, 2002.

[113] M. Hosseini, A. Pirhadi and M. Hakkak, "A Novel AMC with little sensitivity to the angle of incidence using 2-layer Jerusalem cross FSS," *Progress in Electromagnetics Research, PIER,* vol. 64, pp. 43-51, 2006.

[114] N. Marcuvitz, *Waveguide Handbook (IEE Electromagnetic Waves)PBEW0210 (IEE Electromagnetic Waves).* ,New Ed ed.Institution of Engineering and Technology, 1986, pp. 446.

[115] Leitch, P.: Tassinari, T. H., "Interactive Textiles: New Materials in the New Millennium," *Journal of Industrial Textiles,* vol. 29, pp. 173-190, 2000.

[116] K. C. Gupta and A. Benalla, *Microstrip Antenna Design.* Norwood, MA: Artech House, 1988, pp. 397.

[117] K. Wong, *Planar Antennas for Wireless Communications.* Hoboken, NJ: J. Wiley-Interscience, 2003, pp. 301.

[118] R. Garg, *Microstrip Antenna Design Handbook.* Boston, MA: Artech House, 2001, pp. 845.

[119] Z. N. Chen and M. Y. W. Chia, *Broadband Planar Antennas : Design and Applications.* Chichester, England ; Hoboken, NJ: John Wiley & Sons, 2006, pp. 243.

[120] http://www2.rohde-schwarz.com/ - Retrieved 30th Sep 09.

[121] J. Krupka, "Frequency domain complex permittivity measurements at microwave frequencies," *Measurement Science and Technology,* vol. 17, pp. 55-70, 2006.

[122] J. krupka, R. G. Geyer, J. Baker-Jarvis and J. Ceremuga, "Measurements of the complex permittivity of microwave circuit board substrates using split dielectric resonator and reentrant cavity techniques," in *Seventh International Conference on Dielectric Materials, Measurements and Applications,* 1996, pp. 21-24.

[123] Linfeng Chen, C. K. Ong and B. T. G. Tan, "Amendment of cavity perturbation method for permittivity measurement of extremely low-loss dielectrics," *Instrumentation and Measurement, IEEE Transactions on,* vol. 48, pp. 1031-1037, 1999.

[124] J. R. Mosig, J. E. Besson, M. Gex-Fabry and F. E. Gardiol. (1981, no. 1). Reflection of an open-ended coaxial line and application to nondestructive measurement of materials. *IEEE Transactions on Instrumentation and Measurment Vol. IM-30*pp. pp. 46-51.

[125] J. Baker-Jarvis, M. D. Janezic, J. H. Grovenor Jr and R. G. Geyer, "Transmission/reflection and short-circuit line methods for measuring permittivity and permeability," NIST Technology, Tech. Rep. 1355, 1993.

[126] J. krupka, "Operating manual of 2.4GHz SPDR,"

[127] http://www.muirhead.co.uk/sti/muirhead/muirhead_home.asp- Retrieved 30th Sep 09.

[128] C. A. Winterhalter, J. Teverovsky, P. Wilson, J. Slade, W. Horowitz, E. Tierney and V. Sharma, "Development of electronic textiles to support networks, communications, and medical applications in future U.S. Military protective clothing systems," *Information Technology in Biomedicine, IEEE Transactions on,* vol. 9, pp. 402-406, 2005.

[129] http://www.lessemf.com/ - Retrieved 30th Sep 09.

[130] R. Waterhouse, *Microstrip Patch Antennas: A Designer's Guide.* Springer, 2003, pp. 432.

[131] S. Dey and R. Mittra, "Compact microstrip patch antenna," *Microwave Opt Technol Lett,* vol. 13, pp. 12-14, 1996.

[132] A. Shackelford, Kai-Fong Lee and D. Chatterjee, "On reducing the patch size of U-slot and L-probe wideband patch antennas," in *Antennas and Propagation for Wireless Communications, 2000 IEEE-APS Conference on,* 2000, pp. 35-38.

[133] T. Huynh and K. -. Lee, "Single-layer single-patch wideband microstrip antenna," *Electronics Letters,* vol. 31, pp. 1310-1312, 1995.

[134] M. Tanaka and J. Jang, "Wearable microstrip antenna for satellite communications," *IEICE Trans. Commun.,* vol. E87-B, pp. 2066-2071, 2004.

[135] Fan Yang and Y. Rahmat-Samii, "Wire antennas on artificial complex ground planes: a new generation of low gain antennas," *Antennas and Propagation Society International Symposium, 2004. IEEE,* vol. 1, pp. 309-312 Vol.1, 2004.

[136] http://uk.rs-online.com/web/- Retrieved 30th Sep 09,

[137] Z. Duan, D. Linton, W. Scanlon and G. Conway, "Using EBG to Improve Antenna Efficiency in Proximity to the Human Body," *Wideband, Multiband Antennas and Arrays for Defence Or Civil Applications, 2008 Institution of Engineering and Technology Seminar on,* pp. 173-180, 2008.

[138] H. Mosallaei and K. Sarabandi, "Antenna miniaturization and bandwidth enhancement using a reactive impedance substrate," *Antennas and Propagation, IEEE Transactions on,* vol. 52; 52, pp. 2403-2414, 2004.

[139] P. Salonen, M. Keskilammi and Y. Rahmat-Samii, "Textile antennas: Effect of antenna bending on radiation pattern and efficiency," *Antennas and Propagation Society International Symposium, 2008. AP-S 2008. IEEE,* pp. 1-4, 2008.

[140] T. Weiland, "A discretization model for the solution of Maxwell's equations for six-component fields," *Archiv Elektronik Und Uebertragungstechnik,* vol. 31, pp. 116-120, 1977.